Inaugural dissertation
for
obtaining the doctoral degree
of the
Combined Faculty of Mathematics, Engineering and Natural Sciences
of the
Ruprecht - Karls - University
Heidelberg

Presented by

M.Sc. Alicia Alonso de la Vega
born in: Madrid, Spain

Oral examination: 09.12.2022

Uncovering the role of APOBEC3B in lung cancer and RNA editing

Referees: **Prof. Dr. Michael Boutros**

Prof. Dr. Stefan Wiemann

Para mi abuela Alicia. Todo esto es para ti.

SUMMARY

De novo genetic alterations such as DNA mutations, chromosomal instability and other mechanisms like RNA editing, can all induce tumor heterogeneity. Members of the APOBEC3 family of cytosine deaminases have been implicated in increased cancer genome mutagenesis, thereby contributing to intra- and inter tumor genomic heterogeneity and therapy resistance. Among the APOBEC3 family, APOBEC3A (A3A) and APOBEC3B (A3B) have been causally linked to the observed APOBEC mutation signature in several cancers. It is essential to understand how these conserved enzymes with a key role in innate defense can turn against the host endangering the genome. Recent studies on A3B, have generated new insights into how A3B mutagenesis and chromosomal instability fuels tumor evolution. However, there is still a long way to go in understanding the actual impact of A3B expression in cancer and its implication in other possible mechanisms driving diversity, such as RNA editing.

To better understand the impact of A3B in tissue homeostasis and tumor evolution, we engineered a novel doxycycline-inducible mouse model of A3B-overexpression. The data in this thesis uncovered that A3B can influence tumorigenesis at different stages. First, long-term A3B expression fueled tumor initiation in different tissues. In addition, A3B expression combined with a well-described model of Kras-driven lung adenocarcinoma promoted malignant progression. Although overexpression of A3B did not affect overall survival, tumors acquired advanced disease features similar to those seen in human lung malignancies. The aggressiveness of A3B expression was also reflected in partial tumor regression upon direct oncogene inhibition. Finally, A3B tumor cells downregulate the p53 pathway as a bypass mechanism to tolerate A3B-induced damage. In summary, the first part of this thesis unveils that A3B expression enables tumor cells to evolve and acquire traits to drive tumor evolution.

To study a potential role of A3B as and RNA editing enzyme I engineered a mouse model that achieves strong and persistent levels of A3B in healthy tissues, leading to disruption of cellular fitness and causing sudden animals' death. Liver and pancreas were the main organs affected, correlating with being the tissues with higher A3B expression. Importantly, strict analysis of whole exome and transcriptomic data from A3B tissues revealed hundreds of A3B-driven RNA editing events localized in a particular sequence context: UCCGUGUG. In addition, the labile nature of RNA editing was confirmed by undetectable editing activity in the absence of A3B expression. Finally, I discovered that RNA editing activity is dependent on the deaminase catalytic domain of A3B. This work illustrates how elevated levels of A3B are toxic

and dramatically compromise cell and tissue homeostasis and identifies, for the first time, a new function of A3B in editing the RNA.

Zusammenfassung

De-novo-Genveränderungen wie DNA-Mutationen, chromosomale Instabilität und andere Mechanismen wie RNA-Editing können zu Tumorheterogenität führen. Mitglieder der APOBEC3-Familie von Cytosindeaminasen werden mit einer verstärkten Mutagenese des Krebsgenoms in Verbindung gebracht und tragen so zur genomischen Heterogenität innerhalb und zwischen Tumoren und zur Therapieresistenz bei. Von der APOBEC3-Familie wurden APOBEC3A (A3A) und APOBEC3B (A3B) mit der bei verschiedenen Krebsarten beobachteten APOBEC-Mutationssignatur in Verbindung gebracht. Es ist wichtig zu verstehen, wie sich diese konservierten Enzyme, die eine Schlüsselrolle bei den angeborenen Abwehrmechanismen spielen, gegen den Wirt wenden und das Genom gefährden können. Jüngste Studien zu A3B haben neue Erkenntnisse darüber erbracht, wie die Mutagenese von A3B und chromosomale Instabilität die Tumorevolution vorantreiben. Weitere Forschung ist notwendig um die tatsächlichen Auswirkungen der A3B-Expression bei Krebs und ihre Implikation in andere mögliche Mechanismen, die die Diversität vorantreiben, wie z. B. RNA-Editing, zu verstehen.

Um die Auswirkungen von A3B auf die Gewebehomöostase und die Tumorevolution besser zu verstehen, haben wir ein neuartiges Doxycyclin-induzierbares Mausmodell der A3B-Überexpression entwickelt. Die Daten dieser Arbeit haben gezeigt, dass A3B die Tumorentstehung in verschiedenen Stadien beeinflussen kann. Zunächst förderte die langfristige A3B-Expression die Tumorentstehung in verschiedenen Geweben. Darüber hinaus förderte die A3B-Expression in Kombination mit einem gut beschriebenen Modell des Kras-getriebenen Lungenadenokarzinoms die maligne Progression. Obwohl die Überexpression von A3B keinen Einfluss auf das Gesamtüberleben hatte, wiesen die Tumoren fortgeschrittene Krankheitsmerkmale auf, die denen von menschlichen Lungenkrebsen ähnelten. Die Aggressivität der A3B-Expression spiegelte sich auch in der teilweisen Rückbildung des Tumors bei direkter Hemmung des Onkogens wider. A3B-Tumorzellen regulieren den p53-Signalweg als Umgehungsmechanismus herunter, um A3B-induzierte Schäden tolerieren zu können. Zusammenfassend zeigt der erste Teil dieser Arbeit, dass die A3B-Expression es Tumorzellen ermöglicht, sich weiterzuentwickeln und Eigenschaften zu erwerben, die die Tumorevolution vorantreiben.

Um die potenzielle Rolle von A3B als RNA-editierendes Enzym zu untersuchen, habe ich ein Mausmodell entwickelt, in dem starke und anhaltende A3B-Konzentrationen in gesundem Gewebe erreicht werden, was zu einer Störung der zellulären Fitness und zum plötzlichen Tod

der Tiere führt. Leber und Bauchspeicheldrüse waren die am stärksten betroffenen Organe, was damit korreliert, dass sie die Gewebe mit der höchsten A3B-Expression sind. Eine strenge Analyse der gesamten Exom- und Transkriptomdaten von A3B-Geweben ergab Hunderte von A3B-gesteuerten RNA-Editing-Ereignissen, die in einem bestimmten Sequenzkontext lokalisiert sind: UCCGUGUG. Darüber hinaus wurde die labile Natur des RNA-Editings durch eine nicht nachweisbare Editing-Aktivität in Abwesenheit der A3B-Expression bestätigt. Schließlich entdeckte ich, dass die RNA-Editing-Aktivität von der katalytischen Deaminase-Domäne von A3B abhängig ist. Diese Arbeit veranschaulicht, wie erhöhte A3B-Spiegel toxisch wirken und die Zell- und Gewebehomöostase dramatisch beeinträchtigen, und identifiziert zum ersten Mal eine neue Funktion von A3B im Bezug auf RNA-Editing.

Introduction

1. AID/APOBEC family

The AID/APOBEC (apolipoprotein B mRNA editing catalytic polypeptide-like) family of enzymes catalyzes the chemical reaction of deamination, which involves the conversion of cytosines to uracils. In primates and humans, this family of deaminases consists of 11 gene members: activation-induced-deaminase (AID), APOBEC1 (A1), APOBEC2 (A2), APOBEC3 (A3, with 7 isoforms) and APOBEC4 (A4). The APOBEC field was born when ApoB C to U editing by A1 was discovered (S.-H. Chen et al., 1987; Powell et al., 1987; Teng et al., 1993). However, phylogenetic analysis showed that it was more than 500 million years ago when the first AID ancestor gene appeared in jawless fish. The requirement for adaptive immunity and after duplications in AID ancestral genes, the genes that encoded for AID and A2 emerged in bony fish. Later, A1, A3, and A4 first appeared in reptiles, birds, amphibians and mammals. Finally, A3 underwent one more round of evolution in primates, leading to the emergence of seven distinct isoforms, ranging from A to H (Conticello et al., 2005).

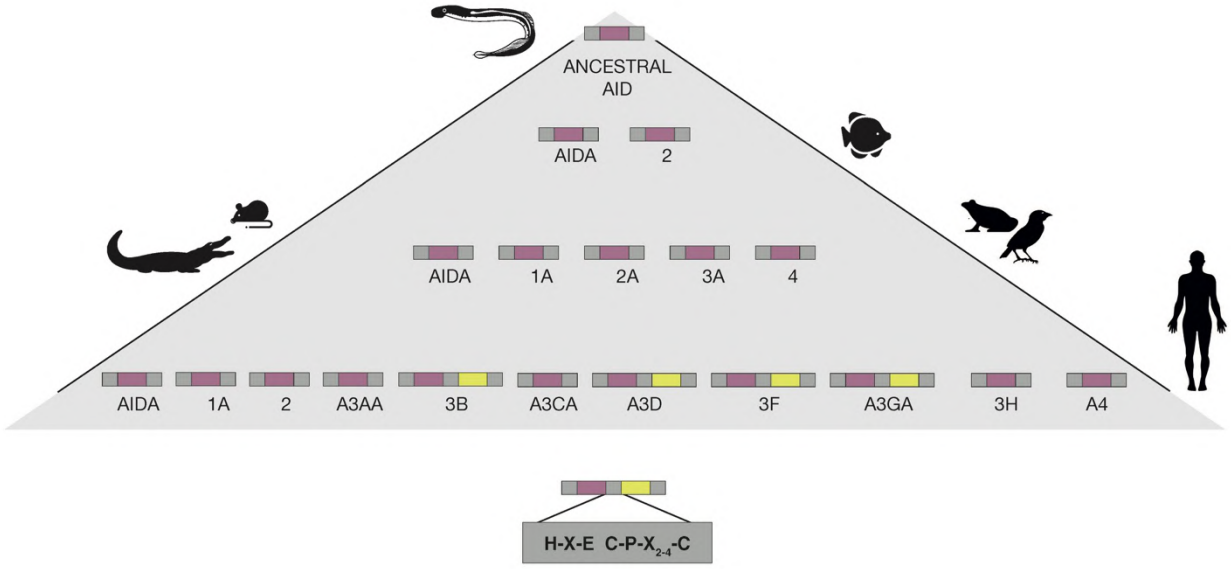

Figure 1: Evolution of the APOBEC family

The APOBEC family in humans is composed by single zinc-dependent deaminase domain (ZDD) enzymes (purple) AID, A2, A1, A3A/C/H, and A4 and double ZDD enzymes (purple and yellow) A3B/D/F/G. Both domains contain a canonical amino acid sequence shown in the bottom of the panel. The cartoon also shows the emergence and evolution of APOBEC family members since the first AID ancestor genes in jawless fish to humans.

1.1. Structural features and deamination reaction

According to crystallographic evidence, the catalytic core of the AID/APOBEC family contains a conserved amino acid sequence with modest variations. A zinc ion (Zn^{2+}) found in the catalytic subunit or zinc-dependent deaminase domain (ZDD) coordinates the deamination process in nucleoside and nucleotide substrates. The overall structure consists of a core of five hydrophobic ß-sheets surrounded by six α-helices (Pecori et al., 2022). Particularly, the conserved ZDD is formed by α2 and α3 domains with the amino acid sequence H-X-E and C-P-X_{2-4}-C. The histidine and the two cysteines coordinate the ZDD, to keep the Zn^{2+} in place forming the catalytic pocket where the deaminated cytosine will bound (Conticello, 2008). The deamination reaction starts with the nucleophilic attack of the Zn^{2+} in the cytosine atom's C4. Then, the conserved glutamate functions as a proton donor, donating a proton to the departing ammonia group and transferring a proton from the water molecule to the N3 molecule of the cytosine, which ultimately produces a uracil nucleobase (Fig) (Salter & Smith, 2018).

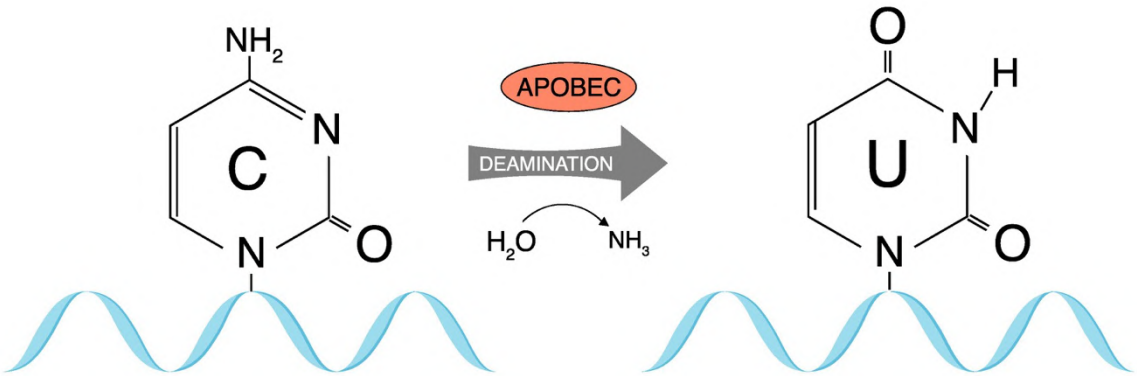

Figure 2: Cytosine deamination reaction

Schematic of the single-stranded DNA cytosine deamination reaction catalysed by the APOBEC family.

The majority of the APOBEC genes have one ZDD domain (APOBEC3A/C/H, AID, and APOBEC1). However, in some species, the original gene has undergone rounds of duplication and fusion to form deaminases containing a double ZDD domain (APOBEC3B/D/F/G) (Salter et al., 2016; Salter & Smith, 2018). The emergence of two ZDD domains in a single enzyme most likely resulted from selective pressure and diversification in mammals (Sawyer et al., 2004; J. Zhang & Webb, 2004). In double-domain enzymes, only the C-terminal domain is catalytically active; the N-terminal domain is structurally identical to the catalytic domain but is catalytically inactive. The biological function of this domain is thought to be connected with regulatory processes and subcellular localization.

APOBEC enzymes work in distinct cellular compartments and identify diverse nucleic acid motifs and structures. Although they have a common enzymatic core, the 11 members of the family differ in their preferred targets, binding affinities and catalytic rates. All APOBEC

members prefer to deaminate single-stranded-DNA (ssDNA) substrates, although some enzymes in the family also target RNA molecules. Moreover, sequence and structural variations in loops 1 and 7, surrounding the ZDD domain, control over substrate access to the active site. Importantly, co-crystal structures of the different APOBECs with ssDNAs shed light on substrate selectivity. The nucleobase at position -1 upstream of the target C was discovered to determine each enzyme's intrinsic preference (review in (Salter et al., 2016; Salter & Smith, 2018)).

1.2. Repair mechanisms after deamination

Deamination is a multi-step process that is often completed by base excision repair (BER). First, the uracil-DNA glycosylase (UNG) removes the uracil from ssDNA, resulting in an apyrimidinic (AP) site that is then nicked by the endonuclease APE1 and repaired by X-ray repair cross-complementing protein 1 (XRCC1) through the recruitment of polymerases and ligases. However, the following alternatives might also occur:

- If replication interrupts UNG-base excision, the replication machinery will insert an A in front of the U, resulting in a C to T transition.
- If the uracil is removed by UNG-base excision prior to replication, translesion synthesis (TLS) polymerases may replicate the AP site, resulting in C to T transitions or C to G transversions.
- Double strand breaks may result from simultaneous deamination of two nearby cytosines in opposing strands.

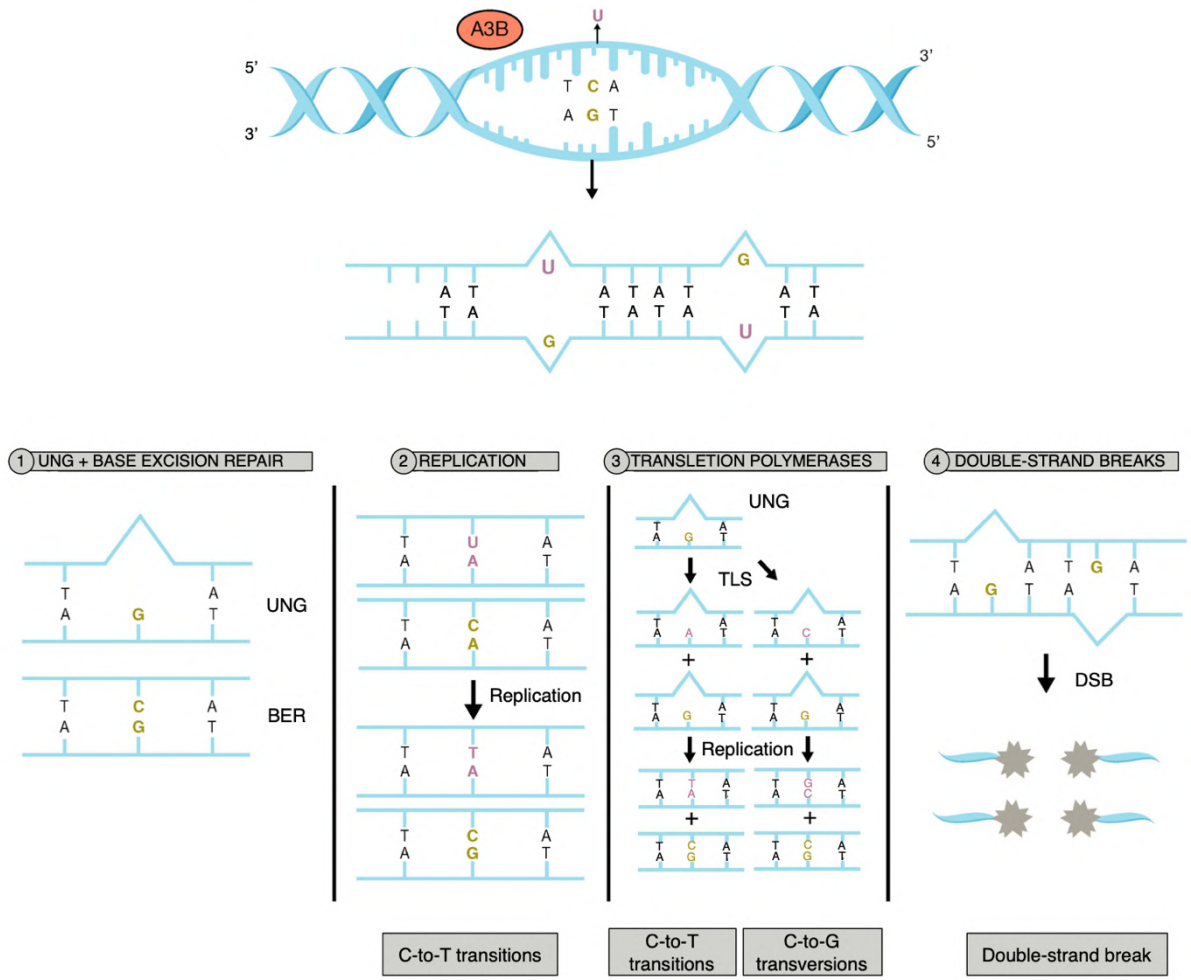

Figure 3: Processing of genomic uracil after APOBEC-mediated cytosine deamination

Schematic of the multiple repair mechanisms that can follow cytosine deamination in single-stranded DNA by the APOBEC family.

APOBECs' expression is mostly confined to the cytoplasm; nevertheless, dysregulation and malfunction of the repair machinery might render nuclear genomic DNA susceptible to APOBEC activity. Genomic stability could be compromised by deamination-induced transitions or transversions in the host DNA that may result in mutations, and/or double-strand breaks (DSBs), which could create translocations (Henderson & Fenton, 2015).

2. APOBEC family members

2.1. AID

AID was first discovered in 1999 as part of the host defenses having a determinant role in the adaptive immune responses (Muramatsu et al., 1999). AID is expressed in activated B cells and vital for antibody diversification and maturation through somatic hypermutation (SHM) and class-switch recombination (CSR) (Muramatsu et al., 2000). In SHM, AID deamination

induces hypermutation in the immunoglobulin (Ig) genes, resulting in changes in antibody affinity that allows the antibody to identify the presented antigen more effectively (Storb, 2014). Only B cells producing Ig with increased antigen affinity are favorably chosen for further maturation. In CSR, AID deamination induces DSBs, resulting in the rearrangement of the Ig locus and antibody isotype switching (Methot & Noia, 2017).

AID prefers to deaminate ssDNA cytosines in 5'WRC motifs (W=A/T, R=A/G) that correlate with the motif of Ig variable regions (Nabel et al., 2012; Rogozin & Diaz, 2004; Rogozin & Kolchanov, 1992). Even though AID can bind to both RNA and ssDNA, no catalytic activity toward RNA has yet been found (Bransteitter et al., 2003; Larijani & Martin, 2007).

Finally, deregulation in AID activity can induce off-target mutations and chromosomal translocations in non-Ig genes, which have been associated with the development of lymphomas and other hematological malignancies (Klemm et al., 2009) and in a minority of cases, solid tumors (L. Li et al., 2019). Several studies have shown that constitutive and ubiquitous expression of AID in transgenic mice led to T-cell lymphomas resulting from mutations in oncogenes (Okazaki et al., 2003) or Ig-associated translocations (Pasqualucci et al., 2008).

2.2. APOBEC1

APOBEC1 was the first APOBEC member discovered as the enzyme responsible for apolipoprotein B (ApoB) mRNA C to U editing (Teng et al., 1993). Human APOBEC1 expression is restricted to the small intestine and its unique proven physiological target is ApoB mRNA. However, mouse Apobec1 is expressed more extensively, primarily in immune cells as well as in the small intestine and in the liver. In fact, several studies in mice have identified hundreds of Apobec1-editing targets in multiple mouse tissues. (Rayon-Estrada et al., 2017; Rosenberg et al., 2011; Soleymanjahi et al., 2021).

APOBEC1 prefers to deaminate ssDNA cytosines in 5'TC motifs that include a broader sequence context. For example, it is consistent that surrounding the edited cytosine there is an enrichment in AU content, a 3' cis-acting sequence, and the formation of secondary structures (Lerner et al., 2018). Like the majority of deaminases, APOBEC1 functions in the nuclear compartment and shuttles between the nucleus and the cytoplasm. Even though it was first described as an RNA editing enzyme, it has been shown that APOBEC1 is promiscuous when selecting its substrate and also has the ability to deaminate ssDNA (Caval et al., 2019; Harris et al., 2002; Petersen-Mahrt & Neuberger, 2003; Saraconi et al., 2014).

While APOBEC1 and C-to-U editing have been associated with a number of biological processes, their deregulation has been linked to the development of several disorders, including cancer (C. Luo et al., 2021; Swanton et al., 2015).

2.3. APOBEC2

APOBEC2 is highly conserved through evolution. However, its biological function has not yet been determined. In mammals and chickens, it is expressed in cardiac and skeletal muscle. In fact, APOBEC2 knockdown animal models have shown that myopathy is caused by mitochondrial abnormalities (Sato et al., 2018). Recently, it was shown that despite the absence of deaminase activity in DNA or RNA, APOBEC2 may still bind to DNA and function as a transcriptional repressor (Lorenzo et al., 2021).

2.4. APOBEC4

APOBEC4 is, along with APOBEC2, the least understood APOBEC enzyme. It has not been reported to have deaminase activity and has been identified to be expressed in the testis of mammals (Rogozin et al., 2005). Although it has been hypothesized to have a role in spermatogenesis, its biological function and substrate specificity remain unknown.

2.5. APOBEC3

The APOBEC3 gene was originated in placental animals and has been exposed to natural selection. While the genome of rodents has only one Apobec3 gene, humans and primates possess seven APOBEC3 genes that code for seven distinct deaminases (A3A-D and A3F-A3H). Their biological role might explain this fast evolution and positive selection. As a major innate defensive barrier, there is a constant need to evolve to combat new threats. APOBEC3s play a crucial function in protecting the host against viruses by hypermutating and degrading the replicating viral genome (Harris & Dudley, 2015). Retrotransposons are retroviral-like sequences that constitute a significant portion of the mammalian genome. These sequences multiply and expand through a copy-and-paste-like process, posing a threat to the genome's integrity. APOBEC3s are the first line of defense in retroelement restriction to protect the genome. However, APOBEC3-induced mutations in retroelements can also be beneficial and positively selected, contributing to the evolution and the formation of new genes (Carmi et al., 2011). Similarly, viral genomes may benefit from these mutations and acquire new characteristics as they evolve (Tasakis et al., 2021; R. Wang et al., 2020).

Through the process of subcellular localization, cells are able to compartmentalize proteins that have the potential to be either genotoxic or cytotoxic. APOBEC3 proteins strictly

regulate their subcellular localization in order to restrict their activities to their targets rather than nuclear DNA. Single-domain human APOBEC3s (A3A, A3C and A3H) are the smallest and are capable to diffuse through the nuclear membrane. They are localized through all cell compartments during interphase. The double-domain human APOBEC3s (A3B, A3D, A3F, and A3G) cannot passively access the nucleus, and during interphase, only A3B is localized in the nuclear compartment. When the nuclear envelope breaks down during mitosis, all human APOBEC3s are blocked from chromatin, likely inhibiting genome mutagenesis (Lackey et al., 2014; Salter et al., 2016). In addition, tissue-specific expression is determined by gene, for example, A3A is mainly expressed in monocytes (Land et al., 2013).

APOBEC3s have been characterized mainly to target ssDNA in 5'TC motifs, with the exception of A3G, which deaminates cytosines in 5'CC. Even though the majority have a significant affinity for DNA substrates, some members have been identified to have deaminase activity on RNA substrates. Overexpression of A3A enhances RNA editing in hypoxic and interferon-stimulated macrophages as well as in human tumors (Jalili et al., 2020; Sharma et al., 2015). In addition, A3G has been found to have RNA editing activity in HEK293T and lymphocyte cells (Sharma et al., 2019).

Deregulation of specific APOBEC3 enzymes, A3A and A3B, has been proposed to compromise genome integrity, and their activity has been associated with cancer. The importance of these two enzymes will be described in more detail in the next sections.

2.5.1. APOBEC3A

A3A is a single-domain enzyme with the most powerful deaminase activity and the highest viral restriction capacity of all APOBEC3 enzymes. It was the first APOBEC3 enzyme described to have a dual function in ssDNA and RNA deamination. Biochemical analysis showed that A3A has an intrinsic preference for YTCA (Y=pyrimidine) motifs for deamination (Chan et al., 2015). Remarkably, A3A preferentially targets stem-loop secondary structures (Buisson et al., 2019). A3A has been identified as a restriction factor for the retroelement LINE-1 and different types of viruses (H. Chen et al., 2006; Harris & Dudley, 2015). A3A expression is carefully regulated by mechanisms involving STAT2 and p65 transcription factors. The cues that trigger A3A activation cascade are interferon type-I (IFN) and are associated with inflammation and genotoxic stress (Oh et al., 2021). Recently, tyrosine kinase inhibitors have also been shown to increase A3A expression (Isozaki et al., 2021). Its expression is mainly restricted to the myeloid lineage, and due to its small size (25kDa) it can shuttle between the cytoplasm and the nucleus (Stenglein et al., 2010). Under normal conditions, A3A is found in the cytoplasm, preventing access to nuclear DNA. However, A3A has also been found to be

genotoxic when overexpressed, causing cell cycle arrest and DNA damage (Land et al., 2013; Landry et al., 2011).

2.5.2. APOBEC3B

A3B is a double-domain enzyme involved in the suppression of retroviruses, such as HIV or HBV, and retroelement restriction (Harris & Dudley, 2015; Refsland & Harris, 2013). It has so far only been described to deaminate ssDNA. There is evidence supporting that A3B interacts with RNA through its non-catalytic CD domain, although this interaction appeared to attenuate DNA deaminase activity (Xiao et al., 2017). Although A3A and A3B are highly homologous, biochemical analysis has shown that A3B has an intrinsic preference for RTCA (R=purine) motifs for deamination different from the one from A3A (Chan et al., 2015). In addition, contrary to A3A, findings on biochemical structures revealed no relationship between A3B substrates and secondary structures (Buisson et al., 2019). A3B is the only member that is constitutively nuclear and has been found to be expressed in hepatocytes and at low levels in lymphocytes (Bonvin et al., 2006; Burns et al., 2013; Koning et al., 2009; Salamango et al., 2018). While some studies indicate that A3B expression is IFN-dependent (Bonvin et al., 2006), new data clearly supports that nuclear factor kappa B (NF-kB) signaling is a powerful promoter of A3B induction (Leonard et al., 2015; Maruyama et al., 2016). Furthermore, DNA

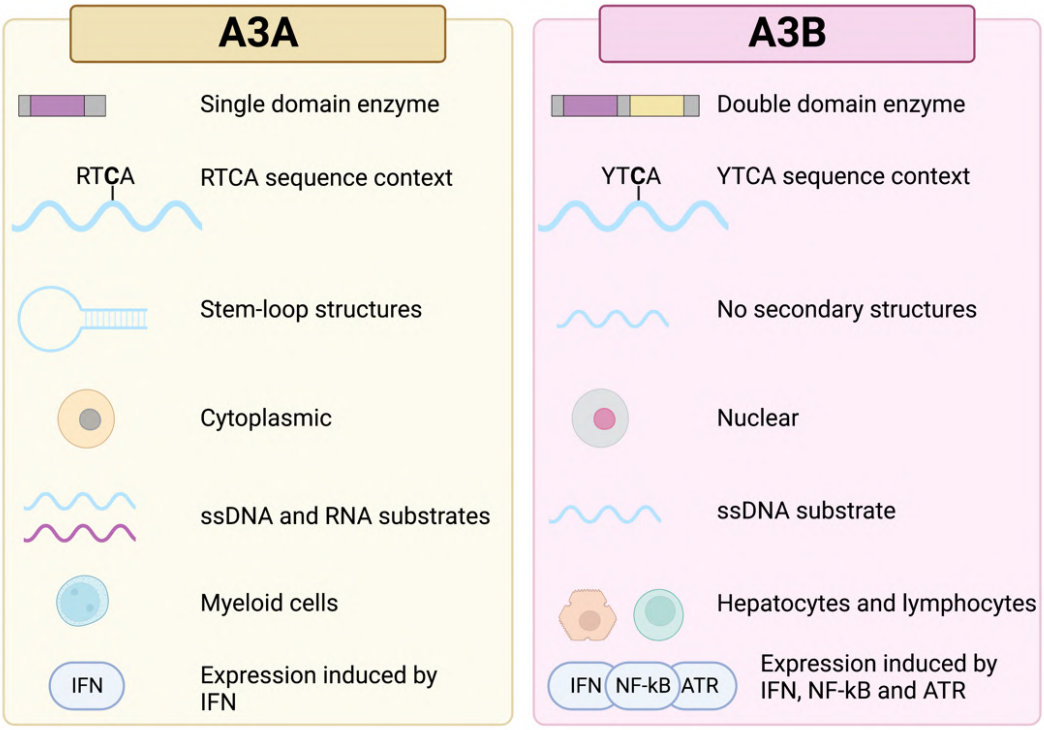

Figure 4: Summary of A3A and A3B differences

Schematic summarizing the differences in substrate preference, localization and regulation of expression between A3A and A3B.

damage and replication stress have been demonstrated to promote A3B expression through the ATR/CHK1 pathway (Kanu et al., 2016; Menendez et al., 2017). Recently, tyrosine kinase inhibitors have also been shown to increase A3B expression (Caswell et al., 2022).

The mutagenic potential of A3A and A3B in the nucleus has made these enzymes to be considered as important contributors to cancer. Many efforts have been made to determine which enzyme is the primary player in carcinogenesis or if both play an equal role, although due to their similar substrate preference and their high homology, this has been challenging. It is critical to clearly understand the role that each enzyme plays in the development of cancer.

3. APOBEC3 mutagenesis in cancer

3.1. Mutational signatures

During life, cells are gradually exposed to endogenous and exogenous mutagens, which can endanger the genome. Failure to repair DNA damage induced by these mutagens during cell division can lead to somatic mutations compromising genomic stability. Although the vast majority of these mutations will be passengers and will not provide any proliferative benefit, eventually, some alterations can promote tumorigenesis. Prior research focused on understanding driving mutations as being responsible for shaping cancer genomes; however, tumors also contain thousands of passenger mutations. Passenger mutations account for the biological mechanisms that have occurred in the tumor. Therefore, cancer genomes reflect the scars of the mutagenic processes that occurred during tumor evolution.

Advances in DNA sequencing over the last decades have revealed characteristic patterns of nucleotide substitutions, insertions, deletions and structural changes. Each combination of mutation types arises from different mutagenic processes, and they have been classified into mutational signatures. The concept was raised when consistent patterns of somatic mutations were found in a whole-genome-sequencing (WGS) dataset coming from 21 breast tumors (Nik-Zainal et al., 2012) Later, an extensive analysis of thousands of tumors from different cancer types revealed 21 different single-base substitution signatures (SBSs) (Alexandrov et al., 2013). Recently, this study was updated by increasing the number of samples and describing a total of 49 different SBSs (Alexandrov et al., 2020).

Among these, SBS2 and SBS13 mutational signatures have been attributed to the APOBEC family and have been broadly found in different human cancers (Alexandrov et al., 2013; Nik-Zainal et al., 2012; Roberts et al., 2013). Several studies correlated the expression levels of APOBEC enzymes with the presence of both signatures in human tumors (Burns et al., 2013; Roberts et al., 2013). These signatures are characterized by cytosine substitutions

occurring in a TCN trinucleotide context. Whereas SBS2 is characterized by C-to-T changes, SBS13 shows C-to-G or C-to-A substitutions. This indicates that even though both signatures occur through APOBEC mutagenesis, each signature employs different repair mechanisms or replicative polymerases to resolve cytosine deamination (Helleday et al., 2014; Roberts & Gordenin, 2015).

A fraction of the APOBEC mutations occurs in clusters that consist in 6 or more mutations that are separated by an average distance of less than or equal to 1Kb. This phenomenon was named *kataegis*, which means thunderstorm in Greek (Nik-Zainal et al., 2012; Roberts et al., 2013). This phenomenon has been described in several types of cancer and is associated with double-strand breaks and chromothripsis (Maciejowski et al., 2015; Nik-Zainal et al., 2012; Roberts et al., 2012; Taylor et al., 2013).

3.2. APOBEC3 enzymes in cancer

It is now well-established that members of the A3 enzyme family represent an endogenous source of somatic mutations that are observed in multiple human tumors such as cervical, bladder, breast, head/neck, and lung cancer (Alexandrov et al., 2013; Harris, 2015; Henderson & Fenton, 2015; Lawrence et al., 2013; Rebhandl et al., 1929; Roberts & Gordenin, 2015; Weinstein et al., 2014). However, there is a continuous debate regarding which A3 enzyme is the main player in cancer. It would be essential to elucidate whether cancer mutagenesis is a direct result of the action of a single deaminase or a combination of many of them. Although distinguishable deamination sequence contexts for each enzyme are now emerging (Chan et al., 2015; Shi, Carpenter, et al., 2017), the high homology across them has been an obstacle to teasing apart which one is responsible for A3 signatures in tumors.

In addition to sequencing studies, work with cancer cell lines was performed to determine the contribution of each A3 in driving SBS2 and SBS13. First, the Harris group examined the expression levels of the various A3 family members and found A3B to be overexpressed in breast cancer cell lines and primary tumor samples. Moreover, knockdown of A3B ablated deamination activity and reduced considerably the load of C-to-T mutations in breast cancer cell lines (Burns et al., 2013). However, the APOBEC signature can also be detected in breast tumors in the absence of A3B. It has been observed that breast cancer risk increases in patients harboring a partial allele deletion of A3B, which deregulates A3A activity by merging the coding sequence of A3A to the 3' untranslated region of A3B (Nik-Zainal et al., 2014). Analysis of sequencing data and *in vitro* experiments using A3A-A3B artificial constructs revealed increased hypermutation activity compared to single A3A expression (Caval, Suspène, Shapira, et al., 2014). Even though high levels of A3B mRNA have been detected

in several types of cancer, A3A has a more potent deaminase activity. Although A3A's dangerous activity is counteracted by its localization to the cytoplasm, some studies have shown that A3A can target genomic DNA and promote tumorigenesis (Caval, Suspène, Vartanian, et al., 2014; Landry et al., 2011). Finally, in a recent study, A3H haplotype I was also proposed to contribute to the bulk of 'APOBEC signature' mutations in cancer (Starrett et al., 2016). Currently, it is challenging to rule out the potential contribution that one or more of these proteins have to cancer mutagenesis.

One important tool for expanding our knowledge of cancer development is the use of mouse models. *In vivo* overexpression studies proved the tumorigenic activity of APOBEC1, APOBEC2 and AID (Okazaki et al., 2003; Okuyama et al., 2012; Yamanaka et al., 1995). Because rodents only have one A3 gene and humans have seven, no reliable animal model for studying individual A3 genes has been published. In 2020, the first *in vivo* study showing a cause-and-effect relationship between human A3A and cancer was published. It demonstrated how A3A catalyzes mutagenesis and promotes tumorigenesis in colorectal and hepatocellular cancer (Law et al., 2020). There is currently no evidence that A3B alone can promote tumorigenesis *in vivo*. Some research has combined the expression of A3B with clinically relevant mouse models. However, these studies failed to induce A3B at sufficient levels to increase A3B-mediated mutagenesis (Boumelha et al., 2022; Caswell et al., 2022; Venkatesan et al., 2021).

Growing evidence highlights the complexity of APOBEC mutagenesis in human tumors and the significance of these enzymes. In addition, the timeframe when these deaminases are expressed and whether their activity is driving tumor initiation or acting later during tumor evolution is still unclear.

3.2.1. Initiation and promotion of cancer

It is generally accepted that cancer is caused by gene mutations that enhance the fitness of cancer cells compared to the surrounding normal cells. The mutagenic activity of A3s is a compelling fuel for initiating transformation in healthy cells.

Some studies have observed that A3s are involved in tumor initiation, as their signature is found at early stages in certain tumors (Henderson et al., 2014; Jamal-Hanjani et al., 2017). Some bonafide driver mutations occur in APOBEC signature motifs. For example, the oncogene *PIK3CA* is mutated at high levels. APOBEC activity has been implicated as a key driver of *PIK3CA* mutagenesis by causing TCA to TTA changes that resulted in E542K and E545K driver mutations (Cannataro et al., 2019; Henderson et al., 2014).

Viral infections may trigger or amplify A3 activity, causing genomic damage to the host. Particularly, human papillomavirus (HPV) infections result in up-regulation of A3A and A3B gene expression, and HPV-associated cancers have a high enrichment of the APOBEC signature (Henderson et al., 2014; Mori et al., 2017; Vieira et al., 2014; Warren et al., 2015).

An elegant study showed for the first time the direct relationship between A3 mutagenesis and cancer *in vivo* (Law et al., 2020). They engineered two transgenic mice for the ubiquitous overexpression of A3A and A3B, separately. Unfortunately, as explained before, A3B mice lost A3B expression. Interestingly, A3A overexpression increased tumor formation in Apc^{min} mice and tumors showed clear evidence of APOBEC signatures. Moreover, they tested the oncogenic capacities of each A3 enzyme by hydrodynamic delivery of vectors to mouse hepatocytes. Correlating with their previous results, A3A promoted tumor initiation, although it was not the case for the other 6 deaminases.

In contrast, there is evidence that claims that APOBEC mutagenesis does not promote tumor initiation. Recent studies have demonstrated that in combination with different oncogenes, A3B has a detrimental effect on tumor initiation, delaying tumor appearance (Caswell et al., 2018; DiMarco et al., 2021). Also, A3A deamination in stem-loop structures occurs in passenger genes (Buisson et al., 2019). Importantly, even though tumors contain thousands of APOBEC-like mutations, these are not shared among patients, demonstrating any selective advantage (Nik-Zainal et al., 2016).

3.2.2. Cancer progression, metastasis and resistance

Cancer is an evolving and heterogeneous disease. As cancer progresses, cancer cell subclones acquire unique molecular fingerprints, providing a substrate for selection. Human tumors are exposed to constant pressures and continuously gain *de novo* mutations that promote progression. Tumor heterogeneity is one of the main causes of metastasis and resistance to therapy (Caswell & Swanton, 2017; McGranahan & Swanton, 2017; Turajlic et al., 2019). A3s have been proposed to be major drivers of tumor evolution.

A3B-mediated mutations are enriched for subclonal mutations, suggesting that A3B is a late mutagenesis process generating branched evolution in cancer (Bruin et al., 2014; Jamal-Hanjani et al., 2017; Roper et al., 2019). Tumors promote an inflammatory microenvironment that could trigger the expression of A3A and A3B, placing them at a later stage of cancer development (Leonard et al., 2015; Maruyama et al., 2016). In addition, A3s mutagenesis could trigger a potent anti-tumor immune response by the presentation of neoantigens to the innate immune system, making tumors responsive to immune therapy (S. Wang et al., 2018). However, *in vivo* studies failed to induce A3B at sufficient levels to increase A3B-mediated

mutagenesis and neoantigen presentation (Boumelha et al., 2022; Caswell et al., 2022). Recently, it has been described that APOBEC mutagenesis is not the only factor fueling tumor evolution. A3B and A3A have been proposed to induce DNA damage and chromosomal instability, contributing to tumor heterogeneity (Landry et al., 2011; Venkatesan et al., 2021; Wörmann et al., 2021).

It has been demonstrated that A3B mutagenesis is the seed for targeted therapy failure (Law et al., 2016). Non-responder patients with BRAF V600-mutant melanomas treated with BRAF inhibitors harbored APOBEC-like mutations in MEK1 and MEK2 genes (Allen et al., 2014). Consistent with the potent diversification activity of these enzymes, sequencing data from metastatic tumors showed an increase in APOBEC signature compared to primary tumors (Angus et al., 2019; Bertucci et al., 2019; Roper et al., 2019).

The significance of APOBEC as a continuous mutagenesis process, which contributes to subclonal diversity and intratumor heterogeneity, highlights the need for developing future diagnostic and therapeutic strategies to suppress these enzymes and restrict tumor evolution.

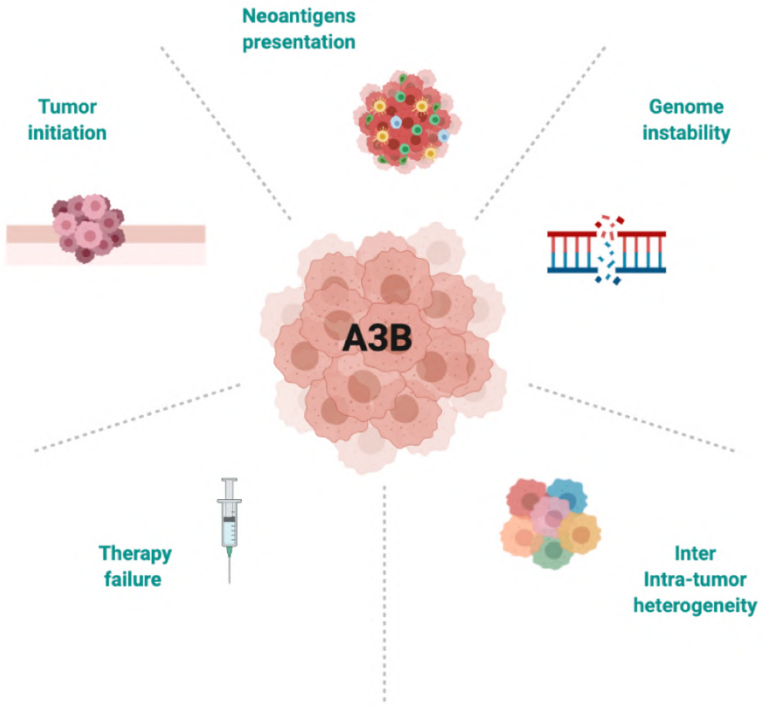

Figure 5: Diverse functions of A3B in cancer

Research is now focus on understanding the contribution of A3B expression in cancer. Some studies claimed a role of A3B in tumor initiation as it signatures has been found in early stages of tumor formation. In addition, the mutagenic activity of this enzyme leads to high levels of inter and intra-tutor heterogeneity, which has been associated with incomplete therapy response or relapse in patients. A3B-induced mutations can give raise to unique proteins that can serve as neoantigens and make cancer cells visible to the immune system, rendering tumors susceptible to immunotherapy. Finally, A3B can induce replication stress and generate single and double-stranded breaks driving chromosomal instability.

3.3. Lung cancer

Lung cancer is the leading cause of cancer-related deaths worldwide, with around 2.2 million new cases in 2022 (Siegel et al., 2022) Lung cancer is classified into two main types: small cell lung cancer (SCLC) and non-small cell lung cancer (NSCLC). Among them, NSCLC accounts for 80% of all lung tumors and is classified into three subtypes: adenocarcinoma, squamous cell carcinoma and large-cell carcinoma (Travis, 2002). Adenocarcinomas represent 40% of the cases, and a large cohort of lung cancer patients is attributed to chronic tobacco exposure. Molecular analyses of these tumors have detected common KRAS activating mutations. The most common mutations in the KRAS gene are a consequence of smoking-induced transversions or transitions that involve substitutions of a glycine residue for a cysteine or an aspartic acid, respectively (G12C or G12D) (Hunter et al., 2015). These mutations dramatically impair the GTPase activity of KRAS and hyperactivate downstream signaling cascades affecting processes such as cell proliferation, migration or differentiation, ultimately promoting tumorigenesis. Moreover, smokers frequently develop more complicated KRAS-mutant tumors, with a larger mutational load and a higher probability of co-occurring mutations in TP53 or STK11 (Ferrer et al., 2018). Alterations in TP53 are found in more than 50% of NSCLCs and are associated with more advanced stages of lung adenocarcinomas.

Several mouse lung cancer models have been generated to study the effects of KRAS (Fisher et al., 2001; Jackson et al., 2001; Johnson et al., 2001; Meuwissen et al., 2001). Human lung adenocarcinomas generally progress to advanced stages of the disease, presenting features such as metastasis, whereas these models only resemble early stages of lung adenocarcinomas. Therefore, to recapitulate all the aspects of human tumors, KRAS mutant models together with TP53 alterations were engineered (Jackson et al., 2005).

Despite significant efforts, NSCLC patients have seen very little clinical benefit from targeted treatments that directly block KRAS-related signaling pathways. However, the development of immunotherapy has shed light on the outcome for these patients. Unfortunately, not all patients respond to these therapies (Drosten & Barbacid, 2022). The use of preclinical models that properly capture the interactions between tumor cells and the immune system is necessary to develop strategies to increase the clinical effects of the existing immunotherapies in NSCLC. Typically, genetically engineered mouse cancer models use a handful of driver genes to induce tumor formation and acquire a few de novo mutations during tumor progression (McFadden et al., 2016). Therefore, these tumors present a low mutational burden with low antigen presentation and weak anti-tumor immune responses, which does not reflect what happens in human tumors.

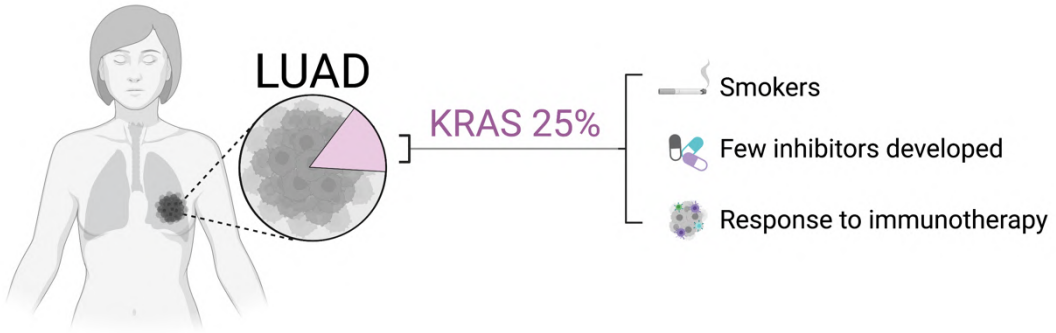

Figure 6: Kras-induced lung adenocarcinomas

Mutations in the *Kras* oncogene account for the 25% of the cases of lung adenocarcinomas. Typically, patients with Kras mutations are smokers. Unfortunately, the number of inhibitors designed to specifically target Kras is limited, and patients with NSCLC have shown little therapeutic benefit. Some patients, however, respond well to immunotherapy.

3.4. A3B in lung cancer

In addition to smoking, the expression of APOBEC enzymes, particularly A3B, has been identified as a prominent source of mutations in NSCLC. Expression analysis of the APOBEC enzymes showed that A3B was upregulated at different stages in lung adenocarcinomas (Venkatesan et al., 2021) and was reported to correlate with poor prognosis in lung cancer patients (H. Zhang et al., 2021). Moreover, it has been demonstrated that the overexpression of oncogenes such as RAS causes an initial hyperproliferation, increasing A3B activity (Kanu et al., 2016).

Much effort has been done to decipher the timing when A3B is expressed and exerts its mutagenic activity. Multiregional sampling of early-stage NSCLCs allowed to examine the mutational events that occurred throughout tumor progression, establishing the temporal dynamics of APOBEC mutational processes. When compared to early clonal truncal mutations, the APOBEC signature was shown to be enriched in the branches of tumor evolutionary trees, affecting driver genes, fueling subclonal evolution and cancer heterogeneity (Bruin et al., 2014; Mcgranahan et al., 2015; J. Zhang et al., 2014). Chromosomal instability is another mechanism promoting cancer variety, and it was recently discovered that A3B drives chromosomal instability through replication stress and chromosome missegregation (Venkatesan et al., 2021). In addition, it has been shown that in lung adenocarcinomas treated with tyrosine kinase inhibitors, A3B is increased, driving aggressive subclonal populations and enhancing tumor resistance to therapy (Caswell et al., 2022). Altogether, these findings imply an essential role for A3B in lung adenocarcinoma progression.

Tumor heterogeneity induced by A3B activity, converts this enzyme into a druggable target for achieving more sustained therapeutic responses. It was hypothesized that A3B inhibition might slow down cancer progression, yet there are no existing drugs that inhibit A3B

expression or activity (Grillo et al., 2022). Immunotherapy is a potential treatment for patients with NSCLC; however, it is not yet known which patients will be responsive to checkpoint blockade inhibitors. A3B expression has been shown to correlate with immunotherapy response biomarker expression and therapy response in NSCLC patients. Moreover, the mutational signature of APOBEC is enriched in patients who have a sustained therapeutic response after immunotherapy (S. Wang et al., 2018). It is believed that APOBEC-induced mutations create neoantigens that trigger potent immune responses (Driscoll et al., 2020). However, another study showed that tumor cell lines expressing A3B and carrying subclonal APOBEC-induced mutations were not immunogenic and did not respond to immunotherapy (Boumelha et al., 2022). Therefore, the impact of A3B expression in NSCLC should continue to be investigated.

4. RNA Editing

The assumption that genetic information directly predicts gene products has been widely accepted. However, in eukaryotic cells the number of coding sequences in the genome does not account for the composition and complexity of the proteasome. Because of this, the genetic code had to be rewritten and the central dogma had to be changed. Now is clear that protein diversity can be produced by a combination of post-transcriptional and post-translational modification mechanisms. Within the post-transcriptional modifications, changes at the RNA level, such as alternative splicing or polyadenylation, can recode the genome.

Recently, epitranscriptomics has emerged as an important field in research. It involves the enzymatic modification of RNA molecules at a single-base level, such as RNA editing (Kumar & Mohapatra, 2021). RNA editing is defined as a co- or post-transcriptional modification that involves the deamination reaction that converts cytosine to uracil (C-to-U) or adenosine to inosine (A-to-I). The APOBEC family is in charge of C-to-U alterations, whereas the adenosine deaminases (ADAR) family is responsible for A-to-I changes. RNA editing could result in a variety of functional effects, for example, affecting mRNA localization or stability. In addition, edited microRNAs (miRNA) and miRNA binding sites could influence gene expression and mRNA abundance. Another example is the modification of splicing sites that could result in the synthesis of alternative proteins. Furthermore, if the editing happens in coding regions, an alternative protein could be formed (Christofi & Zaravinos, 2019).

4.1. A-to-I editing

Millions of editing sites have been found in humans, being the most prevalent type of RNA editing in mammals A-to-I. This editing is performed by the ADAR family of deaminases, which

consists of three members: ADAR1 (which has two isoforms, ADAR1p150 and ADAR1p110), ADAR2 and ADAR3. While ADAR1 and 2 have been demonstrated to be catalytically active, ADAR3, which is only found in the brain, has no deaminase activity and is thought to operate as a negative regulator of ADAR1 and ADAR2 mediated editing (CHEN et al., 2000; Oakes et al., 2017). Both ADAR1 and ADAR2 are ubiquitously expressed, although ADAR1 is expressed more robustly and is mainly responsible for the editing activity. ADAR2 and ADAR1p100 are localized in the nucleus, whereas the IFN-inducible ADAR1p150 isoform shuttles between the nucleus and the cytoplasm (Eisenberg & Levanon, 2018). Recent work suggests that the interplay between RNA editing and DNA mutagenesis might be shared among several deaminases and that ADARs could also act at the DNA level (Tasakis et al., 2020).

ADAR enzymes convert adenosines to inosines (I), which the translational machinery recognizes as guanines, resulting in A-to-G transversions (Nishikura, 2016). ADARs deamination activity requires the identification and binding of double-stranded RNAs (dsRNAs) with a hairpin-loop secondary structure. A-to-I RNA editing does not require an exact sequence; however, it has been shown that ADARs prefer to edit adenines adjacent to a 5′ uridine and a 3′ guanosine (UAG). The majority of ADAR targets are found in non-coding regions such as the 3'- and 5'-UTRs of mRNAs and introns. Interestingly, Alu repetitive elements are the most common targets of A-to-I RNA editing, and a small percentage of ADAR editing sites have been identified in coding regions.

The first A-to-I RNA editing site was identified in the subunit of the glutamate receptor (GRIA2), which is crucial for proper neurotransmission (Higuchi et al., 1993). ADAR affects the translation of the protein by acting on the coding sequence of GRIA2 mRNA. As a consequence, the conversion of glutamine to arginine alters the function of neurotransmitter receptors. In fact, mice lacking ADAR2 die several weeks after birth due to epileptic episodes (Higuchi et al., 2000). ADARs seem to play a significant role in the innate defense system. Through editing, ADARs prevent endogenous dsRNAs from being recognized as foreign (like viral dsRNA) and block the activation of the interferon signaling pathway. As expected, ADAR1 null mice are embryonic-lethal, displaying an aberrant activation of interferon signaling (Liddicoat et al., 2015; Mannion et al., 2014).

4.2. C-to-U editing

The APOBEC family is responsible for the second type of RNA editing, which involves the deamination of cytidines to uracils. While APOBEC mutagenesis has been widely studied, C-to-U editing has been investigated to a lesser extent. Moreover, only a few members of the family have been identified as RNA editors. The ApoB mRNA is the first C-to-U editing

described in the literature. ApoB mRNA is deaminated at cytidine 6666, which converts a glutamine codon into a stop codon and results in a shorter and truncated isoform, ApoB48 (Powell et al., 1987). Some years later, APOBEC1 was shown to be responsible for the editing of ApoB mRNA (Teng et al., 1993).

ApoB editing was used as a model system to study the requirements for C-to-U editing. APOBEC1 deaminates single-stranded RNAs (ssRNA) and it is regulated by several trans and cis-activating factors. A deep examination of the regions flanking the edited cytosine demonstrated the preference for AU-rich sequences. ApoB editing also requires the formation of the editosome, a multiprotein complex that involves the binding of APOBEC1 with APOBEC1 complementation factor (A1CF) and RNA-binding motif protein 47 (RBM47). Both cofactors are essential in recognizing the targeted sequences. In particular, ACF binds an 11-nucleotide mooring sequence several bases downstream of the edited cytidine in apoB mRNA. Similar to ADARs, the majority of editing occurs in non-coding regions, mainly 3'UTRs and Alu elements. Although ApoB editing is the APOBEC1 target that has been better studied, other novel murine transcripts have been identified (Rosenberg et al., 2011; Soleymanjahi et al., 2021).

The second RNA editor identified was A3A, which had previously been proven to deaminate ssDNA. In line with the expression of A3A in monocytes, it has been shown that in hypoxic conditions and in response to interferon stimulation, A3A is upregulated and is responsible for increased RNA editing in macrophages (Sharma et al., 2015). A3A activity on RNA has also been connected to a physiological function, since A3A editing is essential for the polarization of M1 macrophages (Alqassim et al., 2021). Furthermore, overexpression of A3A in non-immune cells, such as HEK293T cells, led to editing in a significant number of genes, which might be connected to various diseases (Sharma, Patnaik, Kemer, et al., 2016). Importantly, a recent study showed that human cancers with high levels of A3A also have a high fraction of altered transcripts (Jalili et al., 2020). Similar to A3A's preferences in DNA substrates, biochemical analysis has shown that A3A also deaminates 4 nucleotides in stem-loop RNA structures. However, while in the DNA stem loops the TpC motif is usually preceded by C or T in the RNA there is an A or U before the UpC motif (Jalili et al., 2020; Sharma & Baysal, 2017). Uncertainty surrounds the substrate selectivity of A3A, however, recent research revealed that while DNA deamination is favored and more adaptable, RNA editing is reduced because the substrate features required for editing are stricter (Barka et al., 2022).

RNA editing by A3G has been poorly described, and it was first shown in HEK293T cells (Sharma, Patnaik, Taggart, et al., 2016). Later, the same group found that natural killer (NK) cells and lymphocytes had increased RNA editing in response to mitochondrial stress (Sharma

et al., 2019). Like A3A, A3G has also been described to target stem-loop RNA structures (Sharma & Baysal, 2017).

Due to the high homology between the APOBEC3 enzymes, RNA editing activity by other family members may have been overlooked. Research must focus on gaining a deeper understanding of the range of C-to-U editing targets, the underlying enzymes and the mechanism.

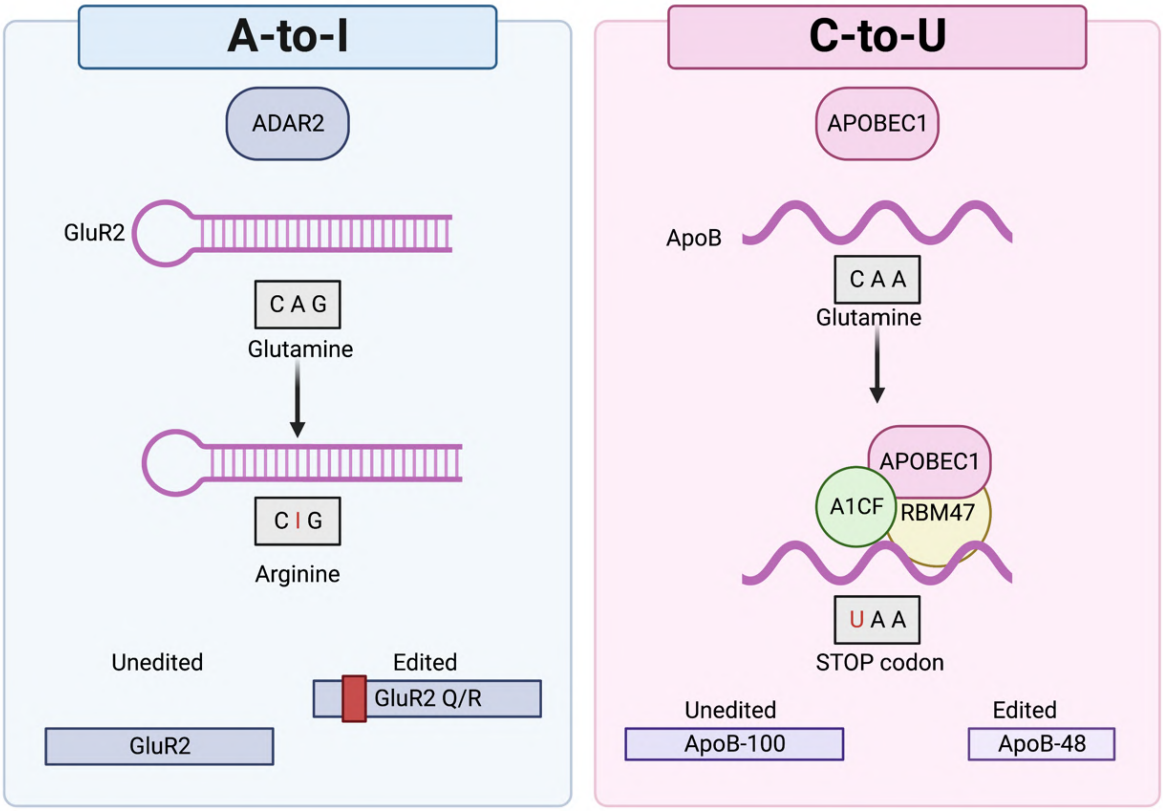

Figure 7: Types of RNA editing

Cartoon representing the two types of RNA editing in mammals (A-to-I and C-to-U). RNA editing examples of the main targets for APOBEC1 (ApoB) and ADAR2 (GluR2) enzymes.

4.3. Unconventional RNA editing

Several forms of unconventional editing, including G-to-A and U-to-C modifications, have been described in B lymphocytes, complicating the editing paradigm (M. Li et al., 2011). In computational analyses, these non-classical mutations are often ignored or ascribed to misalignment with the opposite strand. Due to the absence of a recognized chemical mechanism responsible for these non-classic alterations, the nature of such editing remains unknown. Researchers hypothesize that APOBEC enzymes may be responsible for this type of editing. Unconventional G-to-A RNA edits were identified in the mRNA of Wilms Tumor 1

(WT1) and promote tumorigenesis. RNA interference and overexpression experiments identified A3A as responsible for WT1 editing (Niavarani et al., 2015).

4.4. RNA editing in disease and cancer

The impact of aberrant RNA editing may be comparable to that of diseases caused by mutations in the genome. RNA editing is a tightly regulated process; however, uncontrolled enzyme expression or activity and changes in substrate availability may be important elements in the development of pathologies. Interestingly, it has been shown that the effect of editing on proteome diversity is comparable to, or even greater than, that of somatic mutations (Peng et al., 2018). Even though the majority of targets occur in non-coding regions and have no impact, these modifications may trigger novel splicing sites or alter microRNAs activity. However, certain alterations result in non-synonymous mutations. Some of these alterations have been reported to play crucial roles in carcinogenesis by generating inactive or active proteins, such as tumor suppressors and oncogenes, respectively. Moreover, RNA-edited products could be a source of neoantigens that trigger immune system activation (Roth et al., 2018). Importantly, RNA molecules are volatile and the alterations create temporal diversity that leaves no trace in the genome. Unlike DNA mutations, deleterious edits will not be transmitted to the daughter cells, facilitating a fine balance and improving fitness.

Mutations that impair the editing function of ADARs are implicated in a number of syndromes, including metabolic and brain disorders and skin lesions. It has also been shown that overexpression of ADARs is linked to the development of cancer (Baysal et al., 2017; Kung et al., 2018; Kurkowiak et al., 2021). Their implication in cancer has been associated mainly with specific editing sites. For example, the edited isoform of antienzyme inhibitor 1 (AZIN1) promotes cell proliferation and is increased in hepatocellular carcinoma (L. Chen et al., 2013). In addition, several publications have shown the widespread consequences of RNA editing by ADARs in human cancer (Fumagalli et al., 2015; Han et al., 2015; Paz-Yaacov et al., 2015). ADAR1 seems to be the most relevant member since its expression is changed in several tumor types. For instance, activation of the IFN pathway and subsequent overexpression of the ADAR1p150 isoform, promotes chronic myeloid leukemia by driving hematopoietic differentiation towards the myeloid lineage. (Jiang et al., 2021). In addition, ADAR1 deletion in breast cancer cells led to a reduction in proliferation and an increase in apoptosis (Fumagalli et al., 2015).

APOBEC1 is responsible for ApoB editing, a protein crucial in the transport of lipids in the blood and incorrect editing increases the risk of cardiovascular disease (Powell-Braxton et al., 1998; Xie et al., 2007). In addition, some studies have linked APOBEC1 RNA editing activity

with cancer. Similar to its capacity to modify the ApoB transcript, APOBEC1 also targets the tumor suppressor neurofibromin 1 mRNA (NF1), which controls the inhibition of the RAS/MAPK pathway. In neuronal tumors, APOBEC1 produces a stop codon that results in a truncated and inactive form of the NF1 protein (Cappione et al., 1997; Mukhopadhyay et al., 2002; Skuse et al., 1996). In addition, transgenic mice overexpressing APOBEC1 developed liver tumors and showed hyperediting of NAT1 mRNA which regulates the expression of p21 (Yamanaka et al., 1997). However, whether there is a direct relationship between APOBEC1 editing and cancer development remains unclear. Insights from animal models with APOBEC1 loss and gain of function linked RNA editing to cancer development. For instance, Apobec1 overexpression in transgenic mice and rabbits led to hepatocellular carcinomas showing hyperediting at different locations than the conventional one on the ApoB mRNA, indicating that elevated levels of APOBEC1 cause loss of editing fidelity (Yamanaka et al., 1995). Loss of mouse Apobec1, and hence lack of editing, has shown a decrease in tumor development (Blanc et al., 2007; Nelson et al., 2012). A more recent study linked APOBEC1 mutagenic activity with the onset of esophageal cancer (Saraconi et al., 2014). Therefore, whether APOBEC1 RNA editing or DNA mutagenic activity is connected to cancer is still not clear.

Even though A3A and A3G have been characterized as RNA editing enzymes, the relationship between their editing activity and pathology is poorly understood. Analysis of mRNA data from breast cancer tumors identified RNA modifications at previously described known APOBEC3 RNA editing sites (Asaoka et al., 2019). However, the editing events were not attributed to any APOBEC3 member in particular. In another study, A3A-signature was detected in different types of human tumors that expressed high levels of A3A (Jalili et al., 2020). However, the functional importance of A3A-mediated RNA editing in cancer cells remains unknown. This research also confirmed that even though there are mutational footprints in the genome, these mutations do not always correspond directly with the enzymes' ongoing activity. On the contrary, RNA edits correlated with A3A expression. This demonstrated that RNA editing is a dynamic process that can only be observed if the responsible enzyme is expressed. Therefore, RNA editing could be potentially employed as a reporter of A3A expression and activity.

5. APOBEC deaminase independent functions

The only well-described function of the APOBEC family is deamination of DNA and RNA substrates. It is unclear whether they participate in additional mechanisms that do not need deaminase activity. Several studies have reported deaminase-independent mechanisms of the APOBECs in viral restriction. Moreover, APOBECs have been described to inhibit

retrotransposons activity and alter microRNA activity, although the mechanism is still unknown. Reviewed in: (Hakata & Miyazawa, 2020)

In cancer, A3B influences tumor development through independent deaminase activity (Ma et al., 2019). It has been shown that A3B drives epigenetic modifications in the trimethylation at the 27th lysine residue of the histone H3 protein (H3K27me3), leading to aberrant chemokine expression and cancer progression (Ma et al., 2019; D. Wang et al., 2019). Similarly, A3A has been connected to epigenetic reprogramming; however, it is not yet known if this is related to its deaminase activity (DeWeerd et al., 2022). In addition, a recent study demonstrated that A3A expression, independently of its deaminase activity, can induce replication stress and DNA damage, resulting in chromosomal instability and activation of the DNA sensing program cGAS–STING (Wörmann et al., 2021).

Therefore, a thorough understanding of the molecular processes underlying these deaminase-independent actions will be crucial for viral disease and cancer research.

AIM OF THE THESIS

Since the discovery and characterization of the APOBECs, their role in cancer has been studied in great detail. In particular, recent studies on A3B have generated new insights into how A3B mutagenesis fuels tumor evolution. De novo genetic alterations such as DNA mutations, chromosomal instability and other mechanisms like RNA editing, can all induce tumor heterogeneity. However, the processes by which A3B causes the development of tumors remain poorly understood, and A3B's potential role as an RNA editing enzyme has not yet been studied. Thus, this thesis aims to:

- Investigate the possible role of A3B in tumor initiation by overexpressing the human A3B in a doxycycline-inducible mouse model.
- Study the contribution of A3B in tumor development, treatment resistance and recurrence in different KRAS-driven lung adenocarcinoma mouse models.
- Uncover whether A3B can function as an RNA editing enzyme promoting diversity.

Results

1. Deciphering the role of A3B in tumor initiation progression and resistance

Some of the findings presented in this part of the thesis are now being submitted for publication in the manuscript (Vega et al., 2022). Parts of the text, figures, and figure legends were adapted from the mentioned manuscript, which I co-wrote (see author contributions for more details).

1.1. Generation of a doxycycline-inducible mouse model for human APOBEC3B

Numerous studies have tried to investigate the role of A3B in carcinogenesis by *in vitro* experiments and computational analyses, all of which lack the influence of the immune system. Recently, Reuben Harris developed an A3B mouse model which constitutively overexpressed the human A3B, but did not achieve sustained and high levels of expression (Caswell et al., 2022). Therefore, in our lab, we sought to generate a new mouse model to achieve stronger A3B levels.

To study the effects of A3B activity *in vivo*, Kalman Somogyi created a construct fusing the cDNA of the human APOBEC3B to turboGFP, used as a reporter (thereafter A3B). Rocio Sotillo and Lorena Salgueiro electroporated the A3B vector into the *Collagenase I* locus (ColA1) of KH2 mouse embryonic stem cells (ES cells) (Beard et al., 2006a), which contain the rtTA in the *Rosa26* locus. A3B expression is regulated by a tetracycline-inducible operator (tetO) sequence which is induced by the tetracycline-dependent activation of the reverse tetracycline transactivator (rtTA) (Figure 8A). Doxycycline treatment (tetracycline analog) of

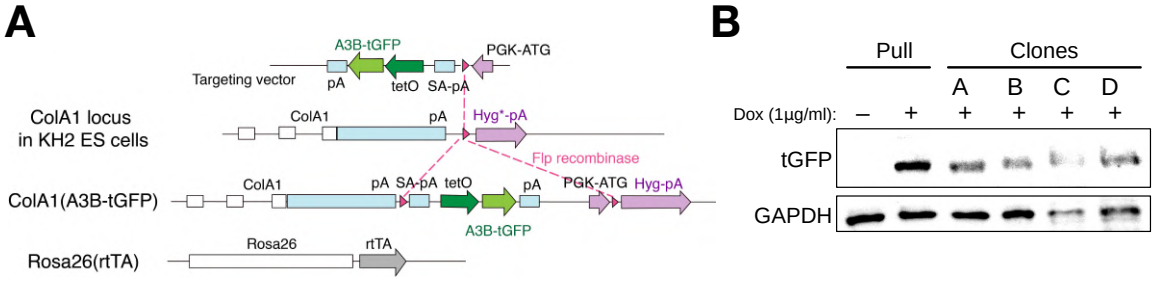

Figure 8: Generation of A3B/Rosa26-rtTA ES cells

(**A**) Scheme of the cloning strategy used to insert the human APOBEC3B cDNA in the *Collagenase I* locus of KH2 ES cells carrying the *Rosa26-rtTA* tetracycline transactivator. (**B**) Immunoblot showing A3B-tGFP levels of the different ES clones (A, B, C and D) treated with doxycycline (Dox) that were later used to generate the *TetO-A3B-tGFP/Rosa26-rtTA* transgenic mice. GAPDH was used as loading control.

different ES cell clones led to the expression of A3B (Figure 8B). The DKFZ transgenic animal facility generated knockin mice after microinjection of these ES cells into developing morulas.

1.2. Overexpression of A3B does not affect proliferation and oncogenic transformation *in vitro*

Mouse embryonic fibroblasts (MEFs) provide a system to answer mechanistic questions that can help the validation of *in vivo* phenotypes. I generated MEFs from *A3B/Rosa26-rtTA* mice to initially evaluate the effects of A3B overexpression *in vitro*. The induction of the A3B transgene was confirmed by performing western blot against tGFP after treatment with doxycycline for 24h (Figure 9A). While MEFs treated with doxycycline had increased A3B mRNA levels, the same MEFs without doxycycline had undetectable A3B expression, suggesting that transgene expression was not leaky (Figure 9B). Cell growth was monitored for 6 days and overexpression of A3B in primary MEFs led to no changes in proliferation (Figure 9C). As A3B has been described to be detrimental to tumor initiation (Caswell et al., 2022; DiMarco et al., 2021), we transformed primary MEFs with oncogenic HrasV12 and E1A.

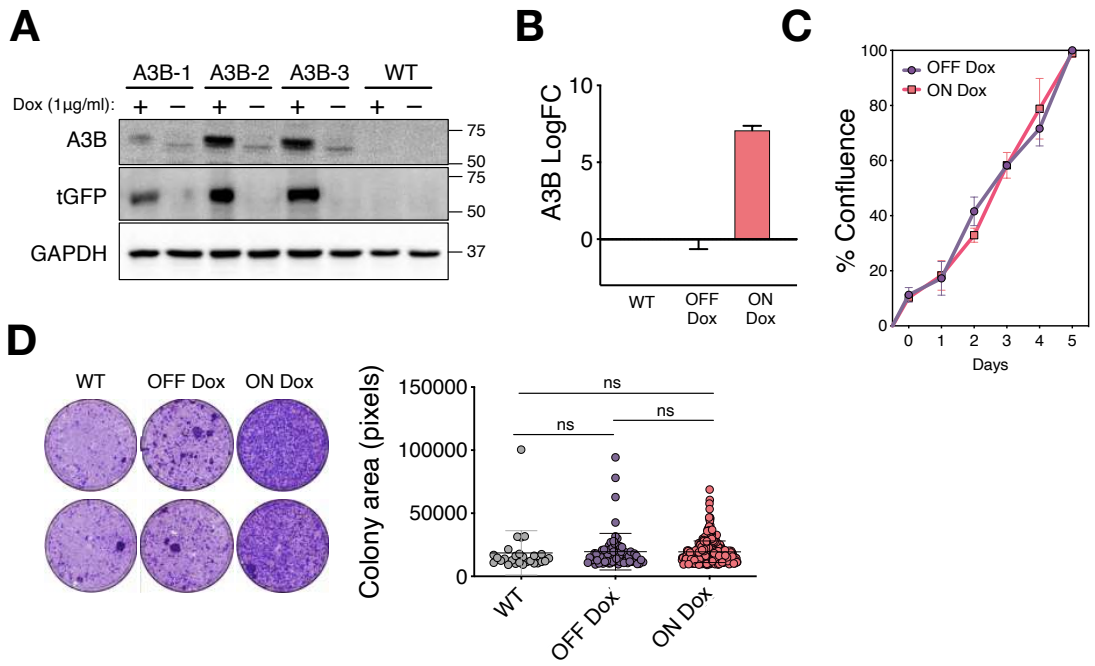

Figure 9: Effects of A3B overexpression in vitro

(**A**) Immunoblot showing A3B and tGFP levels in *(+/A3B);(+/rtTA)* and wildtype (WT) mouse embryonic fibroblasts (MEFs) obtained from the *TetO-A3B-tGFP/Rosa26-rtTA* transgenic mice treated with (+) and without (-) Dox. GAPDH was used as loading control. (**B**) Quantitative RT-PCR of A3B expression levels in *(+/A3B);(+/rtTA)* and WT MEFs with (+) and without Dox (-). 18S and Actin were used as house keeping genes for normalization. Data are expressed as means ± SD (**C**) Proliferation assay of *(+/A3B);(+/rtTA)* MEFs in the presence (+) and absence (-) of Dox. Data are expressed as means ± SD. All time points are not statistically significant; Two-way anova (**D**) Colony formation assays of *(+/A3B);(+/rtTA)* and WT MEFs transfected with oncogenic HrasV12 and E1A in the presence (+) or absence (–) of Dox. Colony area (in pixels) is quantified in the right plot. Each dot represents one colony. Data are expressed as means ± SD. One-way anova; ns, not significant;

A3B overexpression induced by doxycycline in transformed MEFs led to no significant differences in the area of colonies formed (Figure 9D). However, A3B overexpressing MEFs seemed to slightly increase the number of transformed foci, suggesting that A3B overexpression may promote oncogenic transformation *in vitro*.

1.3. *A3B/Rosa26-rtTA* mice show weak A3B levels

Once the A3B transgenic mice were born, I did an initial characterization to check the expression and functionality of the A3B transgene. The *Rosa26* promoter is ubiquitously expressed and drives A3B expression in the whole body of the mice. To check differences in A3B levels between organs, mice were fed doxycycline-containing food for 15 days. Most of the tissues showed weak A3B levels except for the intestine (Figures 10A and B). Similarly, high deaminase activity was detected in the intestine of these mice (Figure 10C). This data goes in line with studies showing that the *Rosa26* promoter has variable activity in different mouse tissues (Dow et al., 2014).

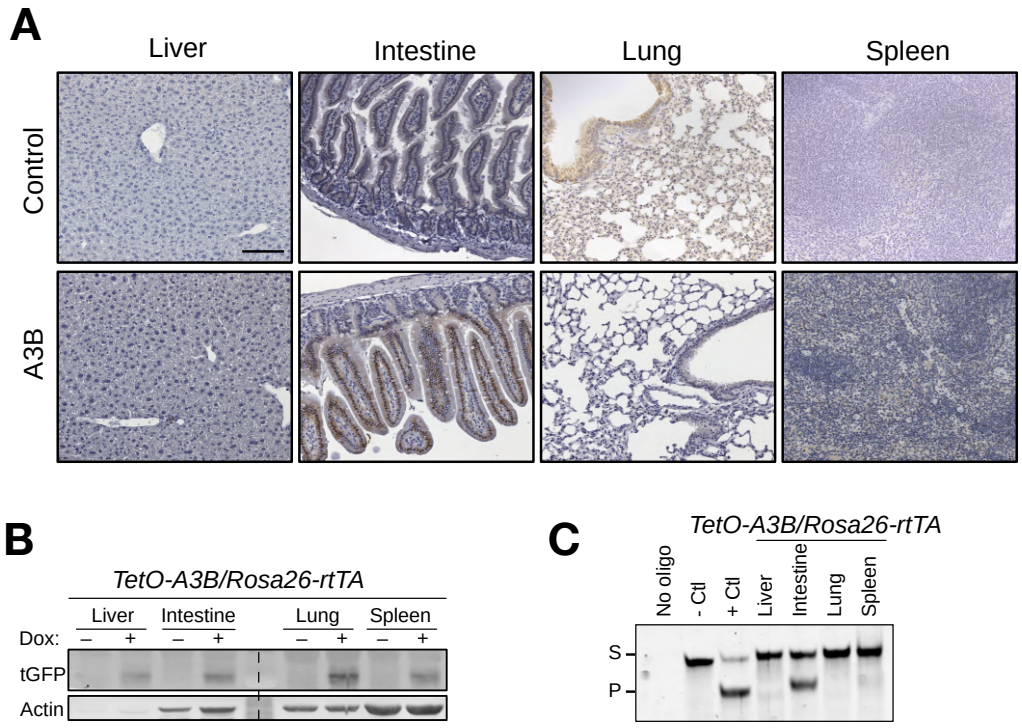

Figure 10: A3B expression and activity in Teto-A3B/Rosa26-rtTA mice

(**A**) Immunohistochemistry of A3B in the indicated tissues from *TetO-A3B/Rosa26-rtTA* and control mice fed with doxycycline (Dox) for 15 days. Scale bar: 100 µm. (**B**) Immunoblot showing A3B-tGFP levels in the indicated tissues from *(+/A3B);(+/rtTA)* mice fed with (+) and without (-) Dox for 15 days. Actin was used as loading control. (**C**) Deamination activity assay in the indicated tissues from *(+/A3B);(+/rtTA)* mice fed with Dox for 15 days. (S, Substrate; P, Product).

1.4. A3B promotes tumorigenesis *in vivo*

In order to detect spontaneous tumor formation, I fed *A3B/Rosa26-rtTA* mice with doxycycline containing food for an average of 460 days. 83% of A3B-overexpressing mice presented tumors compared to 20% in the control group (Figure 11A). Histopathological analysis of these mice showed a wide spectrum of tumors, including lung adenocarcinoma, uterus malignant tumors, lipomas, seminomas and lymphomas (Figure 11B and C upper panel). I next performed immunostaining in tumor and tissue sections. Surprisingly, I found weak or no expression of A3B inside the tumors (Figure 11C lower panel), suggesting that either low levels of A3B alone could promote tumor formation, or that these spontaneous tumors were a result of aging. My results are in line with the data obtained by Reuben Harris lab (manuscript under preparation), where low levels of A3B in mice, using a Cre-inducible model, result in an increase in tumorigenesis. Altogether, there is strong evidence that low levels of A3B promote tumor formation.

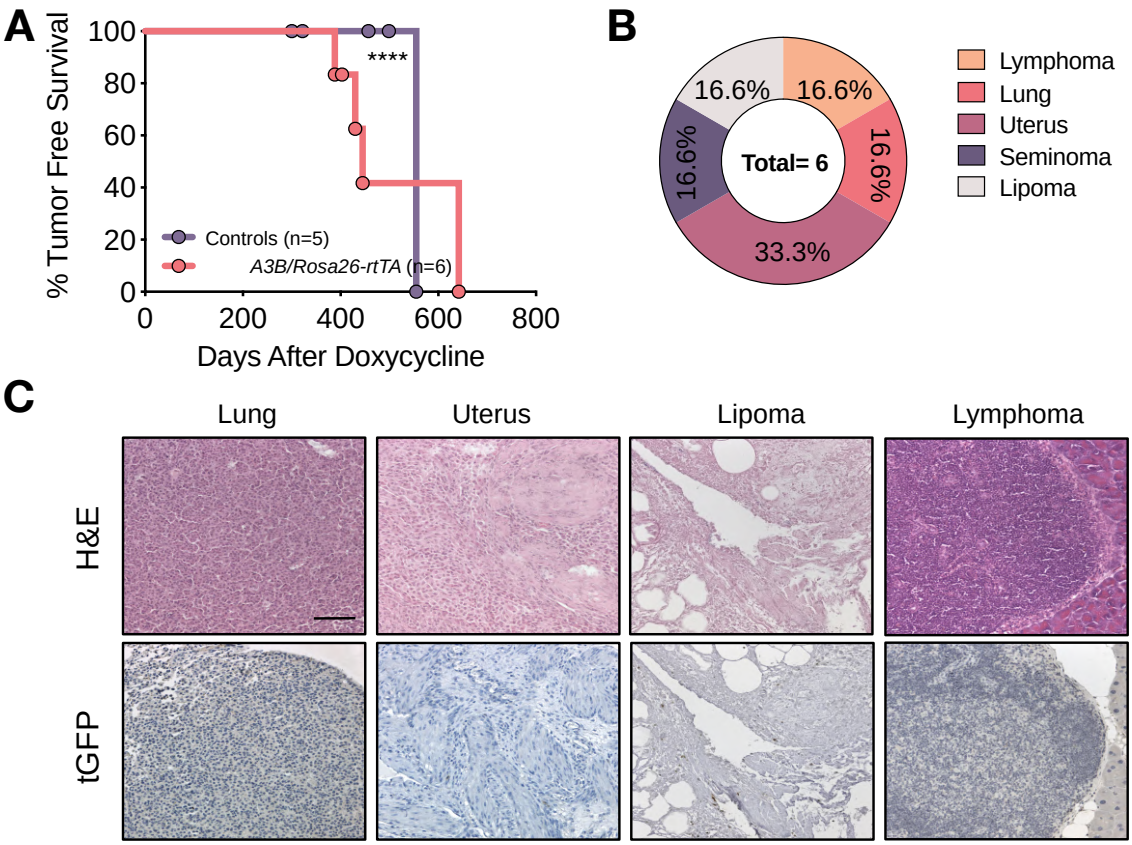

Figure 11: Low levels of A3B promote tumorigenesis in A3B/Rosa26-rtTA mice

(**A**) Tumor free survival from *A3B/Rosa26-rtTA* (n=6) and control mice (n=5) fed with doxycycline (Dox) 1-2 years after birth. ****p < 0.0001; Log-rank (Mantel-Cox) test. (**B**) Pie chart showing the percentage of each tumor type found in *A3B/Rosa26-rtTA* mice (n=5/6). (**C**) Upper panel hematoxylin and eosin (H&E) stainings from the tumors found in *A3B/Rosa26-rtTA* mice. Lower panel: inmunohistochemestry against A3B-tGFP in *A3B/Rosa26-rtTA* tumors. Scale bar: 100 µm.

1.5. A3B does not cooperate with *Kras* in promoting lung adenocarcinomas

It has been widely reported that A3B is upregulated in lung cancer correlating with poor patient outcome (Venkatesan et al., 2021; Yan et al., 2016). A recent publication combined a *Kras* mutant;*p53* deficient lung cancer model with the overexpression of A3B to generate immunogenic mice (Boumelha et al., 2022). Nonetheless, the expression of A3B and more importantly, its mutagenic activity *in vivo* did not reach sufficient levels to induce a dramatic change in their phenotype.

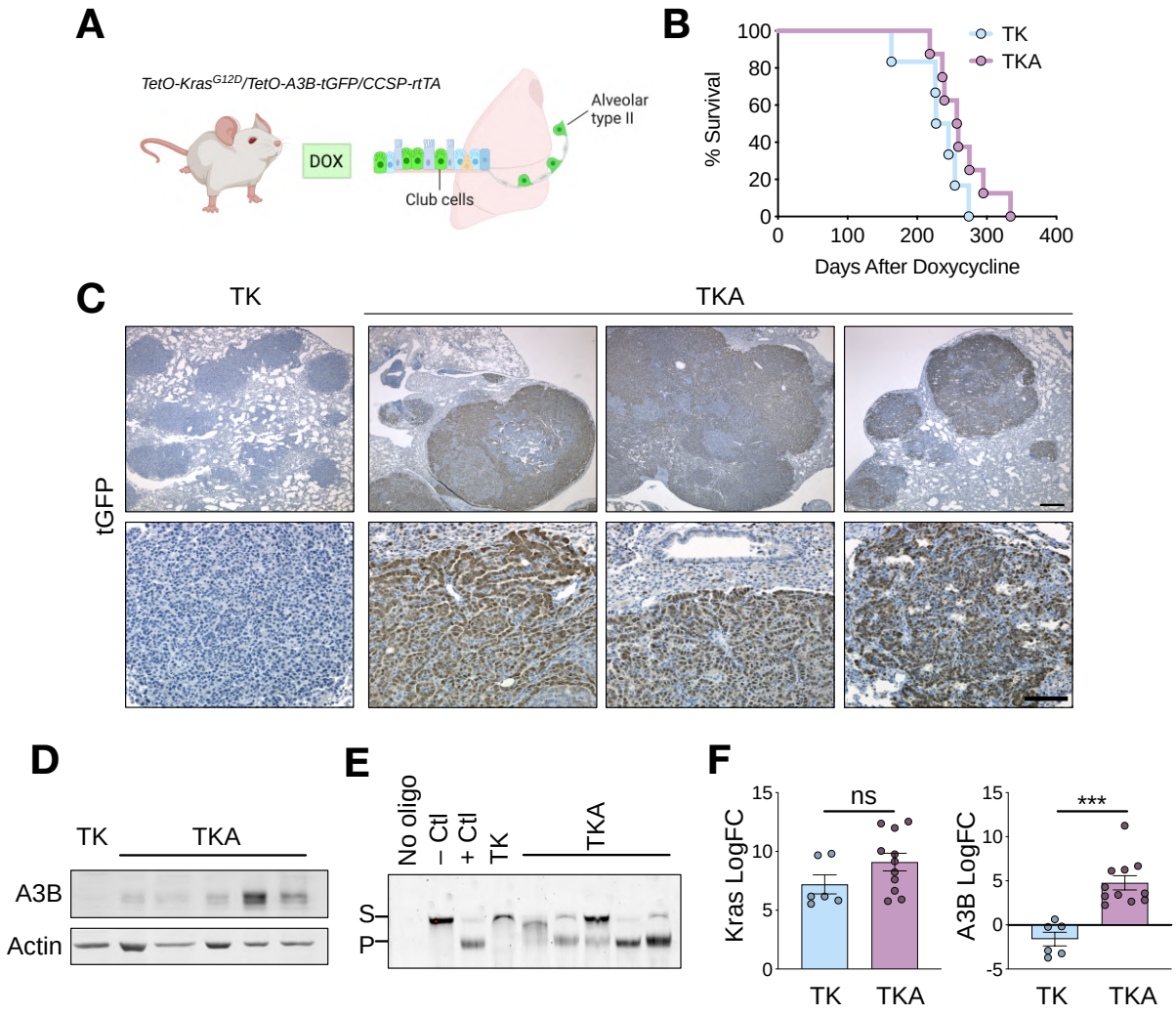

Figure 12: High expression of A3B in Kras-induced lung tumors does not affect survival

(**A**) Scheme of A3B expression in *TetO-Kras^{G12D}/TetO-A3B-tGFP/CCSP-rtTA* mice. The CCSP promoter drives A3B expression in club cells and alveolar type II cells in the lung. (**B**) Percentage of survival of *TetO-Kras/CCSP-rtTA* (TK) and *TetO-Kras/TetO-A3B/CCSP-rtTA* (TKA) after doxycycline (Dox) administration. (TK, n = 7; TKA, n = 8). (**C**) Immunohistochemistry of tGFP in end point tumors from TK and TKA mice Scale bar: upper panels 500 µm; lower panels 100 µm. (**D**) Immunoblot showing A3B levels in single tumor nodules from TK and TKA mice. Actin was used as loading control. (**E**) Deamination activity assay in single tumor nodules from TK and TKA mice (S, Substrate; P, Product). (**F**) Quantitative RT-PCR of Kras and A3B expression levels in single tumor nodules from TK and TKA mice. 18S and Actin were used as house keeping genes for normalization. Data are expressed as means ± SEM. Each dot represents a single nodule. Unpaired t-test; ns not significant; *p<0.001

Previous research in our laboratory showed that doxycycline-inducible mouse models under the clara cell secretory protein promoter (CCSP) result in robust transgene expression (Sotillo et al., 2010). Under this light, I made use of a well-described doxycycline-inducible *Kras* lung cancer model: *TetO-Kras*^{G12D}*/CCSP-rtTA* (TK) in combination with the doxycycline model for human A3B (TKA). In this model, the *Kras*^{G12D} transgene is driven by the *CCSP* promoter that restricts its expression to club and alveolar type II cells in the lung, resulting in the development of LUAD (Fisher et al., 2001) (Figure 12A). Lung tumors were induced by placing mice on a doxycycline-enriched diet and followed for tumor development. Simultaneous overexpression of *Kras*^{G12D} and A3B did not reflect any effect on mouse survival (Figure 12B) even if the expression of A3B in endpoint tumors was strong (Figure 12C and D). Similarly, the majority of single nodules isolated from lung-bearing mice showed high deaminase levels (Figure 12E). In addition, A3B and Kras mRNA expression was also confirmed by quantitative real-time PCR (Figure 12F).

1.6. A3B expression promotes malignant progression of *Kras*-induced lung adenocarcinomas

Several studies have identified alveolar type II pneumocytes and club cells to be the cells of origin in *Kras*-induced lung tumors. Histological analysis of TK and TKA tumors identified malignant cells positive for surfactant protein C (SPC) and club cell protein (CC10), which are markers of alveolar type II and club cells, respectively (Figure 13A). These results indicate that both cell types are the cell of origin in TKA tumors. However, I found that not all TKA tumors were positive for SPC, indicating that these tumors may have lost SPC expression as they progressed.

It has been reported that *Kras*^{G12D} drives lung adenocarcinomas with low aggressiveness (Fisher et al., 2001). Expression of mutant *Kras* in combination with simultaneous loss of *Lkb1* markedly accelerated lung tumor growth with more aggressive and diverse phenotypic features, including squamous cell carcinoma and large cell carcinomas (Ji et al., 2007). Therefore, it is important to determine whether A3B cooperates with *Kras* in inducing more aggressive tumors. Histological analysis of thyroid transcription factor-1 (TTF1) and cytokeratin 5 (CK5) markers for adeno and squamous carcinomas, respectively, showed that while CK5 expression was low, TTF1 was strongly expressed in all TK and TKA tumors (Figure 13A). These results indicate that A3B expression results in lung adenocarcinomas and does not enhance aggressive phenotypes in *Kras* tumors, such as squamous lung carcinomas. (Figure 13A).

Another strategy for ranging tumor progression of lung adenocarcinomas is to classify tumors according to a well-differentiated stage to advance highly dysplastic lesions (Jackson et al., 2001). Low-grade (1-3) tumors, typically exhibit a papillary architecture and can be classified in: grade 1 with cells showing uniform nuclei; grade 2 presenting cells with enlarged nuclei and prominent nucleoli; grade 3 cells containing enlarged and pleomorphic nuclei. More advance tumors such as grade 4 have cells with very large pleomorphic nuclei, nuclear atypia,

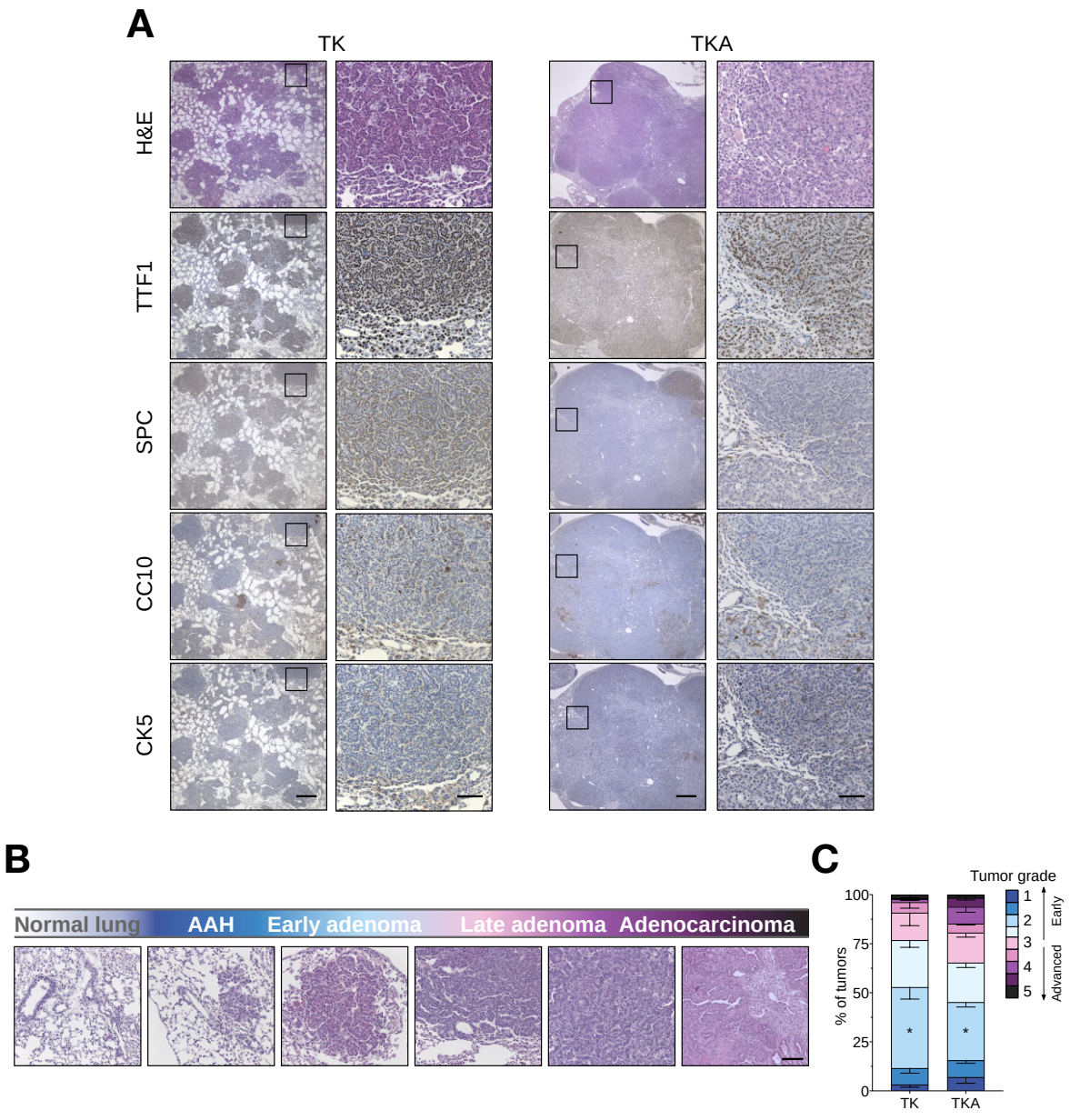

Figure 13: High expression of A3B results in more aggressive Kras-induced lung tumors

(**A**) Hematoxylin eosin stainings and immunostainings of end point tumors from TK and TKA mice fed with Dox. TTF1 marker of lung adenocarcinomas; SPC marker of alveolar type II cells; CC10 marker of club cells; CK5 marker of squamous lung adenocarcinomas. Scale bar magnification 500 µm and closer magnification 100 µm. (**B**) Representative images of the progression of TK lung tumors from early well differentiated atypical adenomous hyperplasias (AAH) and adenomas (Grades 1 and 2) to poorly differentiated adenocarcinomas (Grades 4 and 5). Scale bar, 100 µm. (**C**) Quantification of the percentage of tumors representative of each tumor grade from most differentiated to least differentiated. (TK n=5; TKA n=7). Data are expressed as means ± SEM. Two-way anova, * $p \leq 0.05$.

abnormal mitoses, hyperchromatism and multinucleated giant cells. Finally, grade 5 shows the same features as grade 4 plus stromal desmoplasia (Figure 13B) (Jackson et al., 2005). As previously reported, *Kras* tumors did not develop to aggressive tumors. However, A3B expression in *Kras* lung tumors significantly decreased the number of low-grade tumors and increased the number of advanced and non-differentiated tumors (Figure 13C).

Altogether, these findings suggest that combined lung-specific A3B and *Kras* overexpression leads to the formation of lung adenocarcinomas that are more aggressive than those seen in *Kras* alone tumors.

1.7. A3B expression increases tumor burden in Kras-induced lung tumors

As described above, I found no differences in the overall survival between TK and TKA mice; nevertheless, macroscopically, there were significant differences in tumor burden between the two groups. Whereas TK mice showed multiple and small tumors, TKA mice had fewer but larger tumors (Figure 14A). When lung sections were examined, the overall tumor area was significantly increased in TKA mice compared to TK animals (Figure 14B). Supporting my initial macroscopic findings, the number of nodules per animal in TK mice was much greater than in TKA mice (Figure 14C), although TKA nodules were bigger (Figure 14D). Therefore, TKA mice had increased tumor area due to the size and not to the number of tumors. Taken together, it is tempting to speculate that elevated A3B levels might be detrimental during tumor initiation. Initially, A3B overexpression could cause excessive damage and cell death resulting in fewer cells that get transformed. At later time points, once

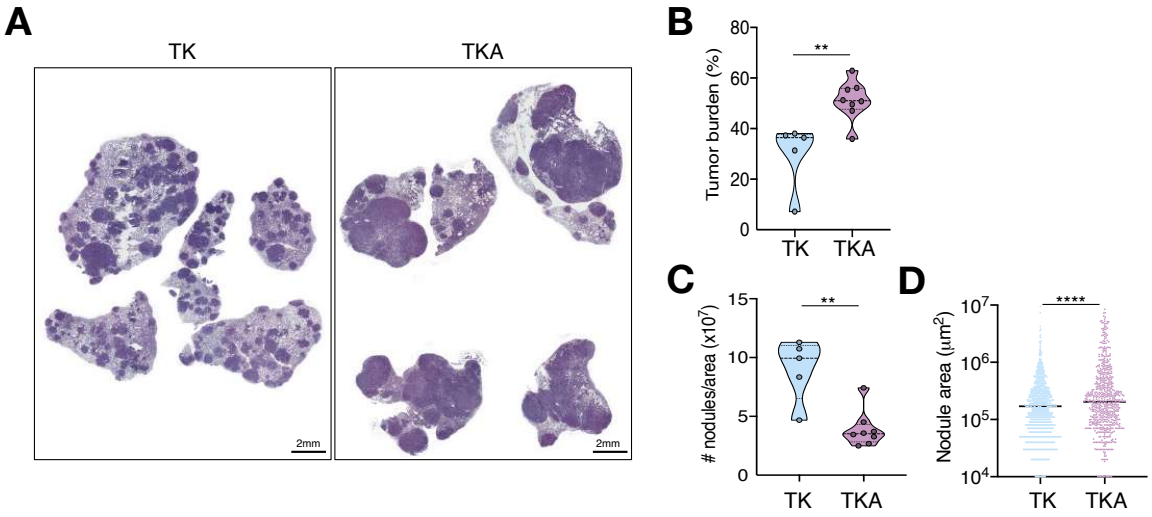

Figure 14: High expression of A3B increases tumor burden

(**A**) Representative hematoxylin eosin images of TK and TKA end point lung tumors. Scale bar: 2mm. (**B**) Tumor burden (tumor area/total lung area) per mouse (TK n = 5, TKA n = 8, each dot represents a mouse). (**C**) Number of nodules per total lung area (x10^7) per mouse (TK n = 5, TKA n = 8, each dot represents a mouse). (**D**) Nodule area in µm^2 (x10^7) (TK n = 5, TKA n = 8, each dot represents a single tumor). Unpaired t-test analysis, ** p ≤ 0.001 and ****p<0.0001.

this detrimental effect is overcome, A3B might give rise to advantageous mutations which accelerate tumor growth.

1.8. A3B expression increases cell death and damage in Kras-induced lung tumors

Expression of A3B has been shown to have a detrimental effect by triggering DNA damage and cell death, causing mutations that may drive ongoing tumor evolution (Burns et al., 2013; Nikkilä et al., 2017). In order to further characterize A3B/Kras tumors, I investigated whether A3B was compromising tumor cell integrity. Immunostaining analyses revealed no differences in proliferation rates. However, lung tumors from TKA mice showed a higher number of apoptotic cells accompanied by an increase in DNA damage (Figure 15A). These findings support my previous hypothesis that A3B causes DNA damage and cell death in LUAD, which may have an influence on tumor initiation and tumor burden.
(Burns et al., 2013; Nikkilä et al., 2017).

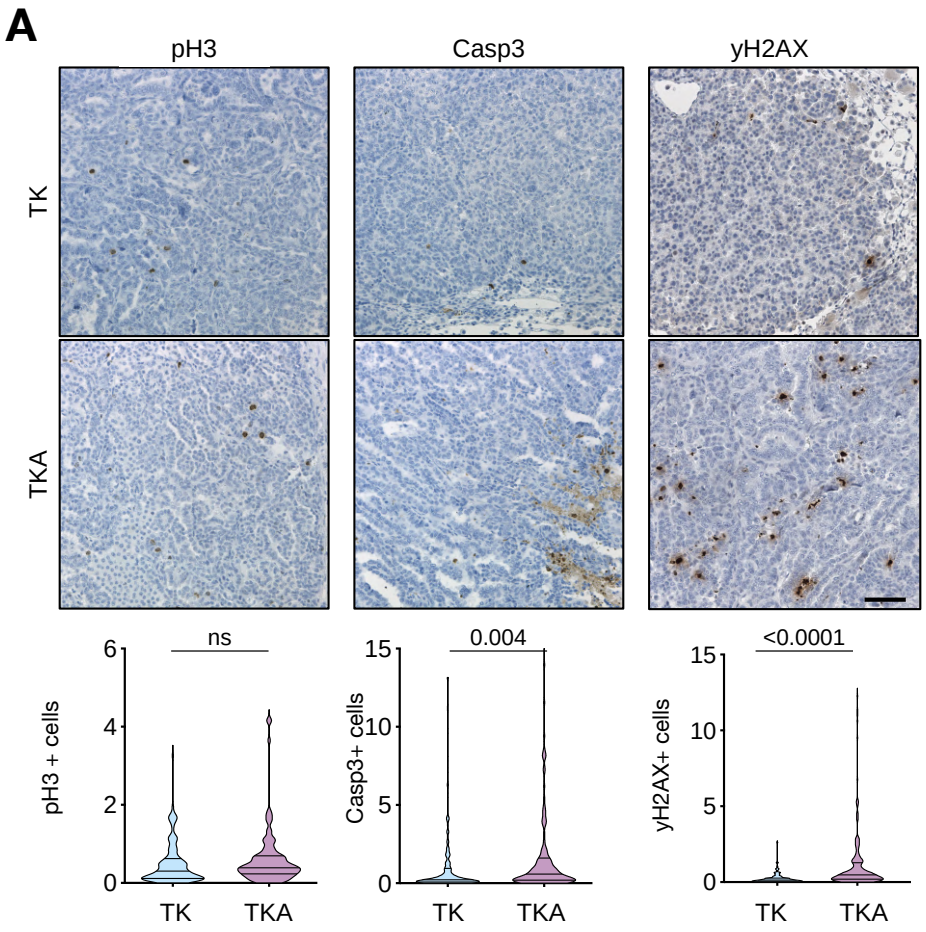

Figure 15: Characterization of TK and TKA tumors

(**A**) Immunohistochemistry against pH3, Casp3 and yH2AX in end point tumors from TK and TKA mice and the corresponding quantifications (TK n = 7, 6 and 4 TKA n = 7, 7 and 8; each dot represents a tumor). Scale bar, 100 µm. Data are expressed as means ± SEM. Unpaired t-test analysis, ns, not significant

1.9. A3B expression inactivates the p53 pathway in *Kras*-induced lung tumors

To investigate the differences between TK and TKA endpoint tumors, DNA and RNA were isolated from single nodules from TK and TKA mice. In addition, to accurately detect mutations and RNA edits, DNA was collected from normal matching ears or tails of identical animals. Five single nodules from 3 mice per genotype (TK and TKA) were submitted for high coverage WES and RNA sequencing, along with matched normal tissue (Figure 16A). Initial PCA analysis from the RNA sequencing data proved that TK tumors shared common features as they clustered together. Interestingly, A3B overexpression led to differences in tumors as they were clustering apart from the TK nodules. Moreover, TKA tumors were different among them (Figure 16B), suggesting increased heterogeneity. In fact, 5013 genes were found to be differentially expressed between the two groups (Figure 16C). Overall, these findings indicate

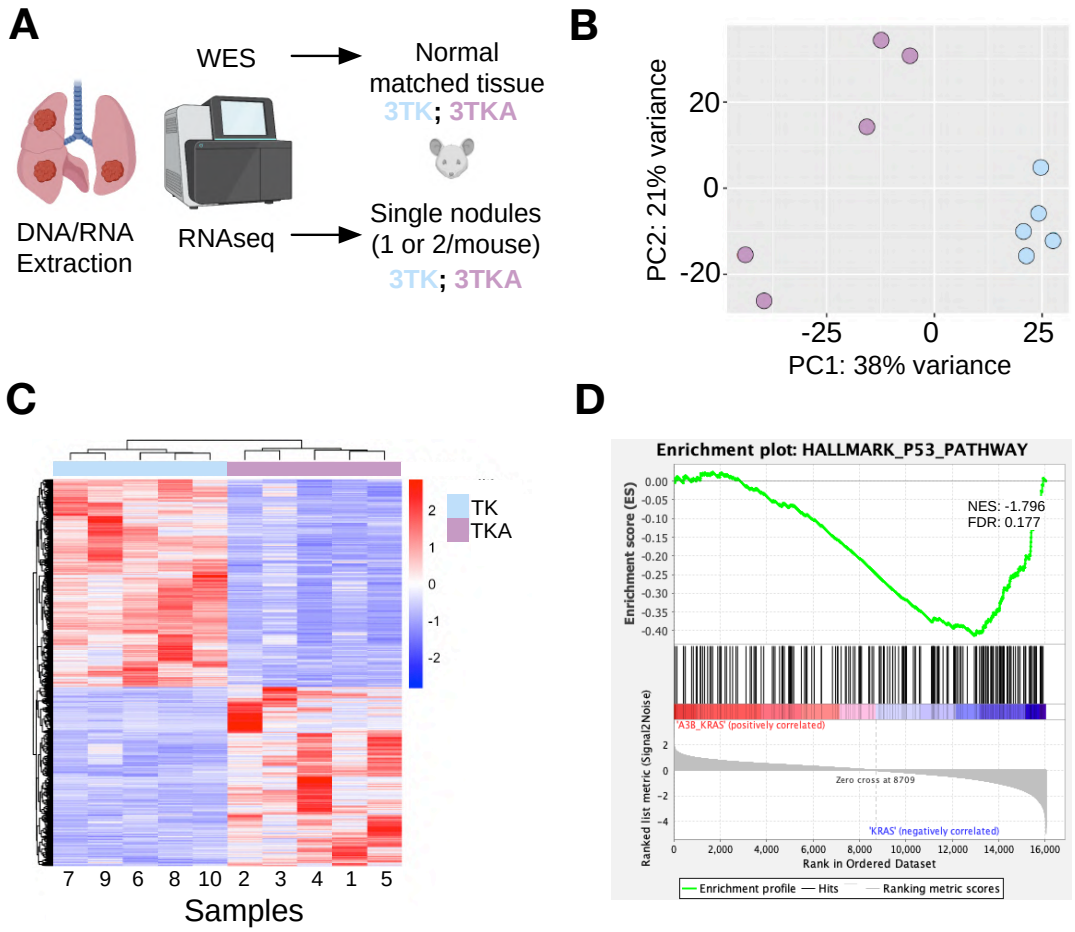

Figure 16: Downregulation of the p53 pathway in TKA tumors

(**A**) DNA and RNA were extracted from single nodules from TK n=3 (5 nodules), TKA n=3 (5 nodules) and sent for RNA-seq and WES. DNA from normal-matched tissue from the same animals was extracted and sent for WES. (**B**) PCA plot obtained from RNA sequencing data from single nodules from TK and TKA mice (n=5 each). Each dot represents a single nodule. (**C**) Heatmap of significantly deregulated genes between TK and TKA nodules (n=5 each). The difference was considered statistically significant when padj<0.05. (**D**) GSEA of "Hallmarks for p53 pathway". RNAseq data of single nodules were used for the analysis. *NES: normalized enrichment score. FDR: false discovery rate.*

that mouse tumors are not heterogenous as they do not acquire the novo mutations as they progress. However, A3B expression confers inter tumor heterogeneity. Whether this heterogeneity is caused by DNA mutations or edits still needs to be addressed. Gene Set Enrichment Analysis (GSEA) comparing control and A3B expressing livers revealed a clear downregulation of the p53 pathway in the TKA group (Figure 16D). Further analysis will be done to understand whether A3B-expressing tumors require the inactivation of the p53 pathway to tolerate A3B mutagenesis.

1.10. A3B overexpression increases the likelihood of non-regression in Kras-induced lung tumors

The results shown in this thesis indicate that expression of A3B in *Kras*-lung adenocarcinomas promotes malignant progression. Consequently, I wondered if A3B could potentially drive the formation of more aggressive subclones that would become resistant to targeted therapy. Although there are currently no inhibitors available against $Kras^{G12D}$, the doxycycline system can mimic targeted therapy. After doxycycline withdrawal, tumors disappear and do not recur as they are completely dependent on Kras expression (Sotillo et al., 2010). Therefore, this is a perfect model for determining if A3B has a role in tumor regression and relapse (Figure 17A).

After 25 weeks of doxycycline treatment, tumor appearance and progression were followed monthly by uCT scans. Once mice harbored tumors, they were scanned every two weeks. Tumor proliferation in TK mice was slow and constant, with almost all the animals exhibiting the same growth pattern. On the contrary, A3B mice seemed to behave differently among them. Initially, tumor development remained steady before exploding in proliferation (Figure 17B). As expected, all TK mice show complete tumor regression 8 weeks after doxycycline withdrawal. Although the majority of TKA tumors disappeared after placing the mice back to a normal diet, some tumors did not completely regress. Moreover, it seems that these non-regressed tumors that were initially regressing, after a few weeks, they resumed growth (Figure 17C and D). Although this experiment is not completed yet, preliminary findings show that A3B expression allows tumor cells to become independent of oncogenic *Kras*.

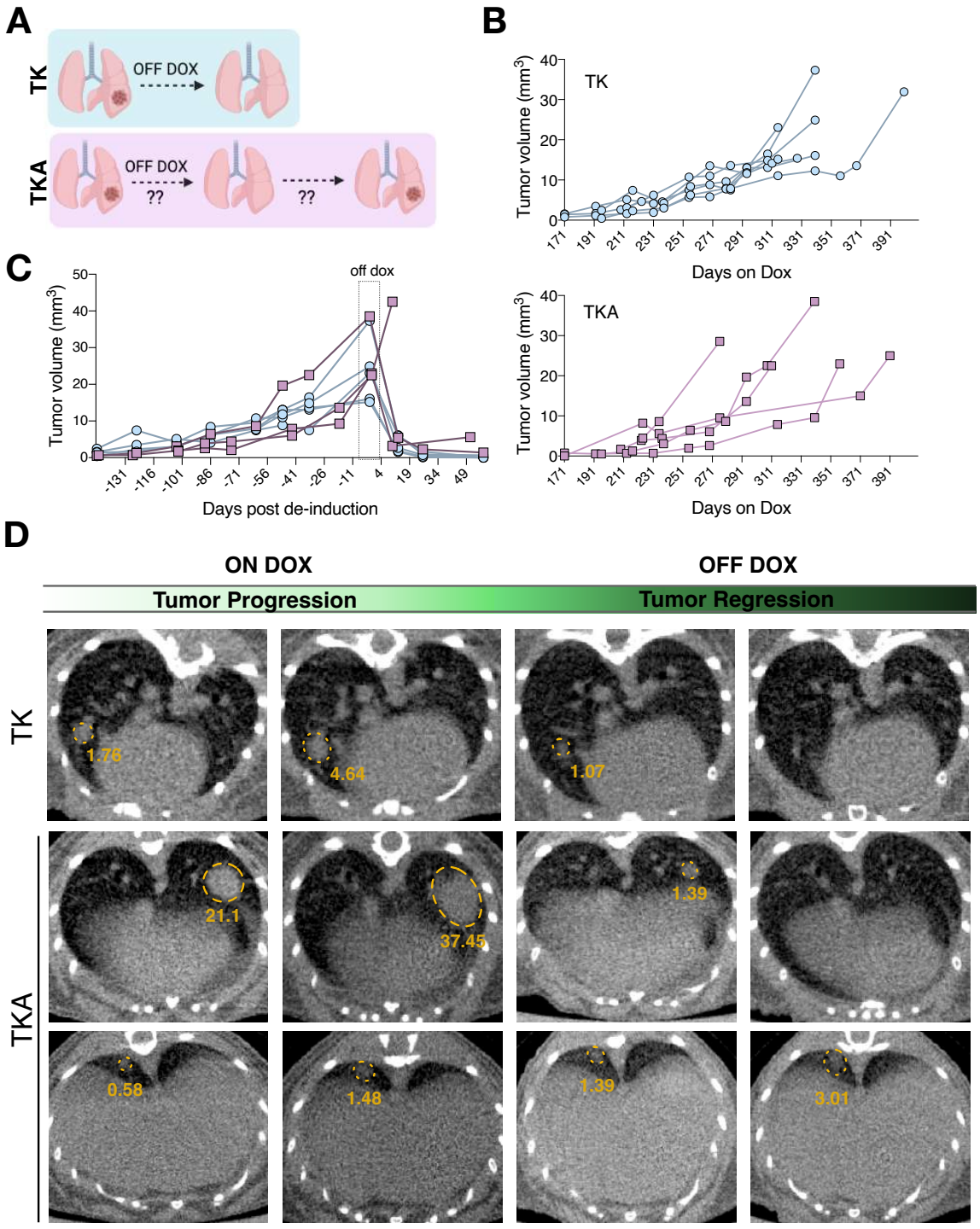

Figure 17: **A3B expression results in incomplete regression of *Kras*-induced tumors**

(**A**) TK mice show complete regression of tumors after Dox withdrawal and tumors do not relapse. Whether A3B expression affects Kras lung tumors regression and recurrence is still unknown. (**B**) Lung tumor volume (mm^3) measured by uCT from TK and TKA mice fed with Dox food. Upper panel: TK tumors; lower panel: TKA tumors. (**C**) Lung tumor volume (mm^3) measured by uCT from TK and TKA after Dox withdrawal. (**D**) uCT from TK and TKA mice on Dox showing progression of lung tumors (yellow circles), after 8-14 weeks of doxycycline withdrawal showing complete regression in TK mice and partial regression in TKA mice. Numbers indicate the volume (mm^3) of each tumor.

1.11. A3B overexpression in an advanced model of LUAD

It has been reported that A3B-mediated mutations are enriched at subclonal mutations, suggesting that A3B is a late mutagenesis process generating branched evolution in NSCLC (Jamal-Hanjani et al., 2017; Roper et al., 2019). However, *Kras*-driven lung tumor models do not recapitulate all the aspects of advanced LUAD. A model that better resembles the features of human LUAD is the commonly used KP model or $p53^{flx/flx}$/LSL-$Kras^{G12D/+}$. Intratracheal injection of an adenovirus expressing Cre recombinase (AdCre) in KP mice leads to expression of oncogenic $Kras^{G12D}$ and simultaneous deletion of p53 in lung epithelial cells, resulting in LUAD (Figure 18A) (Jackson et al., 2005). To further explore the effect of A3B mutagenesis in LUAD, the KP model was combined with the A3B mouse (KPA) allowing the induction of *Kras* and A3B at different time points and thereby mimicking the tumorigenic process closer to what occurs in human cancer. In addition, after the loss of p53, lung epithelial cells will fail to repair A3B induced mutations, likely having important consequences for tumor development and tumor evolution. In fact, p53 mutant tumors have been reported to be enriched in APOBEC signatures (Periyasamy et al., 2017).

Surprisingly, KP and KPA mice (AdCre + doxycycline) died at similar times (Figure 18B). Most of the single nodules isolated from tumor-bearing KPA mice showed high deaminase levels (Figure 18C). In line with this, end point tumors displayed high A3B expression (Figure 18D). Even though the combination of A3B and p53 loss might have been toxic to tumor cells, they did not select against A3B expression and almost every nodule had high A3B levels.

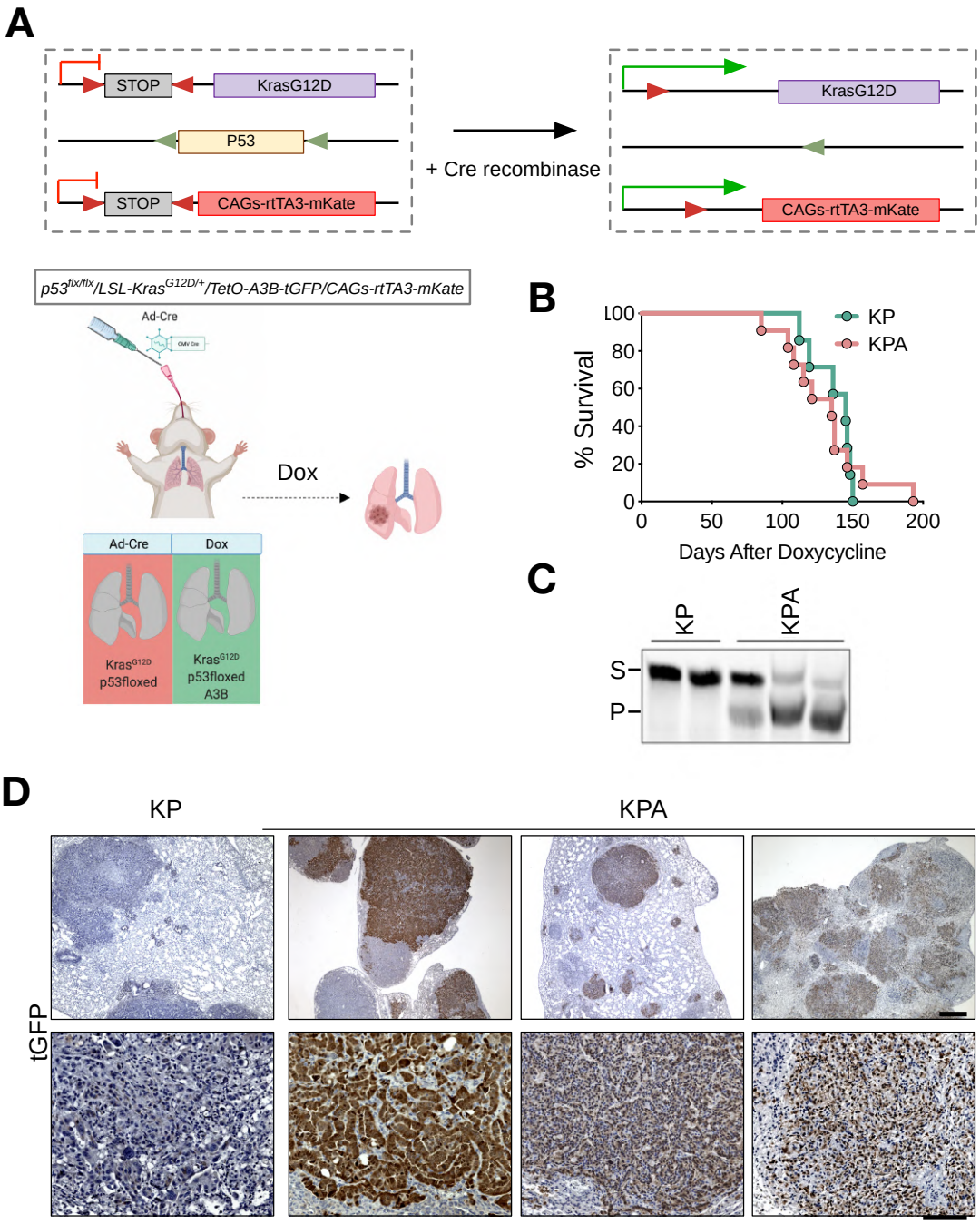

Figure 18: p53 loss and A3B overexpression do not affect survival in Kras-driven LUAD

(**A**) Diagram of *p53*$^{flx/flx}$*/LSL-Kras*$^{G12D/+}$*/CAGs-rtTA3-mKate* alleles. The *p53* allele contains LoxP sites (flx) while *Kras*$^{G12D/+}$ and *CAGs-rtTA3-mKate* have Lox-Stop-Lox (LSL) cassettes. As indicated in the scheme, intratracheal instillation of adenovirus carrying Cre recombinase (Ad-Cre) will allow the expression of *Kras*$^{G12D/+}$ and *CAGs-rtTA3-mKate* and will induce the complete loss of *p53*. In addition, mice containing the *A3B* allele and fed with doxycycline (Dox) will express the A3B transgene. (**B**) Percentage of survival of *p53*$^{flx/flx}$*/LSL-Kras*$^{G12D/+}$*/CAGs-rtTA3-mKate* (KP) and *p53*$^{flx/flx}$*/LSL-Kras*$^{G12D/+}$*/TetO-A3B-tGFP/CAGs-rtTA3-mKate* (KPA) after Ad-Cre infection and Dox administration. (KP, n = 7; KPA, n = 10). (**C**) Deamination activity assay in single nodules from KP and KPA endpoint tumors (S, Substrate; P, Product). (**D**) Immunohistochemistry of tGFP in the endpoint tumors from KP and KPA mice. Scale bar upper panels: 500 µm. Scale bar lower panels: 100 µm.

1.12. A3B does not increase tumor burden in an advanced model of LUAD

As previously described in TK tumors, even though no differences in survival were observed, tumor burden was drastically increased in A3B expressing tumors. In contrast with TKA mice, KP and KPA animals did not show differences in tumor burden (Figure 19A). When lung sections were examined, the overall tumor area and the number of nodules per total lung area showed no differences between KP and KPA lungs (Figure 19B). In addition, it seemed that KP nodules were bigger than KPA tumors when analyzing single nodules (Figure 19D). Taken together, simultaneous overexpression of A3B and loss of p53 did not affect tumor volume in *Kras*-induced LUAD.

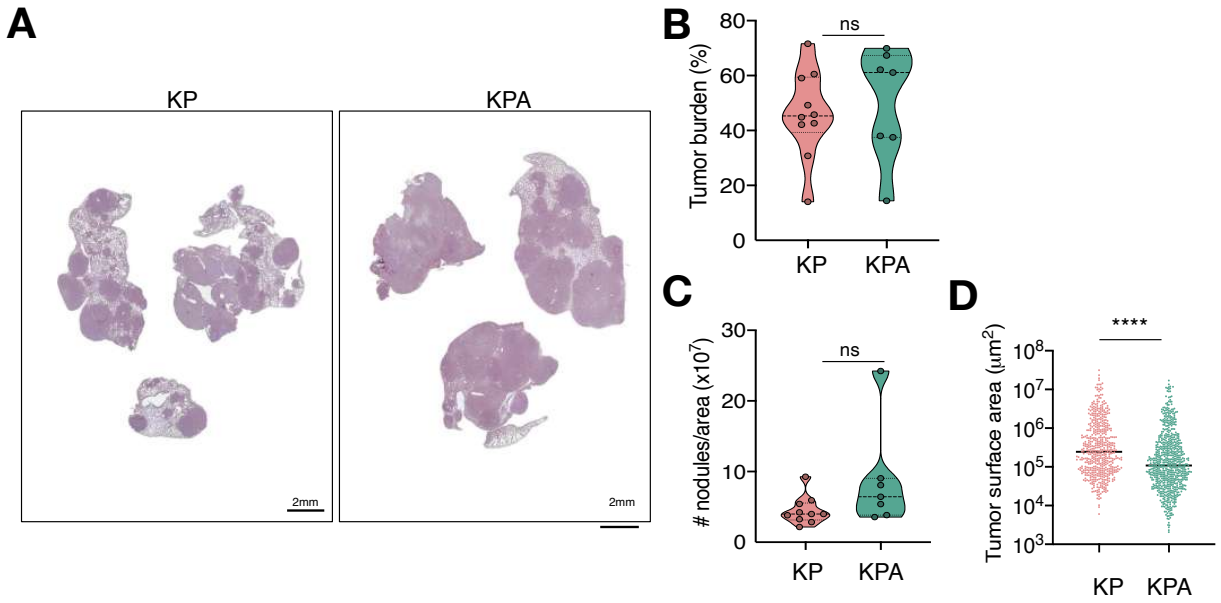

Figure 19: p53 loss and A3B overexpression in kras-driven LUAD show no increase in tumor burden

(**A**) Representative hematoxylin eosin images of KP and KPA end point lung tumors. Scale bar, 2mm. (**B**) Tumor burden (tumor area/total lung area) per mouse (KP n = 10, KPA n = 7, each dot represents a mouse). (**C**) Number of nodules per total lung area (x10^7) per mouse (KP n = 10, KPA n = 7, each dot represents a mouse). (**D**) Nodule area in µm^2 (x10^7) (KP n = 10, KPA n = 7, each dot represents a single tumor). T-test analysis, ns, not significant and ****p<0.0001.

1.13. A3B increases proliferation in an advanced model of LUAD

I next wondered if A3B expression together with the loss of p53 would trigger excessive DNA damage and cell death. Immunostaining analyses revealed a slight increase in DNA damage and cell death, while the growth rate in TKA tumors was significantly elevated (Figure 20A). Based on these findings, the detrimental effect of A3B in *Kras*-induced LUAD is countered by the loss of p53. This compensation may explain why cancers with p53 mutations have been associated with A3B mutagenesis (Mcgranahan et al., 2015; Nik-Zainal et al., 2014). However, evidence favoring an advantage of KPA tumors over KP is still missing.

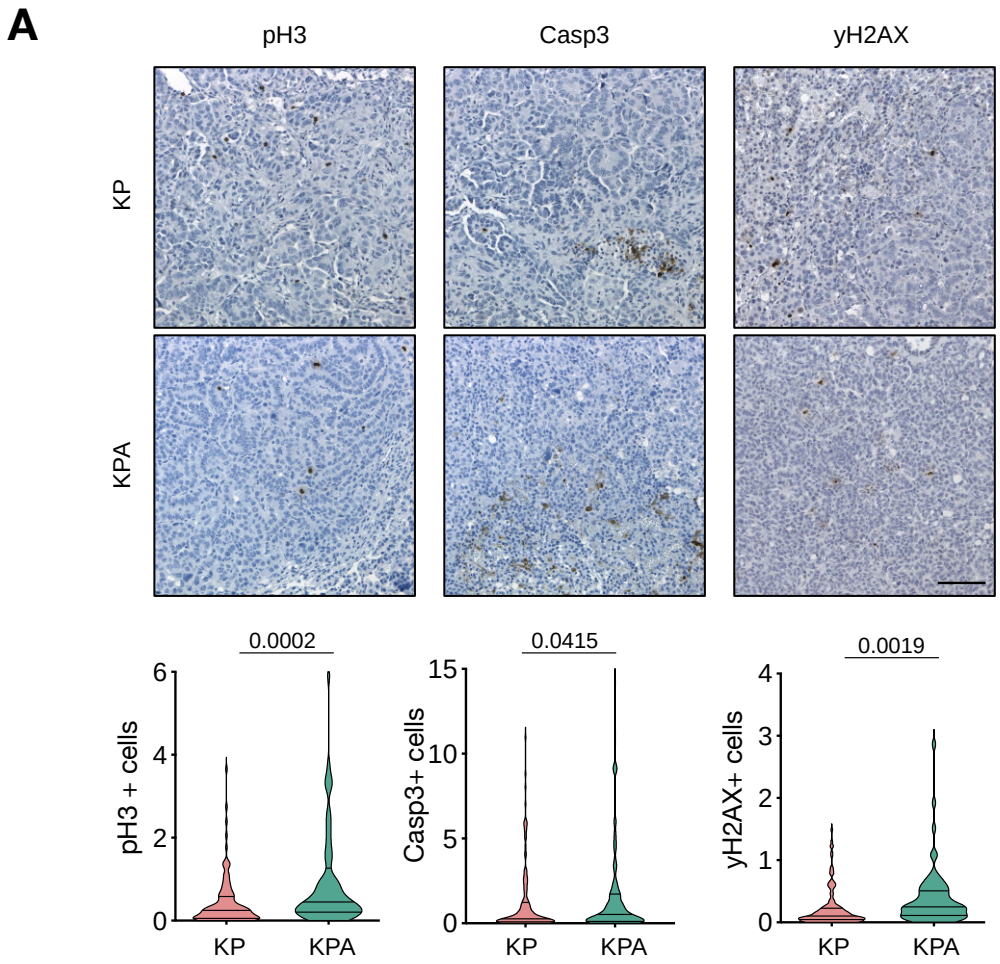

Figure 20: Characterization of KPA tumors

(**A**) Immunohistochemistry against pH3, Casp3 and yH2AX in end point tumors from KP and KPA mice and corresponding quantifications (KP n = 8,9 and 8 TKA n = 7, 6 and 5; each dot represents a tumor). Scale bar, 100 µm. T-test, ns, not significant

Taken together, these results strongly suggest that A3B can influence tumorigenesis at different stages.

2. Acute expression of human APOBEC3B in mice causes lethality and leads to RNA editing

Some of the findings presented in this part of the thesis are now being submitted for publication in the manuscript (Vega et al., 2022). Parts of the text, figures, and figure legends were adapted from the mentioned manuscript, which I co-wrote (see author contributions for more details).

2.1. Overexpression of A3B does not affect proliferation and oncogenic transformation *in vitro*

After finding that low levels of A3B caused tumorigenesis over time, I wondered what would happen if A3B was expressed at high levels. The *Rosa26* promoter activity has shown variable activity in different mouse tissues while the *CAGs* promoter shows a more consistent and robust expression of the rtTA in most adult tissues (Dow et al., 2014). Mice carrying only the A3B transgene were crossed with *CAGs-rtTA3* mice which leads to strong expression of the rtTA transactivator in the majority of adult tissues (Figure 21A).

Prior to *in vivo* studies, I generated MEFs from *A3B/CAGs-rtTA3* mice. The induction of the A3B transgene was confirmed by high deaminase activity 24h after A3B induction (Figure 21B). Cell growth was monitored for 6 days and overexpression of A3B in primary MEFs led to no changes in proliferation (Figure 21C). To understand whether A3B overexpression conferred tumorigenic features such as motility, I performed a wound healing assay. Cells were grown until full confluence before a scratch was generated using a pipet tip. Wound closure was monitored and pictures were taken at start, 18, 24 and 48 hours. There were no differences in wound closure between normal and A3B expressing MEFs (Figure 21D). These findings imply that there is no phenotype *in vitro* at least 6 days after A3B induction at high levels.

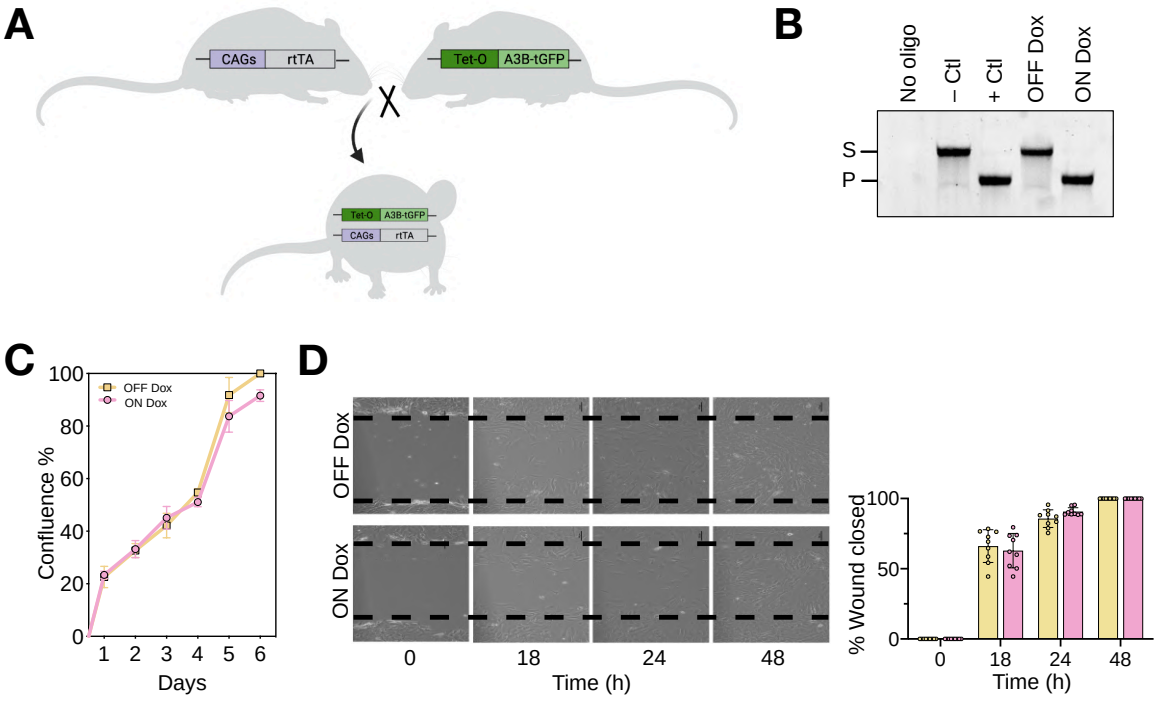

Figure 21: Generation of TetO-A3B/CAGs-rtTA mice and MEFs validation

(**A**) Breeding strategy to generate *TetO-A3B/CAGs-rtTA* mice. (**B**) Deamination activity assay in *(+/A3B);(+/rtTA)* MEFs with (ON Dox) and without (OFF Dox) doxycycline. (**C**) Proliferation assay of *(+/A3B);(+/rtTA)* MEFs in the presence (ON Dox) and absence (OFF Dox) of doxycycline. (**D**) Wound healing migration assay of *(+/A3B);(+/rtTA)* MEFs in the presence (ON Dox) and absence (OFF Dox) at 0, 18, 24, 48 hours. Percentage of the area of wound closure at 0, 18, 24, 48 hours is quantified in the right plot. Each dot represents one well. Three independent biological replicates (each biological replicate contained 3 experimental replicates or wells). Data shown is mean ± SD. Two-way-anova. All values are not significant.

2.2. Generation of a doxycycline-inducible mouse model with high APOBEC3B levels

TetO-A3B/CAGs-rtTA3 (hereafter A3B) adult mice were fed a doxycycline-containing diet to ubiquitously overexpress the A3B transgene. Examination of different tissues under a stereomicroscope after 10 days of daily doxycycline administration, showed that liver, intestinal and pancreatic tissue exhibited the highest amounts of tGFP fluorescence (Figure 22A). Accordingly, I also confirmed that human A3B stains most strongly in liver and pancreatic tissues, and that the enzyme is mainly confined to the nucleus as previously reported (Figure 22B and C) (Salamango et al., 2018).

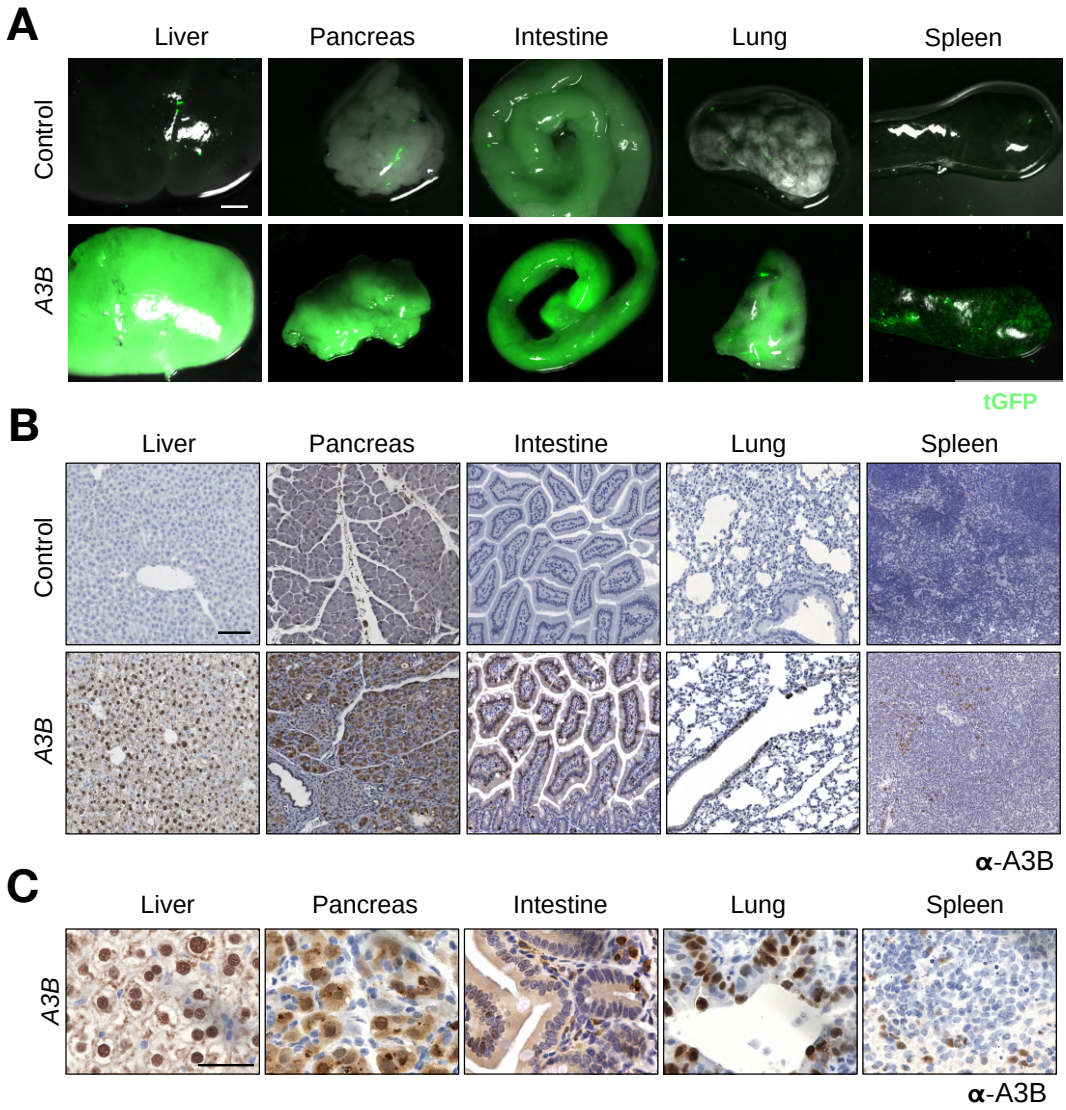

***Figure 22: A3B* is expressed at high levels in *Teto-A3B/CAGs-rtTA* mice**

(**A**) Stereomicroscope images showing tGFP fluorescence in the indicated macroscopic tissues from *TetO-A3B/CAGs-rtTA* and control mice fed with doxycycline (Dox) for 10 days. Scale bar: 3mm. (**B**) Immunohistochemistry of A3B in the indicated tissues from *TetO-A3B/CAGs-rtTA* and control mice fed with Dox for 10 days. Scale bar: 100 µm. (**C**) Magnifications from pictures in panel B demonstrating that A3B has nuclear localization. Scale bar: 50 µm.

2.3. A3B mice show A3B levels similar to those found in human tumors

In order to accurately characterize the new A3B mouse model, I performed immunoblots, which confirmed that A3B is strongly expressed in the liver and pancreas, with moderate levels in the intestine, whereas the lung and the spleen contain only modest levels of this protein (Figure 23A). In order to confirm that A3B retained its deaminase activity, I used soluble protein extracts from A3B-expressing tissues and performed single-stranded DNA C-to-U activity assays. Similarly, the tissues with the highest protein expression showed the strongest deaminase activity (Figure 23B). This induction of A3B was also detected by quantitative PCR

(qPCR) of mRNA from the mentioned tissues (Figure 23C). I next wondered whether the high induction of A3B in some tissues was found in humans and started a collaboration with Prof. Dr. Reuben Harris and Dr. Nuri Alpay Temiz. To compare A3B expression levels in mouse tissues to those in humans, Dr. Nuri Alpay Temiz downloaded mRNA expression data from human tumors available at the Cancer Genome Atlas (TCGA) database. The housekeeping gene encoding TATA-binding protein (TBP) was used for normalization in the analysis. Lung tissues expressed A3B within the range found among human cancers. A3B expression in liver and pancreas was comparable to human tumors with the highest A3B levels, which have been associated with poor patient survival (Figure 23D) (Law et al., 2016; S. Wang et al., 2018; H. Zhang et al., 2021).

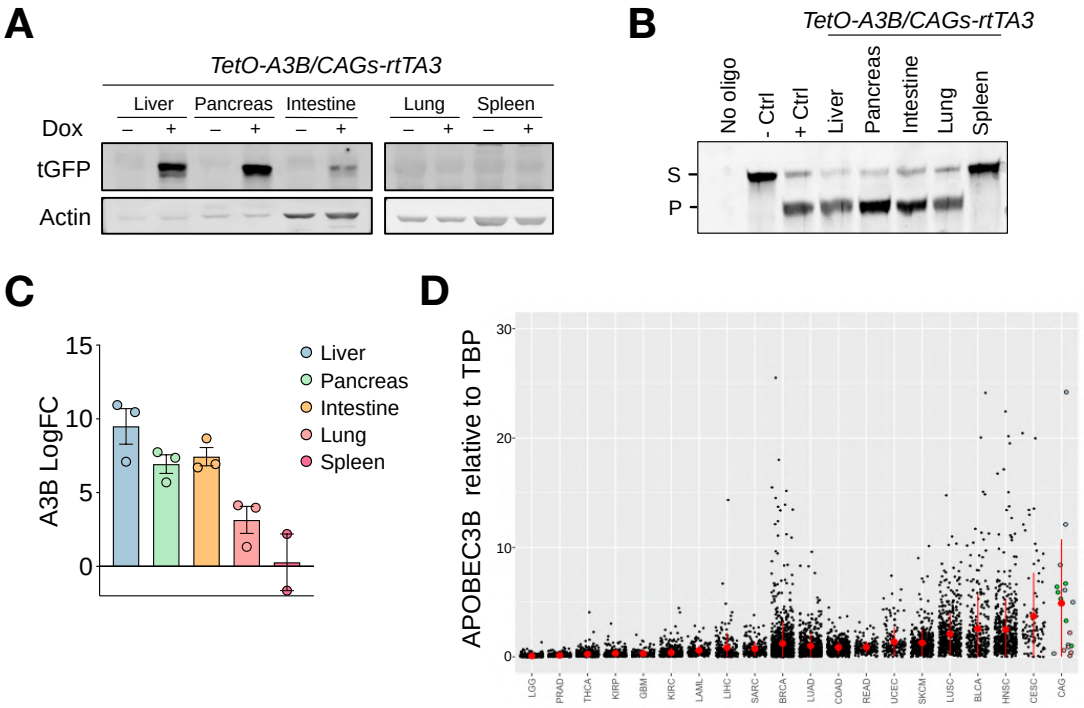

***Figure 23: A3B* is expressed at high levels found in human tumors**

(**A**) Immunoblot showing A3B-tGFP levels in the indicated tissues from *(+/A3B);(+/rtTA)* mice fed with (+) and without (-) doxycycline for 10 days. Actin was used as loading control. (**B**) Deamination activity assay in the indicated tissues from *(+/A3B);(+/rtTA)* mice fed with doxycycline for 10 days. (S, Substrate; P, Product). (**C**) Quantitative RT-PCR of A3B expression levels in the indicated tissues from *(+/A3B);(+/rtTA)* mice fed with doxycycline for 10 days.18S and Actin were used as house keeping genes for normalization. Each dot represents one mouse. Bars show mean and error bars ± SEM. (**D**) Comparison of A3B expression levels relative to TBP in human tumors with liver, pancreas and lung from *A3B/CAGs-rtTA*. Gray dots represent independent TCGA tumors; blue dots liver, green dots pancreas and pink dots lung. Red dots and error bars show mean ± SD.

2.4. Acute A3B levels are toxic and cause lethality *in vivo*

To examine the consequences of expressing high levels of A3B, adult mice were fed with dox-containing food. Unexpectedly, all animals died between 6 and 14 days after receiving dox (Figure 24A). Prior to death, A3B-expressing mice exhibited a "trembling" phenotype, were

immobile and with the inability to respond to stimuli. Macroscopic examination of different organs showed that A3B livers were pale and oily, resembling a fatty acid liver. In collaboration with Prof. Dr. Albrecht Stenzinger and Dr.Tanja Poth, we performed a pathological examination of the organs of these animals. Hematoxylin eosin stainings from paraffin embedded tissues revealed that A3B livers had fatty acid accumulation which is a sign of micro-and macro-vesicular steatosis (Figure 24B). A close examination of pancreatic sections revealed loss of tissue architecture, acinar cell death and evidence of chronic inflammation (Figure 24C). Altogether, these findings indicate that acute A3B expression induces damage in several organs which is incompatible with life.

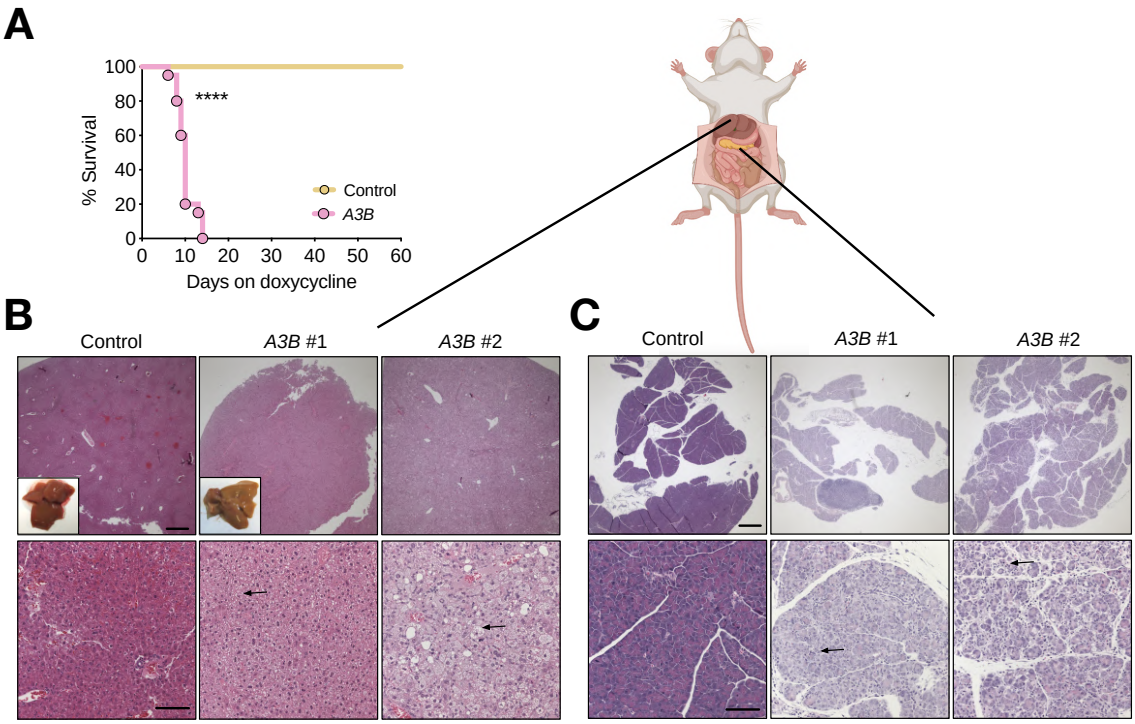

Figure 24: **Acute levels of A3B are lethal in mice and cause dysfunctions in the liver and pancreas**

(**A**) Percentage of survival from *A3B/CAGs-rtTA* (n=12) and control mice (n=11) after doxycycline administration; P<0.001 by Log-rank (Mantel-Cox) test. (**B**) Hematoxylin and eosin (H&E) stainings from livers of *A3B/CAGs-rtTA* and control mice. Insets with macroscopic pictures. Arrows indicate areas presenting micro or macro vesicular steatosis. (**B**) Hematoxylin and eosin (H&E) stainings from pancreas of *A3B/CAGs-rtTA* and control mice. Arrows indicate acinar destruction. Scale bars (**B** and **C**): Upper panels 500 µm; lower panels 100 µm.

2.5. Acute A3B expression causes damage to major vital organs

Further examination of other vital organs such as the lung, intestine, spleen kidney, heart and brain revealed no signs of damage (Figure 25A). Failure in any of these organs could have been the cause of the sudden death of the animals. Taken together, it is tempting to speculate that elevated A3B levels disrupt pancreatic and liver homeostasis resulting in metabolic problems incompatible with life.

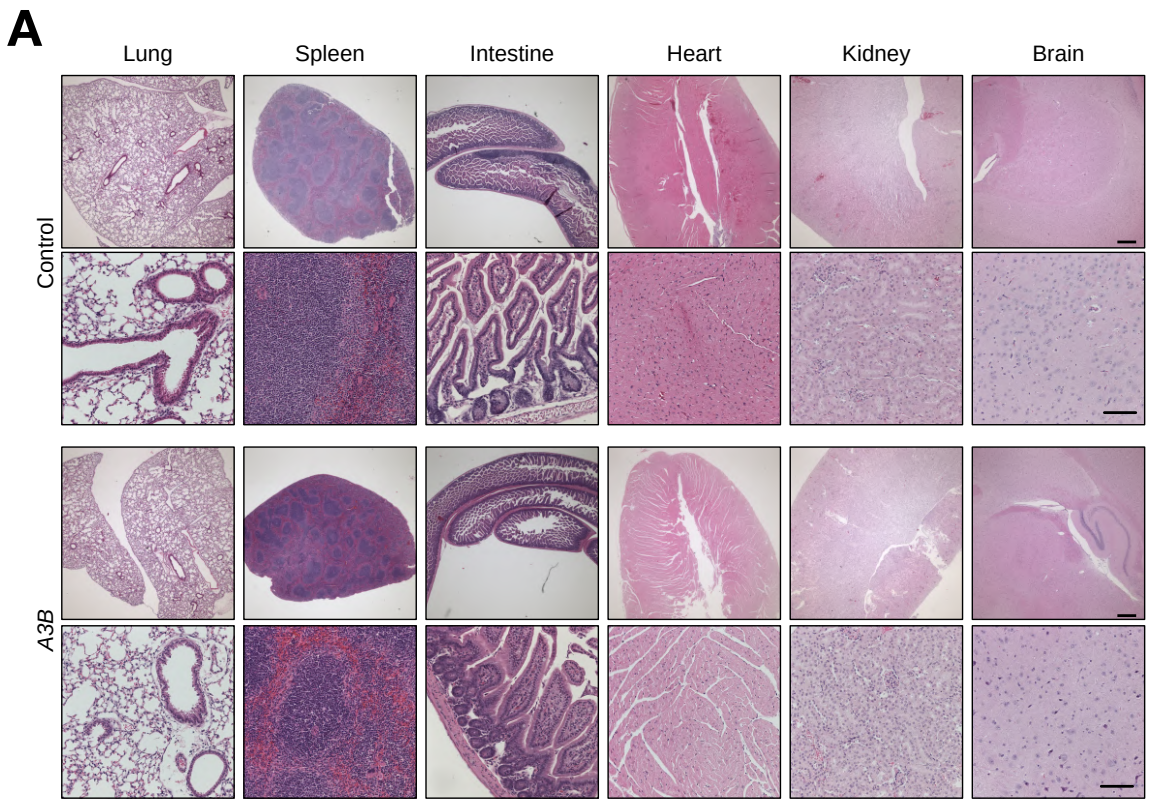

Figure 25: **Acute levels of A3B do not cause pathology in other organs**

(**A**) Hematoxylin and eosin (H&E) stainings from the indicated tissues of *A3B/CAGs-rtTA* and control mice fed with Dox. Scale bars: Upper panels 500 µm; lower panels 100 µm.

2.6. Disruption of metabolism, cell death and DNA damage in A3B expressing livers

To fully understand the consequences of expressing A3B in liver tissues I analyzed makers for apoptosis (caspase3), DNA damage (yH2AX) and proliferation (ki67 and phospho-histone3). Immunohistochemistry of paraffin sections demonstrated an increase in apoptosis and DNA damage in A3B livers compared to controls, whereas no differences in proliferation were observed (Figure 26A and B). In addition, RNA extracted from six A3B livers and two control livers were sent for high coverage RNA sequencing. Differential expression analysis revealed that the expression patterns of the two groups were clearly different (Figure 26C). Gene Set Enrichment Analysis (GSEA) comparing control and A3B expressing livers pointed to a metabolic disturbance, due to the downregulation of the fatty acid and cholesterol metabolism. Moreover, apoptosis and oncogenic pathways such as Kras signaling were upregulated in A3B livers compared to controls (Figure 26D). All these findings support the theory that A3B is detrimental to liver cells causing metabolic failure.

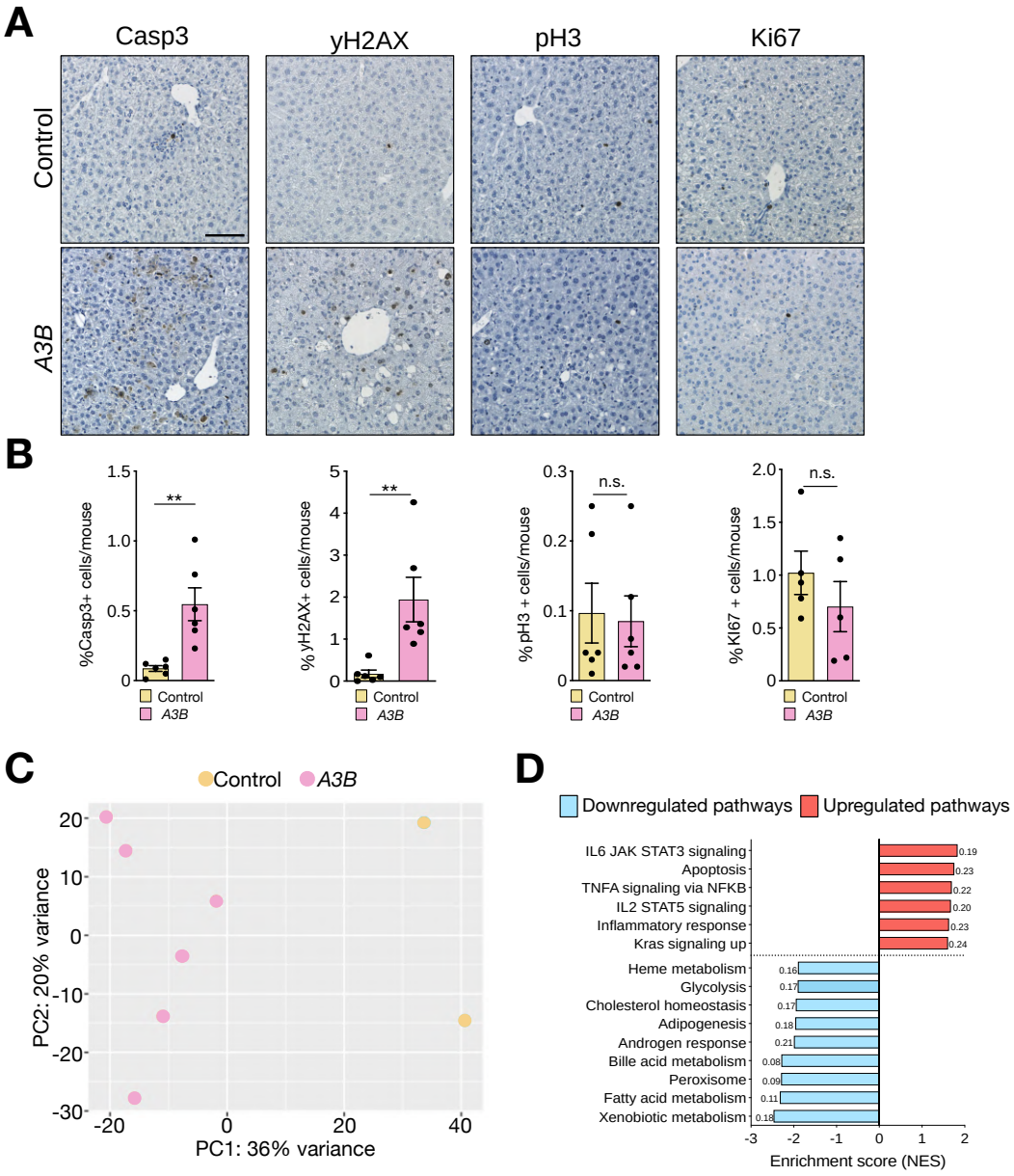

Figure 26: **Livers from *A3B* mice have increased cell death, DNA damage and metabolic dysfunction**

(**A**) Stainings against Caspase3 (Casp3), yH2AX, phosphorus-histone 3 (pH3) and ki67 from *A3B/CAGs-rtTA* and control mice fed with doxycycline (Dox) for 10 days. Scale bar: 100 µm (**B**) Quantification of the percentage of positive cells per mouse in each staining. Each dot represents a mouse. Bars represent the mean and error bars show +- SEM. (**C**) PCA plot obtained from RNA sequencing data from livers from *A3B/CAGs-rtTA* and control mice (n=3 each). Each dot represents a mouse. (**D**) Differential expression analysis GSEA showing the pathways upregulated (red) and downregulated (blue). False discovery rate (FDR) values are annotated at the end of each bar. Normalized enrichment scores (NES); False discovery rate (FDR). T-test analysis: ns, not significant; ** p ≤ 0.01.

2.7. Acute inflammation, cell death and DNA damage in A3B expressing pancreas

Similar to liver tissues, I performed a comprehensive analysis of the pancreatic tissues of A3B expressing mice. Immunohistochemistry of paraffin sections demonstrated an increase in apoptosis and DNA damage in the A3B pancreas compared to controls, whereas no

differences in proliferation were observed. In addition, and correlating with the pathological observations, A3B expressing pancreas showed a striking T cell infiltration (CD3 staining) (Figure 27A and B). To further support these findings, RNA from six A3B pancreas and two controls were submitted for high coverage RNA sequencing. Similar to liver tissues, differential expression analysis revealed that the expression patterns of the two groups were clearly different (Figure 27C). Gene Set Enrichment Analysis (GSEA) comparing control and A3B

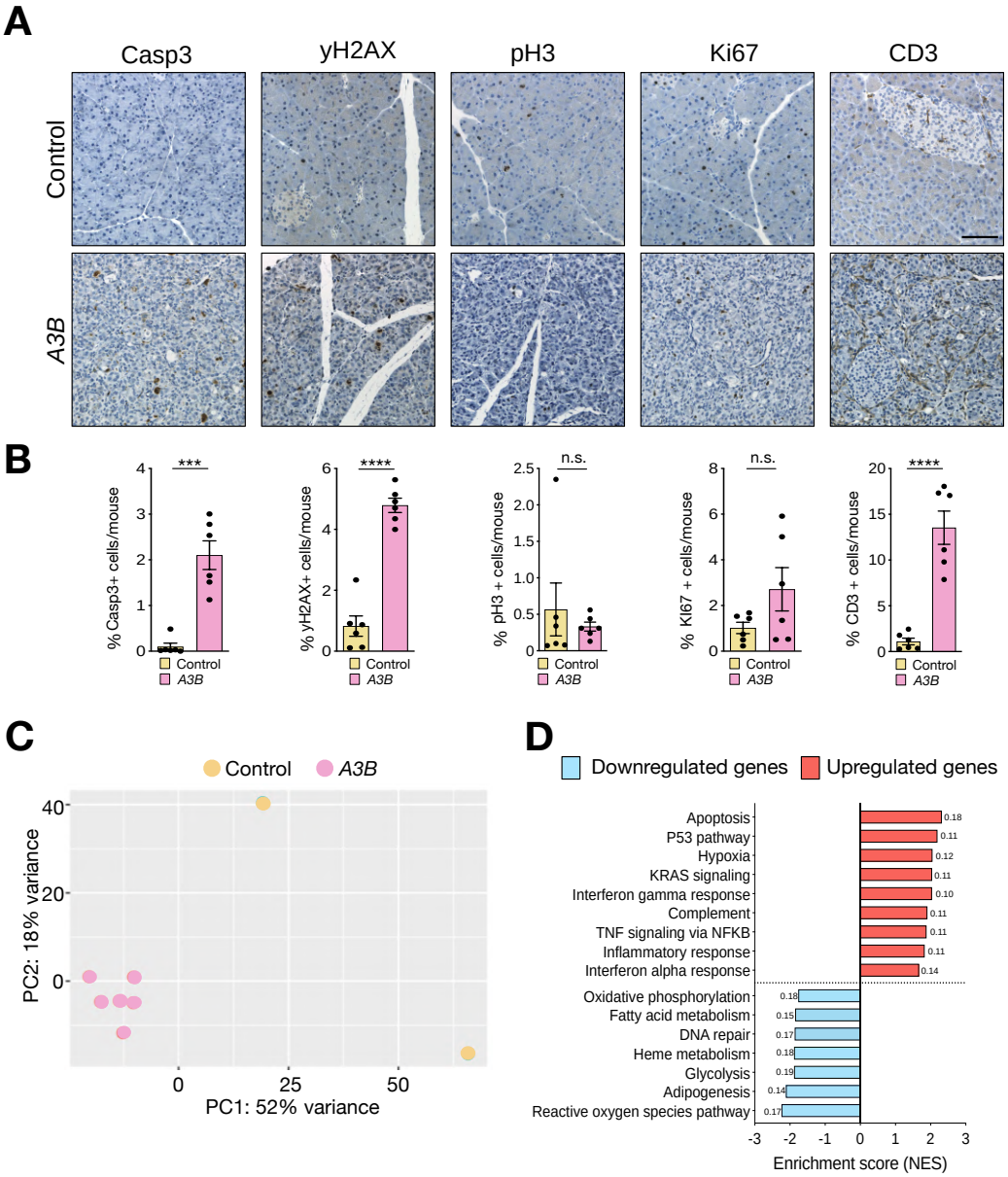

Figure 27: **Pancreas from *A3B* mice have increased cell death, DNA damage and inflammation**

(**A**) Stainings against Casp3, yH2AX, pH3, ki67 and CD3 from *A3B/CAGs-rtTA* and control mice fed with doxycycline (Dox) for 10 days. Scale bar: 100 µm. (**B**) Quantification of the percentage of positive cells per mouse in each staining. Each dot represents a mouse. Bars represent the mean and error bars show ± SEM. (**C**) PCA plot obtained from RNA sequencing data from pancreas from *A3B/CAGs-rtTA* and control mice (n=3 each). Each dot represents a mouse. (**D**) Differential expression analysis GSEA showing the pathways upregulated (red) and downregulated (blue). False discovery rate (FDR) values are annotated at the end of each bar. Normalized enrichment scores (NES); False discovery rate (FDR). Unpaired t-test analysis: ns, not significant; *** $p \leq 0.001$; **** $p \leq 0.0001$.

expressing livers revealed a clear upregulation of inflammatory pathways, apoptosis and oncogenic pathways (Figure 27D).

2.8. Measurements of liver enzymes indicate liver damage in A3B mice

These experiments were performed with the help of Mirian Fernandez from Prof. Dr. Mathias Heikenwälder lab. On the basis of several findings demonstrating a metabolic failure in A3B mice, we conducted comprehensive metabolic profiling of A3B mice. Since the pancreas and the liver participate in glucose metabolism and this might have been a possible cause of mortality in A3B mice, I evaluated the tolerance to glucose by performing a glucose tolerance test. Mice were fasted overnight, with doxycycline administration in the drinking water, and 16 hours later they received an intraperitoneal injection of glucose. Blood samples were taken before glucose injection as well as 15, 30, 60, 90 and 120 min post glucose administration (Figure 28A). Immediately after glucose injection, blood glucose levels will rise and then decrease if glucose metabolism is normal. However, there were no differences in glucose levels between A3B mice and controls, suggesting that glucose metabolism was not affected (Figure 28B). In addition, we measured enzymes related to liver damage in sera from A3B and control animals. Increased serum levels of liver transaminases, such as alanine transaminase (ALT) and aspartate transaminase (AST), indicated liver damage (Figure 28C). Therefore, it is clear that A3B-expressing mice suffer liver and pancreatic failure affecting

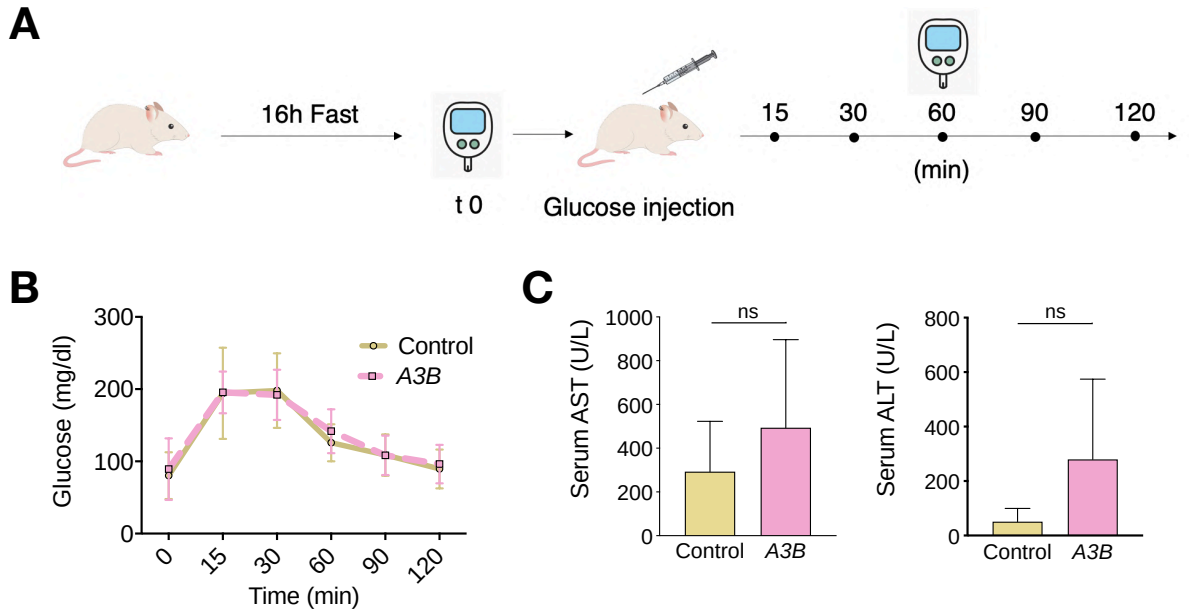

***Figure 28: A3B*-expressing mice show increased levels of transaminase enzymes**

(**A**) Scheme of the experimental procedure of intraperitoneal glucose tolerance test. (**B**) Intraperitoneal glucose tolerance test after 8 days after Dox treatment in A3B mice and controls. (**C**) Analysis of transaminase levels (ALT and AST) in sera of control and A3B mice. A3B n = 6 mice; control n = 5 mice. Data are expressed as means ± SD. Statistical significance was calculated using either unpaired t-test or 2-way anova; ns, not significant.

important processes such as cholesterol and fatty acid metabolism. Overall, our findings imply that elevated levels of A3B result in cell dysfunction and consequently disturbance of tissue homeostasis, systemic organ failure, and early animal death.

2.9. A3B is an RNA editing enzyme

Deamination of single-stranded DNA by A3B has been linked to DNA damage and mutagenesis (Burns et al., 2013; Hoopes et al., 2016). A3A, which is highly homologous to A3B, has been reported to function similarly. However, A3A has also the capacity of deaminating RNA substrates (Jalili et al., 2020; Sharma et al., 2015). To date, RNA editing activity has not been described for A3B. Therefore, it is essential to determine whether A3B represents a mutagenic threat to the RNA and functions in different manners to create diversity.

To address if A3B is editing the RNA, and to find possible editing sites, RNA-seq libraries were prepared in biological triplicates from lung and liver tissues under normal conditions (controls) and under doxycycline induction (10-14 days). After data processing (done by Dr. Rafail Tasakis in Prof. Dr. Nina Papavasilius lab), candidate sites for DNA mutations or RNA editing were defined as C-to-U or G-to-A changes (depending on the sense of the transcribed strand). Only the changes that were not present in the controls and that appeared in the A3B samples in more than 5% of the transcripts for a particular position in the genome were considered. From this analysis, a list with possible candidates was obtained (Figure 29A). Initially, lung and liver tissues had an increased in the number of changes in A3B samples compared to controls. In addition, A3B expressing livers showed more changes when compared to A3B expressing lungs (Figure 29B). This correlated with the higher mRNA A3B expression in liver samples compared to the lungs, which indicates that livers displayed greater deaminase activity (Figure 29C).

To further validate whether these changes corresponded to DNA mutations or RNA editing events, I selected 36 positions (in 36 genes in the liver) and 25 positions (in 13 genes in the lung) for experimental validation of site-specific editing by sanger sequencing of purified DNA and RT-PCR RNA products (Figure 29A). All the 25 positions tested in the lungs were identified as DNA mutations (Figure 29D). In contrast, RNA editing in A3B liver tissues was found in 15 of the 36 positions while the other 21 changes were confirmed as DNA mutations. To further explore whether the RNA editing events found in the A3B liver samples were random or

recurrent events due to A3B overexpression, we sequenced these 15 edited positions in 3 additional A3B expressing livers. I found that 7 of these positions were edited in 100% of the *A3B* mice, 3 positions were edited in 5 out of 6 mice (83%) and the last 5 positions tested were edited in 4 mice (66%), suggesting that A3B RNA editing is a recurrent event in liver samples

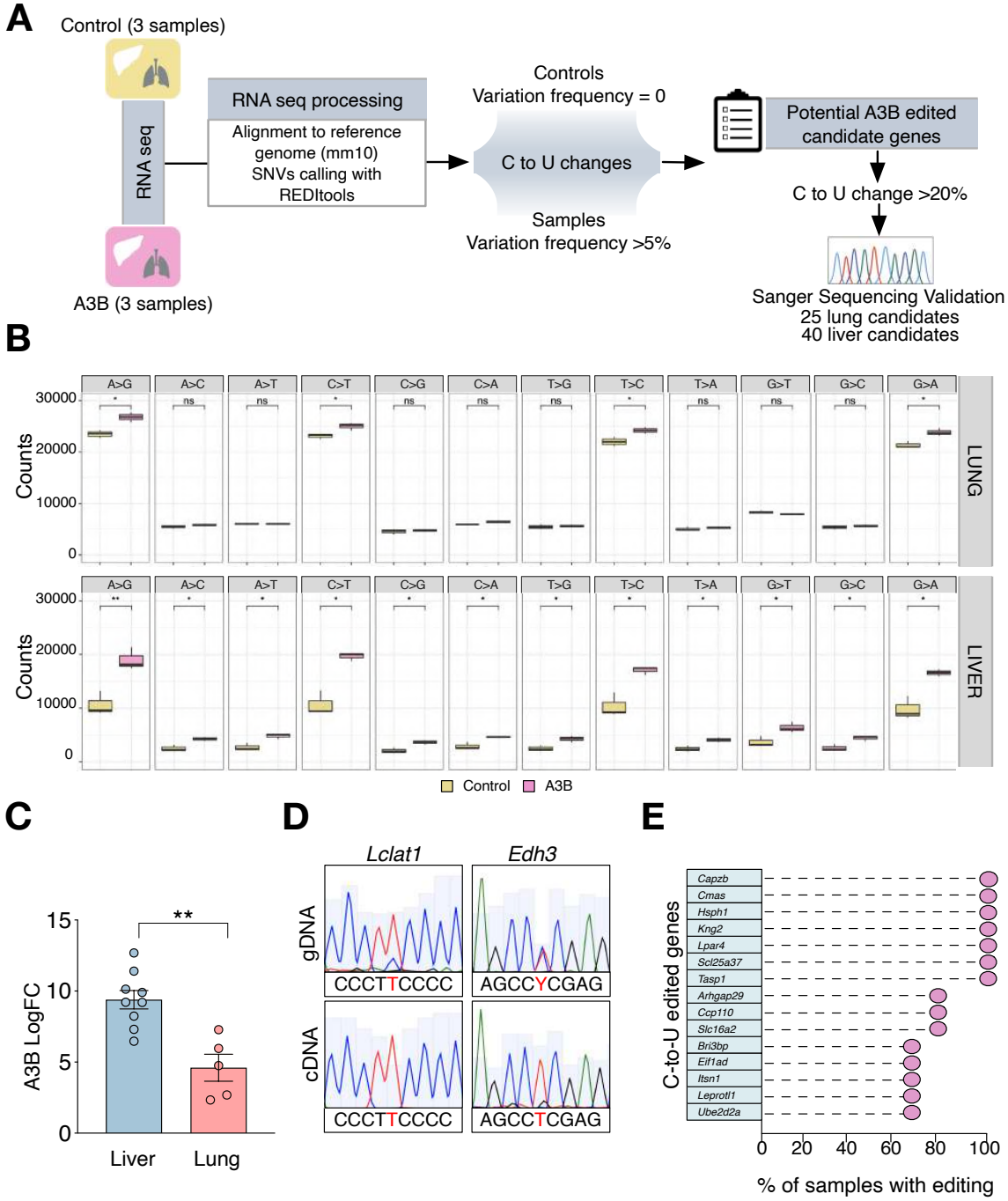

Figure 29: **RNA edits are detected in high A3B-expressing tissues**

(**A**) Schematic of the pipeline used to call potential RNA-editing candidates in the lung. (**B**) Number of single nucleotide variants (SNVs) per type of change in lung and liver of *A3B* mice in comparison to controls (A3B n=3 controls n=3). Data are expressed as means ± SD. (**C**) Quantitative RT-PCR of A3B expression levels in liver and lung from *A3B* mice relative to TBP (mean ± SEM shown by dots and error bars, respectively). (**D**) Sanger sequencing chromatogram indicating examples of A3B-driven mutations in A3B lungs. (**E**) Lollipop plots showing the percentage of mice showing C-to-U editing in candidate targets selected for RT-PCR and Sanger sequencing experimental validation (n=6). Unpaired t-test analysis: ns, not significant; * $p \leq 0.05$; ** $p \leq 0.01$.

(Figure 29E). Based on this analysis, I cannot exclude the possibility of ongoing A3B-mediated RNA editing in the lung, but this result together with a lower mutational load, compared with the liver, correlated with the weak levels of A3B detected in the lung.

2.10. A3B edits the RNA in a preferred motif

The previous analysis demonstrated that A3B can deaminate RNA substrates; nevertheless, it is more accurate to call RNA edits from DNA and RNA data coming from the same sample. Therefore, to demonstrate A3B RNA editing activity in a more precise manner RNA-seq and whole exome sequencing (WES) were performed from liver and pancreatic tissues (high A3B levels) of six A3B mice and two control littermates. Dr. Nuri Alpay Temiz performed the analysis and after applying quality filters and completing data analysis, any single base changes at the DNA or RNA level that were represented by >5% altered reads in A3B samples and no altered reads in control samples were considered to be A3B-specific. For RNA editing analysis, changes that were not found in the matching exome data for each sample were utilized (Figure 30A). Analysis of the various forms of editing in the liver revealed a general increase in A-to-G and C-to-U alterations, perhaps due to endogenous ADAR enzymes (Figure 30B). Even though the majority of the changes in the pancreas were A-to-G transitions, an elevated percentage of C-to-U transitions was also found (Figure 31A). Although an increase in DNA mutations was also observed, only a small number of A3B-preferred TCW motif mutations were detected (Figures 30C and 31B). It is possible that the short time A3B was induced did not allow bulk DNA sequencing from detecting clonal alterations. From the total number of RNA edits, we randomly chose potential candidate genes (C-to-U >20%) that were then validated to make sure our analysis was accurate. We found 7 C-to-U changes in the liver and 7 C-to-U changes in the pancreas (Figures 30D and 31C). Validation in six additional A3B liver and pancreas from the selected genes proved once more that RNA editing by A3B is not a random event (Figures 30E and 31D).

Most of the RNA changes caused by A3B were found in a UCC context, and all of the edited genes that were validated were found in at least two animals. Therefore, we next looked if A3B has a sequence preference near the edited cytosine. Analysis of the nucleotides surrounding the edited cytosine found a wider nucleotide context, 5'-UCCGUGUG-3' (Figure 30F and 31E), that could potentially be used to predict where A3B-catalyzed RNA editing sites are in the liver and pancreas of these mice. In contrast to previous results for A3A RNA editing hotspots, no secondary stem-loop structures containing the deaminated C at the 3′ end of the loop were detected in these sequences (Jalili et al., 2020; Sharma & Baysal, 2017). C-to-U edits were mainly located in 3'UTRs, whereas 30% were in coding exons, causing 1 stop, 13 non-synonymous and 23 synonymous changes (Figure 30G and 31F). These findings confirm

that A3B possesses RNA editing activity in a UCC-specific context, which could be interpreted as hotspots for A3B-driven RNA editing.

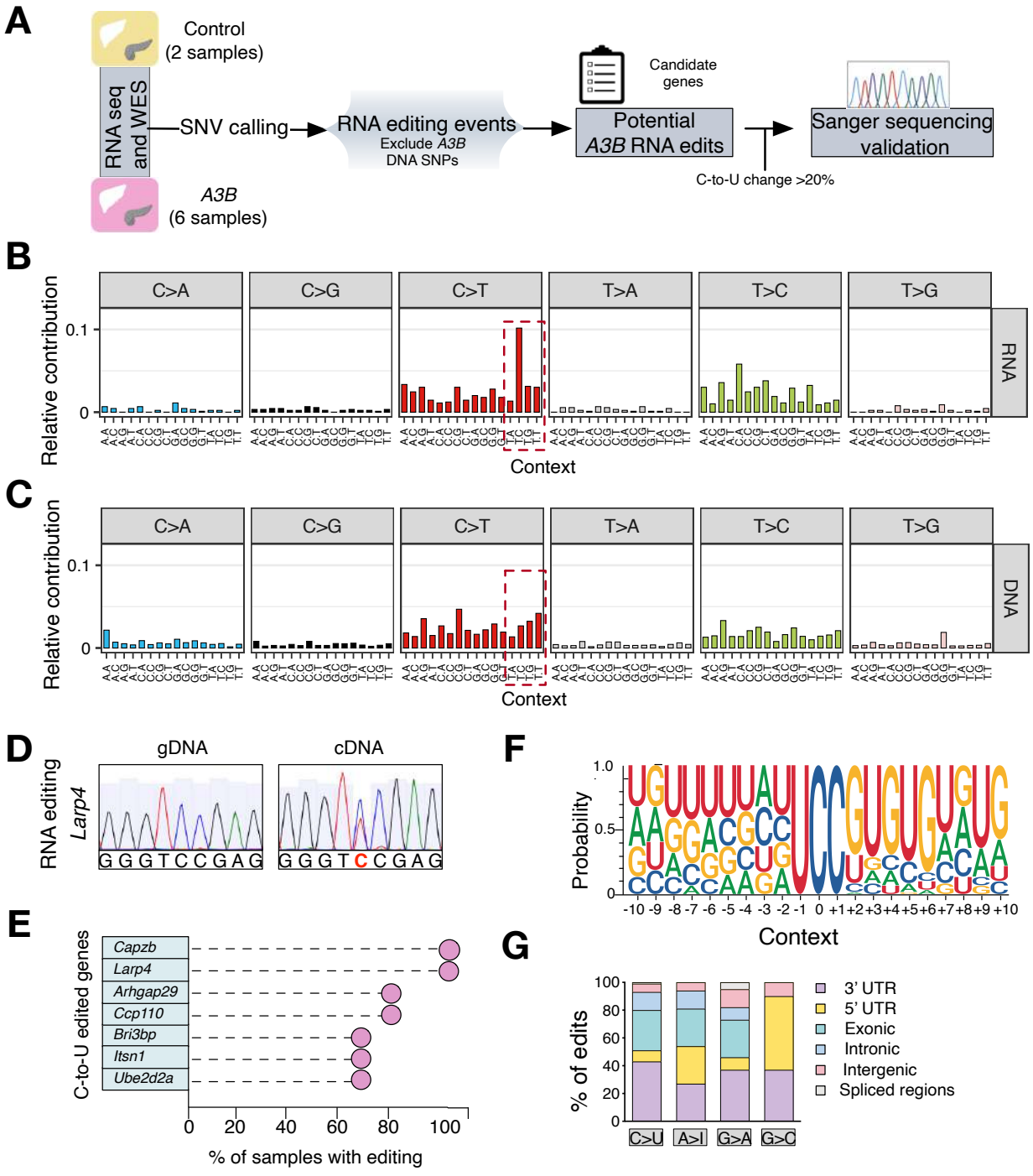

Figure 30: **RNA editing by A3B in liver tissues**

(**A**) Schematic of the pipeline used to call RNA-editing events in liver and pancreatic samples. (**B**) Trinucleotide mutation profiles for all base substitutions at the RNA level in livers from A3B mice. (**C**) Trinucleotide mutation profiles for all base substitutions at the DNA level in livers from A3B mice. (**D**) Sanger sequencing chromatogram indicating an example of A3B-driven RNA editing in A3B livers. (**E**) Lollipop plots indicating the percentage of mice having C-to-U editing in targets selected for RT-PCR and Sanger sequencing experimental validation (n=6). (**F**) Logo representing the sequence context surrounding the C-to-U editing events in 5'-UCC edits in liver. (**G**) Location of the editing sites by type of base substitution in A3B livers.

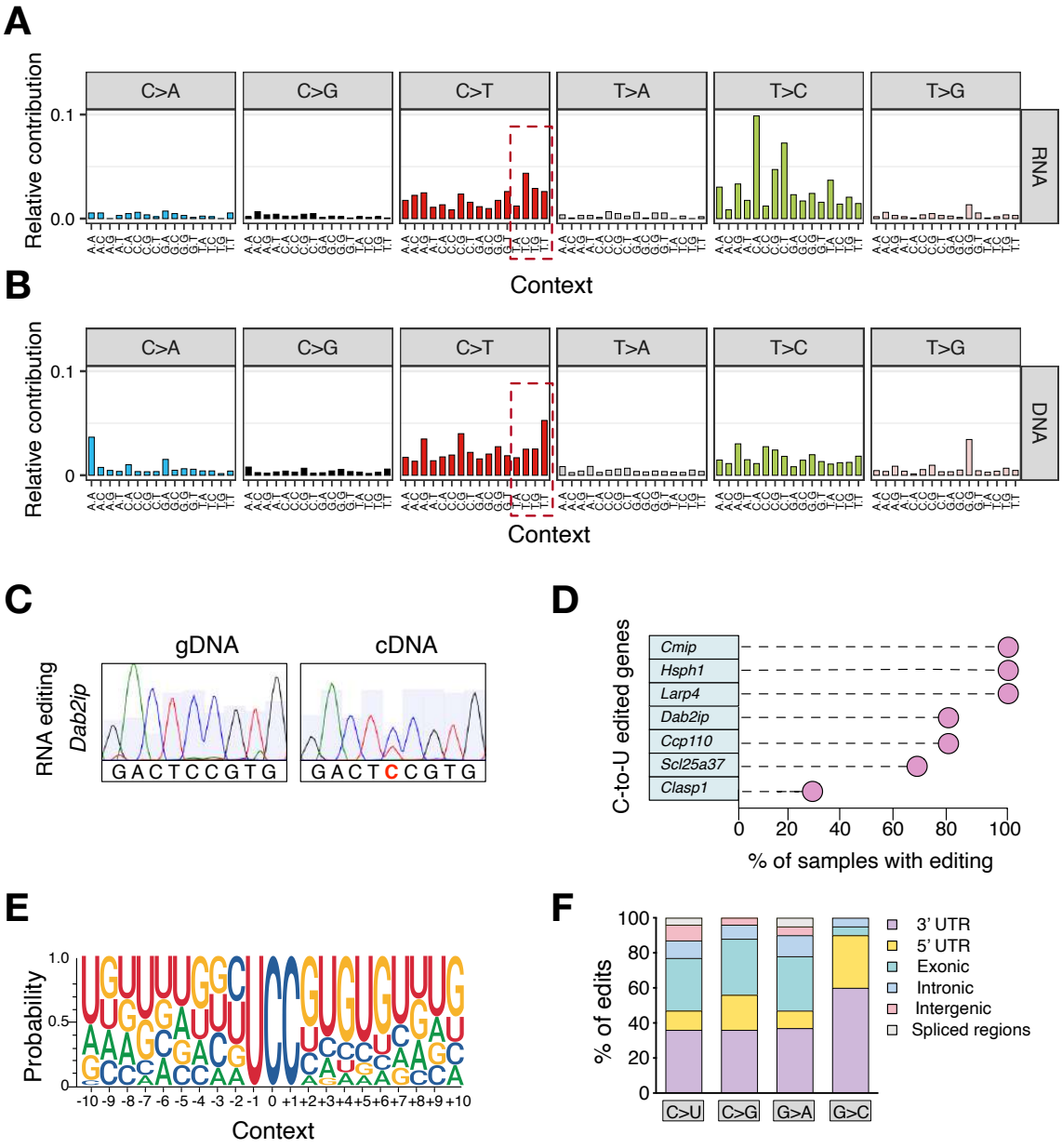

Figure 31: **RNA editing by A3B in pancreas tissues**

(**A**) Trinucleotide mutation profiles for all base substitutions at the RNA level in pancreas from A3B mice. (**B**) Trinucleotide mutation profiles for all base substitutions at the DNA level in pancreas from A3B mice. (**C**) Sanger sequencing chromatogram indicating an example of A3B-driven RNA editing in A3B pancreas. (**D**) Lollipop plots indicating the percentage of mice having C-to-U editing in targets selected for RT-PCR and Sanger sequencing experimental validation (n=6). (**E**) Logo representing the sequence context surrounding the C-to-U editing events in 5'-UCC edits in pancreas. (**F**) Location of the editing sites by type of base substitution in A3B pancreas.

2.11. Endogenous APOBEC and ADAR enzymes are not responsible for the observed RNA editing

Our findings suggest that overexpression of A3B causes an increase in RNA editing events happening in the UCC context. However, a direct connection between A3B activity and the edits was still missing. Mice contain endogenous deaminases that could potentially be

responsible for these edits. To determine if additional enzymes were accountable for the reported editing events and phenotype, Dr. Rafail Tasakis measured the endogenous expression levels of Apobec (Aicda, Apobec1, Apobec2, Apobec3) and Adar (Adar, Adarb1, and Adarb2) genes in liver samples using RNA-seq data. The expression levels of these genes were comparable across samples with and without A3B overexpression, proving it unlikely that the RNA editing events were caused by the activity of one of these enzymes (Figure 32A). Particularly, the focus was set on APOBEC1, since it is a well-established RNA editing enzyme in mouse livers. Since Apobec1 mRNA expression levels were unchanged, I wondered whether A3B overexpression could interfere with the functioning of endogenous APOBEC1. A limiting step in RNA editing by APOBEC1 is the formation of the editosome complex which requires the binding of APOBEC1 to its cofactors: RBM47 and A1CF. To first address, if APOBEC1 activity was altered, Dr. Rafail Tasakis analyzed the expression of APOBEC1 cofactors and found that neither Rbm47 nor A1cf mRNA expression was altered in A3B livers versus controls (Figure 32B). Next, well-known Apobec1 editing targets (Blanc et al., 2014) were examined and found no significant variations in the editing frequencies from the majority of Apobec1 targets. However, the editing of Apobec1 main target, ApoB transcript, was

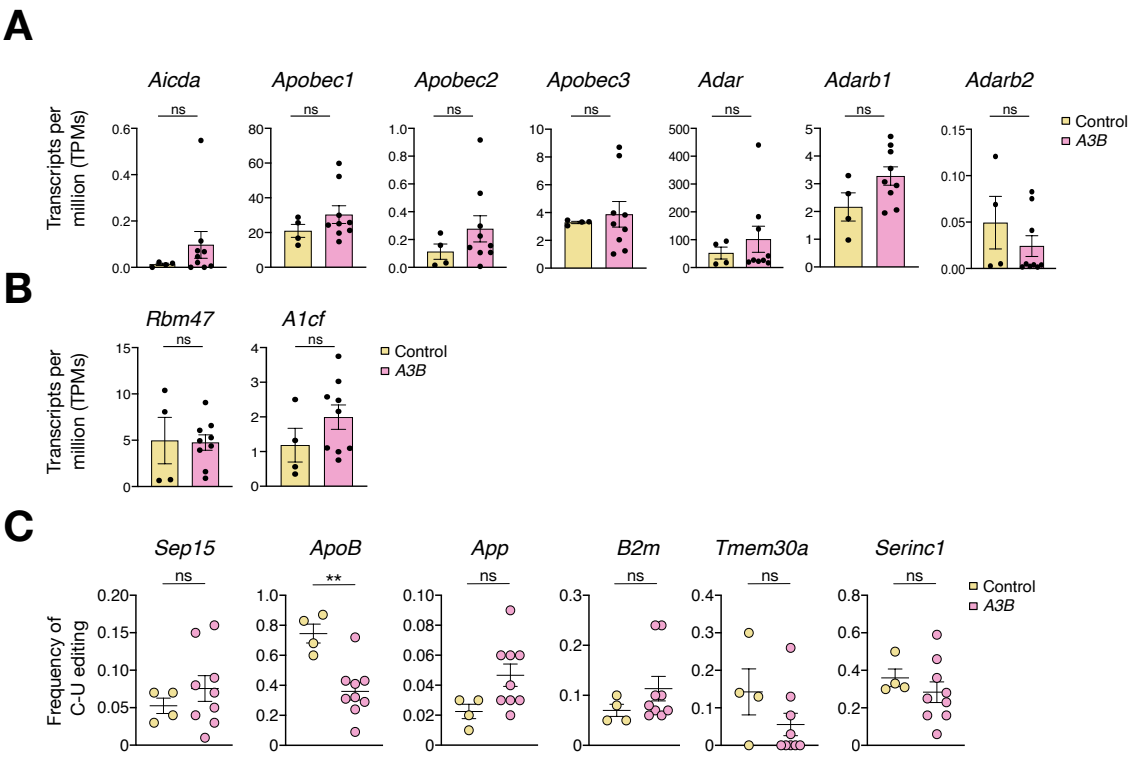

Figure 32: **Endogenous expression of Apobec and Adar enzymes, Apobec1 cofactors and frequency of Apobec1 editing**

(**A**) Expression levels expressed in transcripts per million (TPMs) of the different *Apobec* and *Adar* family members. (**B**) Expression levels expressed in TPMs of the *Apobec1* cofactors. (**C**) Frequency of *Apobec1* editing in well-known target sites. All panels: Data obtained from *A3B* and control liver samples from RNA-seq data (controls, n=4; A3B, n=9; each dot represents one mouse). Data are expressed as means ± SEM.

decreased by half in A3B livers compared to controls (Figure 32C). Since Apobec1 proved decreased editing activity in its primary target ApoB, the newly observed RNA editing events were most likely a direct result of A3B overexpression and not an impact of Apobec1 deamination.

2.12. Apobec1 is not responsible for the editing events in A3B mice

To discard Apobec1 from being responsible of the editing, I next crossed A3B mice with Apobec1 knockout animals (Hirano et al., 1996) (Figure 33A). As expected, *A3B/Apobec1-/-* mice died shortly after doxycycline administration (6-11 days) suggesting that the toxic effect of A3B is independent from Apobec1 expression (Figure 33B). *A3B/Apobec1-/-* mice expressed A3B at similar levels as A3B mice, and A3B deaminase activity was unaffected by Apobec1 deletion (Figure 33C and D). Importantly, recurrent RNA editing events were validated and present in the livers of *A3B/Apobec1-/-* mice (Figure 33E). These findings indicate that A3B, and not endogenous Apobec1, is accountable for the observed RNA editing activity.

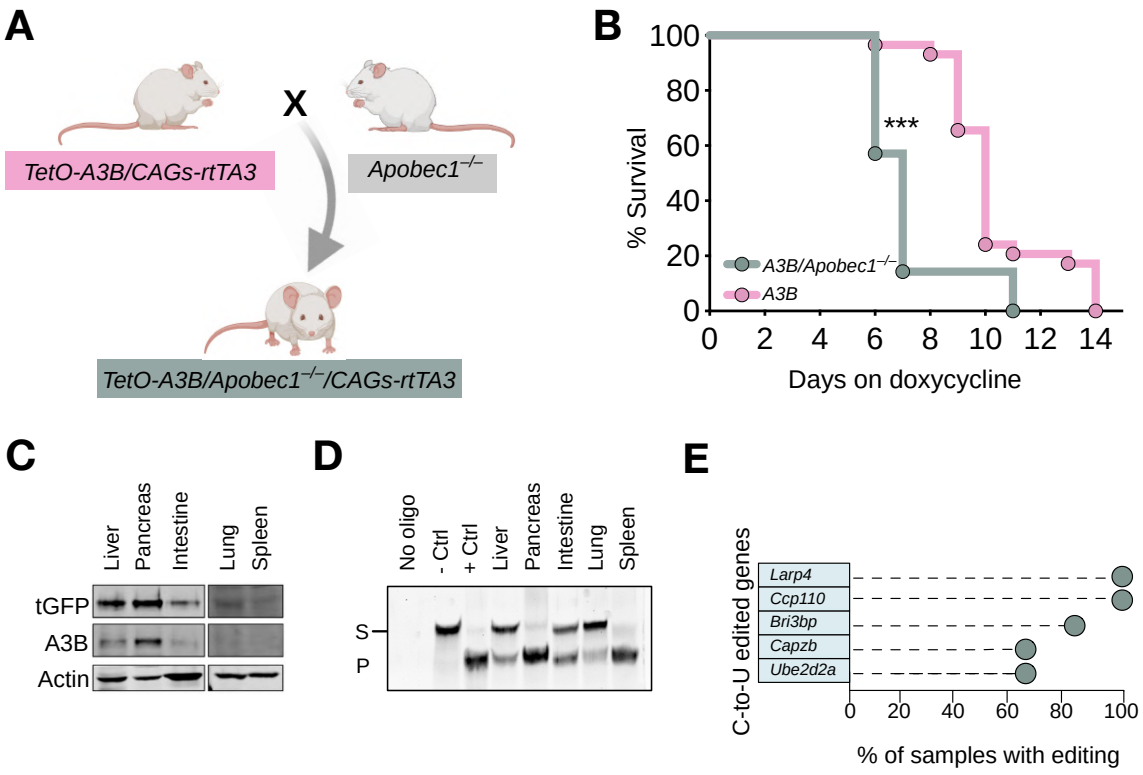

Figure 33: **Loss of Apobec1 has no effect on A3B editing activity**

(**A**) Breeding strategy to obtain *TetO-A3B/Apobec1$^{-/-}$/CAGs-rtTA* mice. (**B**) Percentage of survival from *A3B/Apobec1$^{-/-}$/CAGs-rtTA* (n=6) and *A3B/CAGs-rtTA* (n=12) after doxycycline (**C**) Immunoblot showing A3B and tGFP levels in the indicated tissues from *A3B/Apobec1$^{-/-}$/CAGs-rtTA* mice after doxycycline treatment. Actin was used as loading control. (**D**) Deamination activity assay in the indicated tissues from *A3B/Apobec1$^{-/-}$/CAGs-rtTA* mice after doxycycline treatment. (**E**) Lollipop plots indicating the percentage of mice having C-to-U editing in A3B-edited genes performed by RT-PCR and Sanger sequencing validation (n=6). Data were analyzed by log-rank (Mantel-Cox) test, *** p<0.001.

2.13. Continuous APOBEC3B expression is required for RNA editing

RNA molecules are labile and therefore RNA editing is a passenger and dynamic process. A recent study showed that RNA editing could be used as a predictor of ongoing deaminase activity (Jalili et al., 2020). Therefore, A3B edits should only be detected when A3B is expressed. As the doxycycline system can turn off transgene expression, I could study whether continuous expression of A3B is required to detect RNA edits. Mice were fed with doxycycline for 4 days, followed by doxycycline removal to halt A3B expression and liver samples were

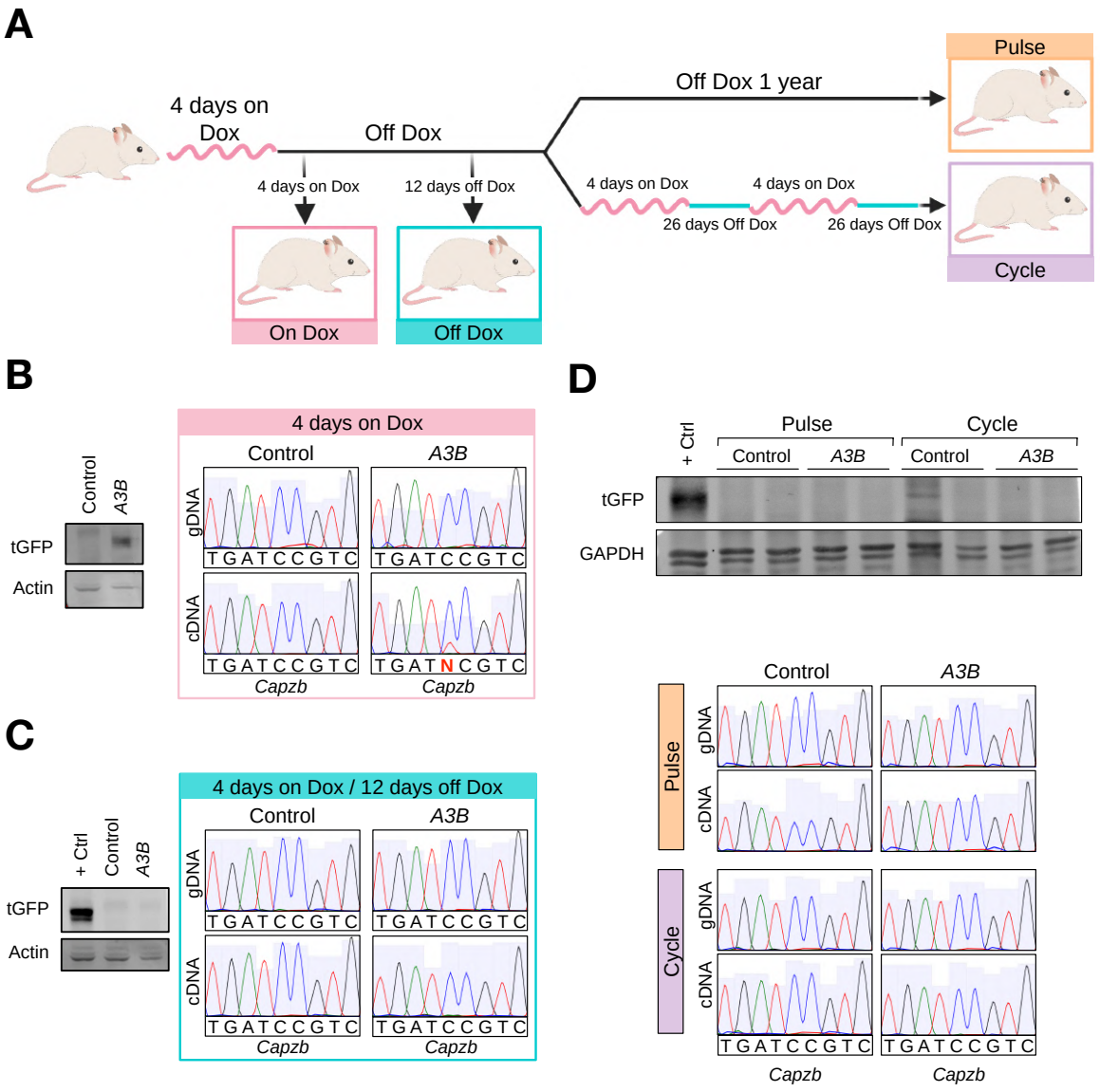

Figure 34: **Continuous A3B expression is required to detect editing**

(**A**) Schematic representation of the strategy used to study whether A3B expression is crucial for RNA editing detection. (**B**) (**C**) and (**D**) Immunoblots showing A3B levels in liver tissues from A3B mice. Anti-actin or Anti-GAPDH were used as loading controls. Example of Sanger sequencing chromatograms from the same livers for the A3B-driven edited positions validation. (**B**) Mice 4 days after doxycycline administration. (**C**) Mice on dox for 4 days and placed back on normal diet for 12 days. (**D**) Mice that received a pulse of A3B expression (4 days dox and up to a year on normal diet) or expressing A3B in a cycle manner (4 days dox-26 days off dox/monthly). Samples were collected at experimental end point (1 year).

collected at defined time points. First, liver samples were analyzed 12 days after doxycycline withdrawal. Second, after 4 days on doxycycline, mice received normal food until the end of the experiment (1 year). Third, mice expressed A3B in cycles (4 days on dox plus 26 days off dox) every month until the end of the experiment (1 year) (Figure 34A). We observed that 4 days of doxycycline administration were sufficient to increase A3B expression and, as a result, induce A3B-driven RNA edits (Figure 34B). Interestingly, 12 days after doxycycline removal stopped A3B expression and A3B-driven RNA edited positions were not detectable (Figure 34C). Accordingly, mice expressing A3B in a pulse or a cycle manner showed no expression of A3B and no detectable RNA editing (Figure 34D). These findings together show that A3B must be continuously expressed at high levels in order to detect its RNA editing activity.

2.14. A3B-driven RNA edits can be detected *in vitro*

RNA editing by APOBEC3s has been mainly detected in immune cells (Sharma et al., 2015, 2019; Sharma, Patnaik, Taggart, et al., 2016). Pancreas and liver tissues where A3B edits were detected showed signs of inflammation and probably an increase in immune cell populations. As whole tissue lysates were submitted for sequencing, I could not conclude which cell population had the ongoing RNA editing activity. Therefore, I wondered whether A3B-induced RNA editing was only restricted to immune cell types. To answer this, I tried to recapitulate A3B-induced editing *in vitro* by overexpressing A3B in MEFs. After 72 hours on doxycycline, DNA and RNA were extracted from cell pellets (Figure 35A). Targeted validation of A3B-driven edits confirmed that A3B overexpression *in vitro* can induce editing, suggesting that A3B editing is not restricted to the immune population (Figure 35B).

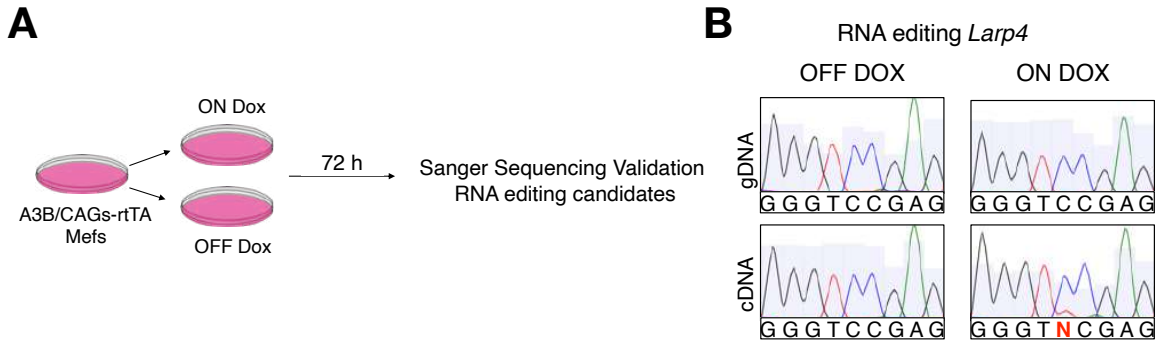

Figure 35: **Overexpression of A3B in MEFs induces RNA editing**
(**A**) MEFs obtained from *A3B* mice were treated with and without Dox for 72 hours. DNA and RNA were extracted from cell pellets for Sanger Sequencing validation of the recurrent A3B-driven edits. (**B**) Example of Sanger sequencing chromatograms from the A3B MEFs treated with and without Dox.

2.15. Generation of A3B-E255A mutant ES cells

To demonstrate that the RNA editing events are a consequence of A3B deaminase activity I attempted to generate a transgenic mouse model carrying the catalytic inactive A3B transgene. It is essential to demonstrate that these editing sites are dependent on A3B activity and absent when the A3B catalytic mutant is expressed.

According to certain studies, A3B is often present in a closed conformation that probably blocks the substrate from entering the active site pocket. This closed conformation is stabilized by the interaction between loops 1 and 7 in the CTD domain. Both the enzymatic activity and the dinucleotide selectivity of the target sequence depend on these loops. When ssDNA is bound to A3B it triggers a conformational change to an open conformation of the active site allowing the entry of the target cytosine into the active site pocket (Hou et al., 2018; Shi, Demir, et al., 2017). Changes in the aminoacid sequence in loop 1, particularly at the Glutamic acid E255 residue, are critical for A3B catalytic activity (Siriwardena et al., 2015). Taking this into consideration, I utilized the tetracycline-regulated A3B-tGFP construct used to generate the A3B mice and turn it into an A3B-tGFP catalytic mutant vector. The A3B inactive vector was created by site-directed mutagenesis to serve by replacing the glutamic acid in residue 255 by an alanine (E255A). Prior to generating the ES cells, the A3B mutant construct was tested in HEK293-T cells (Figure 36A). HEK293-T cells containing the rtTA system were transiently transfected with the A3B-E255A plasmid and treated with doxycycline for 24 hours. Similar A3B levels were found in HEK cells expressing the WT or the mutant A3B constructs (Figure 36B and C). In order to confirm that A3B-E255A abolished any deaminase activity, I used whole protein extracts from A3B-expressing HEK cells and performed single-stranded DNA C-to-U activity assays. HEK cells transfected with the mutant A3B proved to be catalytic inactive with no deaminase activity (Figure 36D).

Next, to generate the mutant A3B transgenic mice I followed the same strategy used for making the A3B WT animals. The ES cells used for generating the transgenic mice contain frt recombination sites located in the *Collagenase I* locus (KH2). Similarly, the mutant A3B-E255A construct carries frt sites flanking the transgene sequence. Electroporation of mutant A3B-E255A and a flipase-containing vector into KH2 ES cells allowed the recombination and integration of A3B-E255A into the *collagenase I* locus. After antibiotic selection, ES cell clones were picked and expanded. Genotyping showed that 100% of the selected clones had inserted the A3B-E255A transgene (Figure 36E). To check A3B expression levels, single ES clones were treated with doxycycline for 24 hours. Western blot against A3B showed low protein levels in all the clones tested (Figure 36F and G). A3B protein might be diluted since ES cells grow on top of feeder cells that do not have A3B expression. On the contrary, while single ES

cell clones treated with doxycycline had increased A3B mRNA levels, the same clones without doxycycline had undetectable A3B expression, suggesting that transgene expression was not leaky (Figure 36H).

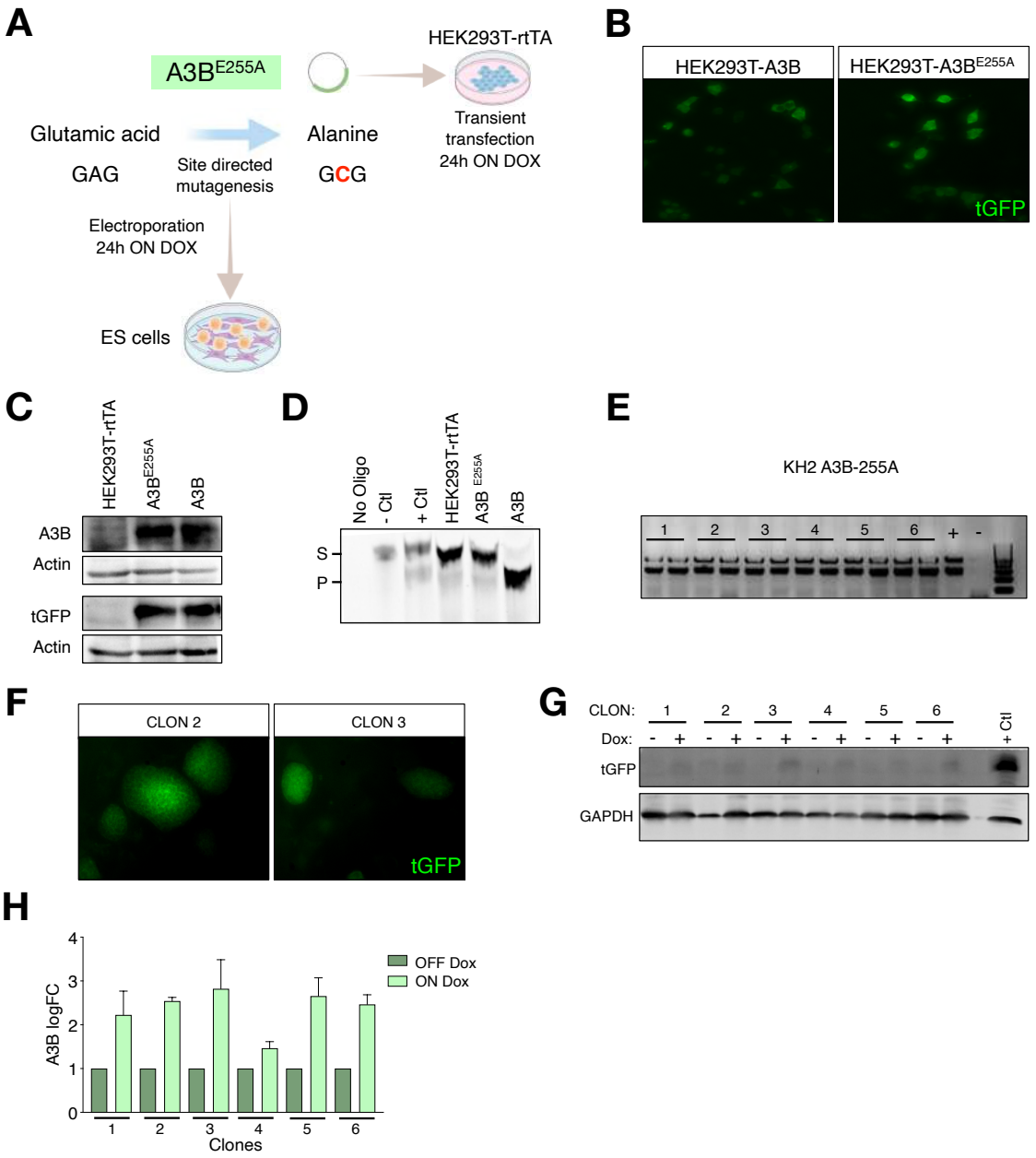

Figure 36: **Generation of A3B-E255A mutant ES cells**

(**A**) Cloning strategy used to create and validate A3B-E255A construct to generate A3B mutant ES cells. (**B**) Endogenous tGFP fluorescence in HEK293T cells carrying A3B or A3B-255A treated with doxycycline for 24 hours. (**C**) Immunoblot showing A3B-tGFP levels in HEK293T cells carrying A3B or A3B-255A treated with doxycycline for 24 hours. Actin was used as loading control. (**D**) Deamination activity assay in HEK293T cells carrying A3B or A3B-255A treated with doxycycline for 24 hours. (**E**) Agarose gel picture from KH2 A3B-E255A PCR products of single ES clones (**F**) Endogenous tGFP fluorescence in single ES cells clones treated with doxycycline for 24 hours. (**G**) Immunoblot showing A3B-tGFP levels in single ES cells clones treated with and without doxycycline for 24 hours. GAPDH was used as loading control. (**H**) A3B mRNA levels from single ES cells clones treated with and without doxycycline for 24 hours. 18S and Actin were used as house keeping genes for normalization. Data are expressed as means ± SEM.

2.16. A3B-driven RNA editing is deaminase dependent

Positive ES cell clones were injected into developing blastocysts and transferred to pseudo pregnant females (Figure 37A). Once *A3B-E225A/Rosa26-rtTA* transgenic mice were born, mice carrying only the A3B-E255A transgene were crossed with *CAGs-rtTA3* mice to achieve strong expression of the transgene. I did an initial characterization to check the expression and functionality of the A3B-E255A transgene. Similar to A3B WT mice, A3B-E255A transgene is strongly expressed in the liver and pancreas, with moderate levels in the intestine, whereas the lung and the spleen contain only modest levels of this protein (Figure 37B and C). In order to confirm that A3B-E255A did not show deaminase activity, I used soluble protein extracts from A3B-E255A-expressing tissues and performed single-stranded DNA C-to-U activity assays. None of the tissues demonstrate deaminase activity (Figure 37D). Surprisingly, 8 days after doxycycline treatment mice died. This result indicates that A3B-induced lethality is independent of its deaminase activity. To determine whether RNA editing activity was deaminase dependent, I selected the recurrent RNA editing events and validated them in the livers of *A3B/E255A* mice. No C-to-U changes were detected in any of the 11 positions examined, suggesting that RNA editing activity requires a functional deaminase domain (Figure 37E).

Taken together, these results strongly suggest that A3B functions need to be further explored. Initially, it was thought to only have deaminase-dependent mutagenic activity. This is the first evidence that A3B also acts as an RNA editing enzyme and in addition, acute expression induces lethality not associated with its deaminase activity. These results highlight the importance of expanding our knowledge of A3B functions and consequences.

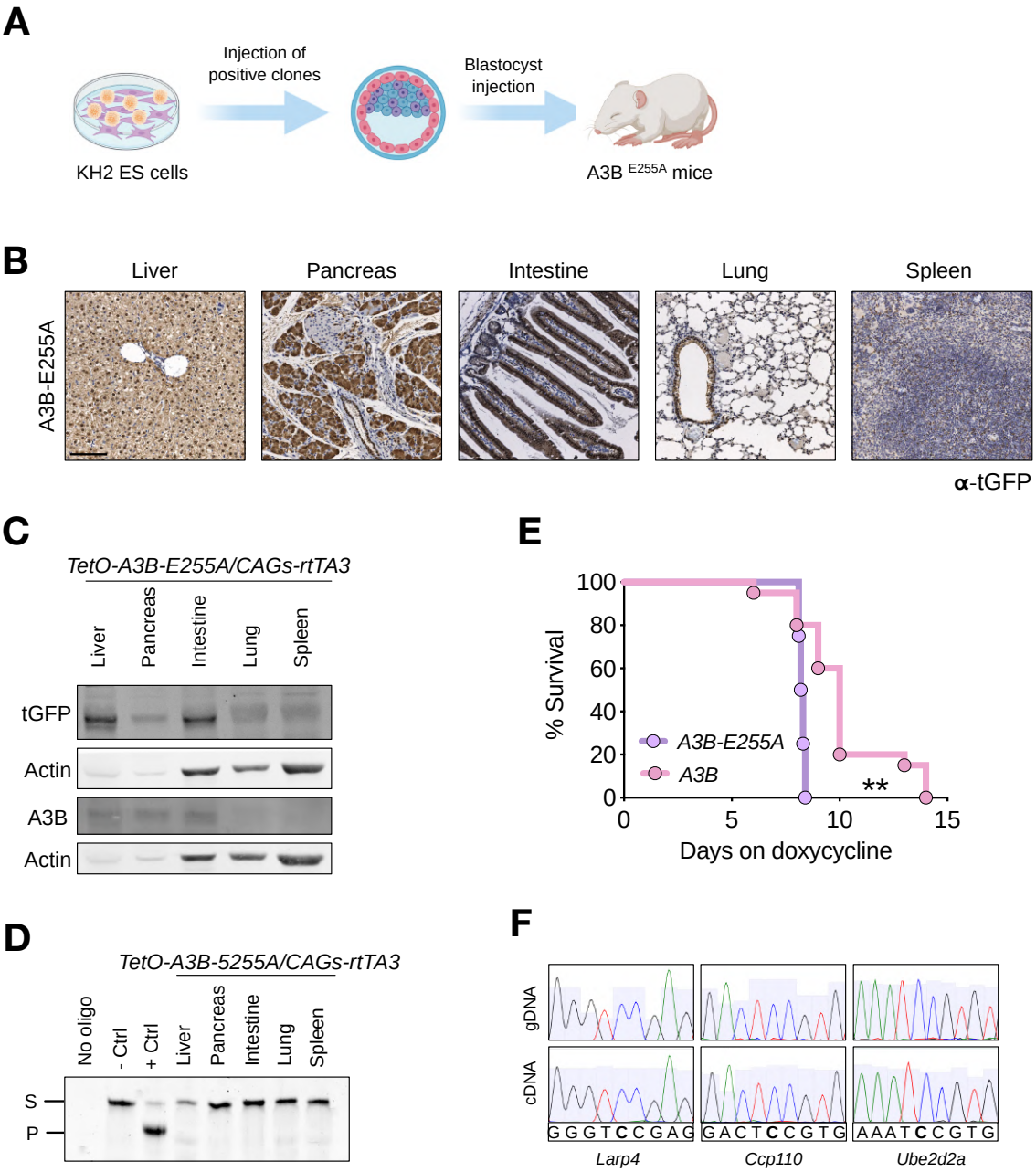

Figure 37: Characterization of A3B-E255A mice

(**A**) Scheme of generation of A3B-E255A mutant transgenic mice (**B**) Immunohistochemistry of tGFP in the indicated tissues from *TetO-A3B-E255A/CAGs-rtTA* fed with Dox for 8 days. Scale bar: 100 µm. (**C**) Immunoblot showing A3B-tGFP levels in the indicated tissues from *TetO-A3B-E255A/CAGs-rtTA* mice fed with Dox for 8 days. Actin was used as loading control. (**D**) Deamination activity assay in the indicated tissues from *TetO-A3B-E255A/CAGs-rtTA* mice fed with Dox for 8 days (S, Substrate; P, Product). (**E**) Percentage of survival from *TetO-A3B-E22A/CAGs-rtTA* (n=4) and *TetO-A3B/CAGs-rtTA* mice (n=12) after doxycycline administration; P<0.001 by Log-rank (Mantel-Cox) test. (**F**) Examples of Sanger sequencing chromatograms from the *A3B-E255A* liver tissues.

Discussion

1. Deciphering the role of A3B in tumor initiation progression and resistance

1.1. A3B expression facilitates tumor initiation

Conventionally, tumor initiation involves the activation of oncogenes and/or the inactivation of tumor suppressor genes (Baylin & Jones, 2011). However, A3B does not match this classical definition, as tumor onset is not a direct consequence of A3B expression. It has been proposed that A3B could function as a cancer enabler since its mutagenic activity facilitates the activation or suppression of tumorigenic driver genes (Harris, 2015). Although several studies have shown how other deaminases, such as AID and APOBEC1, can promote tumorigenesis when overexpressed, there is no clear evidence linking A3B to tumor initiation (Okazaki et al., 2003; Yamanaka et al., 1995). In addition, several studies proposed a model against a role of A3B in tumor initiation, since they claim that APOBEC mutations occur randomly and not at specific targets (Buisson et al., 2019; Venkatesan et al., 2021). The wrong combination of these random mutations could transform a normal cell into a tumorigenic cell, therefore, A3B expression generates a heterogeneous and mysterious scenario with several possible outcomes. The results presented in this thesis show how long-term expression of A3B in mice led to increased tumor formation compared to control littermates, supporting a facilitator role of A3B during tumorigenesis and not simply a consequence of aging. As predicted, A3B overexpression in mice did not follow a predefined pattern and resulted in a broad range of distinct tumors, reflecting the heterogeneity caused by A3B. Importantly, APOBEC mutations have been found in oncogenes such as *PIK3CA* (Henderson et al., 2014), making it crucial to further investigate whether A3B induced tumors contain A3B mutations in driver genes to be able to establish a clear relationship between A3B and tumor initiation.

Recently, Law and colleagues (Law et al., 2020) generated a genetically engineered mouse model that constitutively expressed A3B from the embryonic stage to examine the effect of A3B on tumor development. However, after a few generations, the expression of the transgene was lost. This negative selection was probably due to early A3B-induced mutations that were incompatible with the animal's development and over time, resulted in the loss of transgene expression. In contrast, our approach has the advantage that the A3B transgene can be expressed in a time-controlled fashion (Beard et al., 2006a). Expression of A3B in adult mice showed detectable levels in some tissues, whereas, in tumors, A3B-expressing cells were rare or nonexistent. It is tempting to speculate that once the tumors were formed, A3B

was no longer required and A3B expression was downregulated. This data goes in line with evidence supporting that continuous expression of A3B might render toxicity and be detrimental to cells (Huff et al., 2018; Petljak et al., 2019). Therefore, I propose a model in which A3B is transiently beneficial at the precancerous stage. A3B mutagenesis within a certain threshold would enable cells to gain a mutational combination to become tumorigenic. Cell survival is possible in those cancer cells in which A3B expression does not exceed that threshold, or in which A3B is selected against. It would be important to determine if the silencing of A3B expression is due to the acquisition of mutations in A3B or rtTA transgenes, as previously described (Law et al., 2020; Rowald et al., 2016). Taken all together, this is the first direct evidence for A3B driving tumor initiation.

Recent publications have described that in combination with different oncogenes A3B expression has a detrimental effect on tumor initiation promoting increased mouse survival (Caswell et al., 2022; DiMarco et al., 2021). In contrast, I have shown that A3B in combination with mutant *Kras* and *TP53* loss does not accelerate animal death. One potential reason for this discrepancy is that the *TetO-Kras* model takes longer to develop tumors than the models utilized in the mentioned studies. This additional time could enable the cells to overcome the early deleterious impact of A3B, which was not possible in the aforementioned studies. This theory is consistent with the previously described Rosa26 model, according to which tumor initiation occurs almost two years following A3B expression. In addition, it has been shown that overexpression of the same protein in combination with different oncogenes can have either a tumor-promoting or tumor-suppressing impact (Rowald et al., 2016; Sotillo et al., 2010). Therefore, one possibility could be that the A3B effect might depend on which oncogene is induced.

Finally, the number of mice used for the survival analysis was quite low, and if there were minor differences between groups, there could have not been enough statistical power to detect them.

1.2. A3B activity throughout malignant disease

Throughout the lifetime of a tumor, cancer cells are constantly acquiring *de novo* mutations that could rewire the course of the disease. As tumors develop, they become heterogeneous and selection pressures lead to a bottleneck where only the more advantageous and fitted subclones will survive. Based on these assumptions, A3B mutagenesis could accelerate tumor progression, fueling the appearance of aggressive subclones. In fact, human tumors that express high levels of A3B have been associated with poor patient survival (Law et al., 2016; Periyasamy et al., 2021). In line with this, A3B overexpression confers resistance in mice

harboring mutant EGFR-driven lung tumors after treatment with tyrosine kinase inhibitors (TKIs) (Caswell et al., 2022).

My results show that the survival of Kras mutant mice is not affected by A3B overexpression, although the triple transgenic mice carried larger tumors, significantly impacting the overall tumor volume. How animals with higher tumor load survive the same as animals with less tumor burden is not intuitive. However, this unexpected result has been previously seen in a study in which loss of SMARC4 in the KP model results in a similar tumor burden despite the fact that the animals died at an earlier time point (Concepcion et al., 2021). Similarly, A3B expression in an EGFR mutant lung cancer model had no effect on mouse survival but reduced the overall tumor volume (Caswell et al., 2022). Unfortunately, the authors did not provide an explanation for these unexpected results. The contradictory results of my study could be explained by a model in which A3B overexpression has a negative effect during early stages of tumor growth but accelerates tumor progression in the later stages. Due to the selection of favorable A3B-induced mutations, tumor-initiating cells in TKA mice have probably greater fitness than those in TK animals. Consequently, although malignant growth begins later than in TK mice, TKA cells might have greater proliferation rates, resulting in larger tumors in a shorter amount of time. In accordance with this hypothesis, monitoring tumor growth in mice revealed that although TK tumors grow at a constant rate, TKA tumors first grow slowly before undergoing a fast and exponential expansion.

On the contrary, no differences in tumor burden were found in KPA animals compared to KP mice. Additional p53 loss adds another layer of complexity, which will be discussed in depth in the next sections. As previously described, the KP model gives rise to more aggressive tumors that develop faster when compared to the TK model (Jackson et al., 2005). This rapid progression leaves no time for the KPA cancer cells to reach the exponential growth phase. In fact, endpoint tumors in KPA mice proliferate more compared to KP tumors. Overall, our findings support a scenario in which persistent expression of A3B is initially detrimental to tumor cells but eventually enables the acquisition of features that increase cell fitness. In order to find more evidence to support this hypothesis, I am currently comparing tumor development of tumors in TKA versus TK mice at different time points. Future directions will also include the induction of A3B once the tumors are formed, mimicking what has been described for lung cancer in humans (Swanton et al., 2015; Venkatesan et al., 2021).

A major drawback of using GEMMs in cancer research is that, unlike human cancers, mouse tumors do not accumulate a high number of mutations throughout development (McFadden et al., 2016). It is reasonable to believe that an A3B overexpressing GEMM would provide a closer understanding of human cancers. In line with this concept, Kras-driven lung tumors together with A3B overexpression acquire features of advanced disease not commonly

observed in previous mouse models. In support of these results, A3B expression has been described to develop high-grade lung tumors in an EGFR mutant mouse model (Caswell et al., 2022). Therefore, our A3B mouse model has proved to serve as a preclinical tool that better recapitulates tumor progression in humans. Still, whether our model induces clonal and subclonal mutations in tumors needs to be determined.

1.3. Leveraging APOBEC3 activity for clinical benefit

The rapid evolution of targeted therapies over the last decade has dramatically improved the clinical benefit and outcome for NSCLC patients. Although targeted therapies have benefited other well-known oncogene-dependent NSCLCs, such as those driven by EGFR and ALK mutations, KRAS has been considered to be an undruggable target until recently. A new era in precision oncology has resulted in the identification of potent inhibitors against different KRAS mutations (Molina-Arcas et al., 2021). Despite these drugs having shown outstanding response rates, many patients do not respond and others develop resistance that renders cancers lethal (J. Luo et al., 2022). Nonetheless, the recent development of immunotherapies, which unleash potent anti-tumor immune responses, has revolutionized the treatment of NSCLC, leading to sustained patient responses (Borghaei et al., 2015). Therefore, to assess clinical benefit, an urgent need is to identify new tumor vulnerabilities and to find different possibilities for KRAS treatments.

Overexpression of A3B in lung cancer has been linked with favorable responses to immunotherapies (S. Wang et al., 2018). Emerging literature supports A3B-mutagenesis as a source of tumor neoantigen production, driving immune activation (Driscoll et al., 2020; Faden et al., 2019). To understand the clinical benefits of using combinational therapies in the treatment of KRAS-mutant lung cancers, a recent study used the KP model in combination with A3B overexpression (Boumelha et al., 2022). They attempted to increase the number of mutations in these tumors, which would lead to the formation of neoantigens capable of stimulating antitumor immune responses. Despite increased lymphocyte infiltration, they were unable to trigger tumor recognition by the immune system. This might be due to the variability in A3B expression within tumors, the subclonal nature of neoantigens, or the lack of mutations generated in this mouse model. On the contrary, our model would allow for the selection of clonal neoantigens, since tumor development evolves over a longer period, and A3B expression in tumors is higher. Moreover, I have described how A3B overexpression led to inflammation and T cell infiltration in the pancreas. Therefore, future efforts should focus on determining whether immune infiltration is also present in TKA tumors and gaining mechanistic insights to improve the effectiveness of new therapies in KRAS mutant-lung malignancies.

On the other hand, several studies have associated APOBEC mutagenesis with drug resistance (Law et al., 2016; Sieuwerts et al., 2014). In addition, lung cancer patients who acquired resistance to TKIs had shown APOBEC-related mutations in the EGFR and ALK genes (Caswell et al., 2022; Isozaki et al., 2021). The idea behind targeted therapy is that tumor maintenance is dependent on the expression of the initiating oncogene. Accordingly, KRAS lung tumors are oncogene-dependent, and inhibition of KRAS results in complete tumor regression (Fisher et al., 2001; Sotillo et al., 2010). The data presented here show that A3B expression in KRAS-driven lung tumors does not affect tumor regression. However, this study will continue to investigate whether A3B disrupts oncogene addiction, by conferring the tumor increased adaptive capabilities to relapse.

1.4. Crosstalk between P53 and A3B expression

Inactivation of p53 in cancer has been associated with a higher mutational burden enriched in the APOBEC signature (Periyasamy et al., 2021; Skoulidis & Heymach, 2019). It is tempting to speculate that under the loss of p53, cells will fail to repair A3B-induced mutations. Given p53's role in preserving genomic integrity, I hypothesized that its loss would have a major impact when combined with A3B overexpression. However, correlating with a recent study, A3B overexpression in p53-deficient mice had no impact on survival or tumor burden (Caswell et al., 2022). These findings imply that continuous A3B expression is tolerated in Kras mutant mice in the absence of p53. In contrast, TKA end point tumors, which had an increased tumor volume in comparison to TK tumors, showed downregulation in the p53 pathway. TKA tumors likely acquire mechanisms to inactivate the p53 pathway to overcome the potentially harmful effects of A3B during tumor initiation. In fact, it has been reported that the loss of p53 is used as a mechanism to tolerate the DNA damage induced by A3B-mutagenesis (Nikkilä et al., 2017). Importantly, this work and work from others highlight that inactivation of p53 signaling is positively selected in A3B-expressing tumors as a mechanism to bypass the toxicity induced by continuous A3B expression.

1.5. Is A3B the good or the bad guy?

The results presented in this thesis highlight the importance of A3B during tumor initiation progression and therapy response. Therefore, A3B expression and mutagenesis in cancer need to be further studied to determine a framework for future diagnostic and therapeutic strategies. Some studies have focused on developing small molecules to inhibit A3B and prevent off-target harmful mutations (Grillo et al., 2022). This hypomutation strategy would slow the evolution of aggressive tumors and prevent escape from therapy. On the contrary, a second approach would be hypermutation, which involves amplifying APOBEC's mutagenesis

to exacerbate the detrimental effect of A3B and render lethality to cancer cells (Venkatesan et al., 2018). Paradoxically, increased APOBEC expression helps cancers by triggering immune responses and making tumors more susceptible to immunotherapies. There is little doubt that A3B can be a double-edged sword for tumor cells, and research must figure out how to use it to its advantage.

2. Acute expression of human APOBEC3B in mice causes lethality and induces RNA editing

2.1. Has the RNA editing activity of A3B been overlooked?

Although the incidence and significance of APOBEC3s DNA mutagenesis in cancer are now being determined, the same is not true for APOBEC3s editing the RNA. The high similarity among all APOBEC enzymes in the family makes it logical to consider more members as possible RNA editors. A3A, which is highly homologous and evolutionary close to A3B, has shown RNA editing activity (Jalili et al., 2020; Sharma et al., 2015), supporting the notion that A3B could share these traits and serve as an RNA editing enzyme as well. At the same time, the 90% similarity between both enzymes has made it difficult to establish direct cause-and-effect relationships. Notably, A3A is biochemically more active than A3B, which may explain why A3A has been proposed as the responsible enzyme for the majority of events studied (Byeon et al., 2016). Recent research has shown that A3A and A3B have distinct intrinsic preferences for deaminating DNA substrates (Chan et al., 2015; Jarvis et al., 2022); however, this cannot be extended to RNA. It was initially described that A3A prefers to deaminate YTCA motifs while A3B favors the RTCA motif. However, it has now been shown that although A3A is more likely to deaminate at the YTCA motif, A3B can also do so to some extent (Jarvis et al., 2022). In addition, A3A but not A3B has been found to have a preference for substrate sites in DNA stem loops (Buisson et al., 2019). Based on the distinct sequence and structural preferences of A3A and A3B, editing sites in human cancers were attributed to A3A activity, most likely overlooking the possibility that A3B was responsible for some of these events. Moreover, the problem when looking at RNA editing events in human samples would be to distinguish to whom to attribute these edits. They could likely be performed by any APOBEC3 family member and therefore difficult to attribute them to A3B. Hence, the mouse, containing a single Apobec3 enzyme with no reported editing activity, is an ideal model organism that enabled the first identification of A3B as an RNA editing enzyme.

Another possibility for why A3B has not previously been identified as an RNA editing enzyme could be the challenge of capturing the labile editing landscape. Unlike DNA mutations, RNA editing is a dynamic process that leaves no permanent trace; RNA edits vanish

as soon as the relevant enzymes are no longer expressed. In line with this, the existence of APOBEC mutational signatures in human cancers does not necessarily correspond with A3A/B expression levels (Jalili et al., 2020; Petljak et al., 2019). In fact, clonal DNA sequencing indicated that A3A and A3B may be expressed in episodic bursts (Petljak et al., 2019). The findings given in this thesis demonstrate that continuous A3B expression is required to detect A3B editing activity. Therefore, as patient samples are collected at a certain timepoint and represent a snapshot of the tumor, it is challenging to capture the editing scenario in human cancers. Until now, detection of A3B editing activity could have been diluted by the fact that not every sample analyzed had high levels of A3B. To determine if A3B is an RNA editor in humans, future studies of human tumors should focus on analyzing samples with high levels of A3B expression.

2.2. Monitoring of A3B RNA editing as a predictor of ongoing activity and therapy

Due to the importance of APOBEC mutagenesis in cancer evolution, current research is focused on developing inhibitors against APOBEC enzymes. However, as discussed in previous sections, it is difficult to detect when these enzymes are active since mutational signatures are not accurate predictors. Therefore, it is crucial to create a strategy for monitoring and assigning particular APOBEC enzymes to ongoing activity. Recently, it was shown that RNA edits can be used as a predictor marker of current A3A activity in human tumors (Jalili et al., 2020). Unlike DNA mutations, RNA editing events correlate with A3A expression. My data also indicates that RNA edits are predictors of A3B expression, as RNA changes are not found if A3B is not expressed. Data from us and others support the idea that RNA edits could be used as predictive biomarkers, determining the best time to treat patients and halting or enhancing APOBEC mutagenesis.

An additional problem would be to determine which APOBEC is responsible for the modifications. There is compelling evidence that each enzyme has its substrate preference. According to the observations made in this thesis, the most commonly altered trinucleotide in the RNA of mice expressing A3B is U<u>C</u>C-to-U<u>U</u>C. In contrast, the majority of A3B-catalyzed DNA mutations occur in TCA and TCT patterns, whereas TCC is significantly disfavored. In addition, I observed that A3B-dependent RNA edits also have a broader sequence motif UCCGUGUG. Similarly, APOBEC1 edited RNA cytosines also appear to be part of a broader specific sequence context (AU-rich). In the case of A3A, it deaminates ssDNA and RNA in R loops from stem-loop secondary structures (Pecori et al., 2022). In line with the observations for A3B, the sequence context is dependent on the substrate deaminated by A3A. The sequence around the UpC motif in RNA stem-loops varies from the sequence surrounding the

TpC motif in ssDNA substrates (Jalili et al., 2020). The structural variations between RNA and DNA substrates could explain why the same enzyme has different sequence preferences. However, only A3-ssDNA complexes have been identified by x-ray crystallography and there is no evident atomic explanation for this divergence (Shi, Demir, et al., 2017). Overall, these findings provide a promising opportunity to further investigate the particular editing context to attribute the ongoing activity to a specific deaminase enzyme.

The biological consequences of A3s-induced editing events on cancer development, progression, and immune response also remain unknown. A recent report identified that breast tumors that were enriched in RNA edits had increased immune activity and better disease outcomes. Potentially, the creation of de novo neoantigens renders tumors to be recognized by the immune system (Asaoka et al., 2019). Intriguingly, the pancreas of A3B-expressing mice exhibit signs of inflammation. Preliminary pathway analysis of the edited genes has shown that several edited genes are involved in immune pathways (data not shown). Still, whether A3B editing results in new coding potential or whether it controls mRNA stability or micro-RNA processing needs further investigation. Therefore, it would be worthwhile to examine the biological effects of A3B-edits and whether the presence of edits can predict tumor immunotherapy response.

2.3. A3B might interfere with Apobec1 activity

Apobec1 is the only family member that shows C-to-U RNA editing activity in mice, being highly active in the liver and the intestine (Blanc et al., 2014). It is possible that the editing events detected in the A3B expressing mice were caused by Apobec1 activity rather than A3B. Initially, RNA sequencing data indicated that Apobec1 expression was not affected compared to control samples. However, Apobec1 editing requires the binding to cofactors and the formation of the editosome complex (Soleymanjahi et al., 2021). No changes in the expression of the main Apobec1 cofactors were found in A3B livers compared to controls. Unlike Apobec1, A3B exhibits RNA binding activity (Xiao et al., 2017); however, it is unknown if A3B requires cofactors to deaminate RNA substrates. Surprisingly, as a result of A3B expression, the editing frequency of Apobec1's main target, ApoB, was reduced. This result may suggest that A3B interferes somehow reducing Apobec1 activity. There could be a competition between Apobec1 and A3B targets and cofactors as well as other regulatory mechanisms still unknown. In addition, the use of an Apobec1 deficient mouse model further confirmed that the editing events were a direct effect of A3B expression. Interestingly, loss of Apobec1 negatively affected the phenotype of A3B-expressing mice. Although Apobec1 deficiency does not cause any abnormalities in the mice in short term (Hirano et al., 1996), these findings suggested that the detrimental effect of A3B is "enhanced" upon the loss of murine Apobec1. It has been

reported that aged Apobec1 deficient mice exhibit elevated atherosclerosis levels (Hirano et al., 1996; Nakamuta et al., 1996). Moreover, differential expression analysis of A3B-expressing livers revealed a significant downregulation in fatty acid metabolism. Therefore, the accelerated lethality could be the result of a catastrophic failure in lipid metabolism.

2.4. Acute A3B expression leads to lethality in a deaminase-independent manner

It has been previously reported that continuous expression of A3B and A3A and accumulation of mutations are toxic for the cells (Akre et al., 2016; Burns et al., 2013; Caval, Suspène, Shapira, et al., 2014; Green et al., 2016; Landry et al., 2011; Nikkilä et al., 2017). The data presented in this thesis consistently support the notion that constant expression of A3B is not well tolerated. There are two possible outcomes for cells expressing A3B, one in which A3B is selected against and the other in which cells acquire additional mechanisms, such as the loss of p53, to counteract the deleterious impact. In our mouse model, acute and sustained expression of A3B in the adult mouse disrupts tissue homeostasis and causes lethality. Although these levels are not compatible with life, this mouse model recapitulates the A3B levels found in human cancers. It is essential to keep in mind that these levels are seen in tumor cells that might have acquired distinct mechanisms to fight the damage caused by A3B. Since our model expresses A3B in the whole body, it damages vital organs that are essential for life. Initially, I believed that cells could not handle a large number of mutations, RNA edits, and chromosomal instability caused by A3B deaminase activity in such a short time. Nonetheless, other studies using mouse overexpression models have shown that high levels of an exogenous protein can result in early death, suggesting that exogenous protein accumulation could be toxic (Cárcer et al., 2018; Rubio et al., 2021).

Surprisingly, ubiquitous overexpression of the catalytic inactive A3B resulted in early lethality, similar to mice expressing wild-type A3B, indicating that the deaminase activity is not responsible for the animals' death. A3B-induced DNA damage has been reported as deaminase-independent, although no direct method to explain this has been described (Chapman et al., 2020). In addition, the expression of mutant A3A has also been described to induce replication stress and DNA damage, resulting in chromosomal instability and activation of the DNA sensing program cGAS–STING (Wörmann et al., 2021). Therefore, severe chromosomal instability could account for the rapid death of these animals. A more comprehensive analysis would be required to clarify whether the mortality of A3B mutant mice is due to A3B-induced damage or the toxicity resulting from protein aggregation.

Observations made in this thesis provide new angles that might help to understand the hypothesis of the “just right” levels of A3B. Tumor cells can make use of A3B-induced heterogeneity to adapt to selection pressures. However, excessive genomic instability in any of its forms causes cell-autonomous death. Consequently, a balance between fatal damage and population diversity generates an ideal range in which A3B activity enhances population fitness.

CONCLUSIONS

1. Deciphering the role of A3B in tumor initiation progression and resistance

Summary of this part of the thesis:

• Low levels of A3B are sufficient to promote tumorigenesis

• A3B expression increases the tumor burden in Kras-driven lung adenocarcinoma

• A3B induces gives rise to more aggressive Kras-driven lung adenocarcinoma

• A3B induces abolishes complete tumor regression after Kras silencing

• A3B-expressing tumors require the inactivation of p53 signaling to overcome the A3B-induced damage

In summary, in this thesis, I have demonstrated that A3B not only facilitates tumor initiation but influences tumor progression. The data here has highlighted the importance of inactivation of the p53 signaling to overcome A3B-induced damage. I expect these findings to serve for further research and expand our understanding of how A3B influences every facet of carcinogenesis.

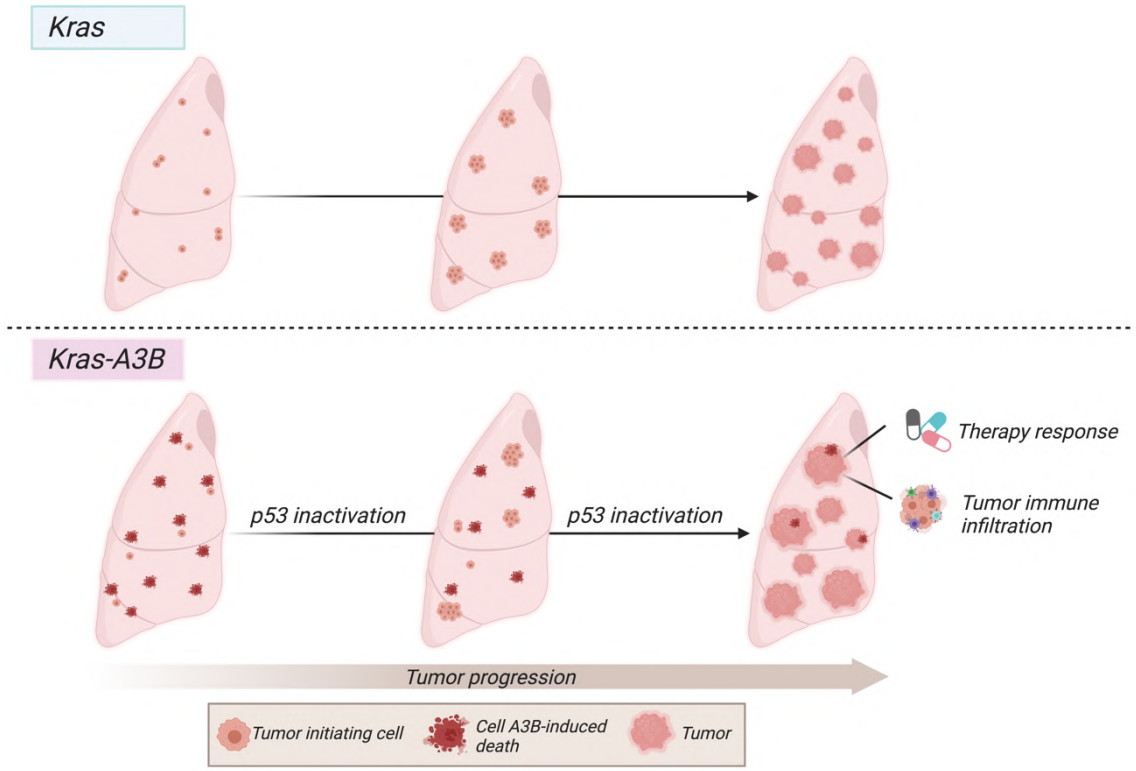

Figure 38: Graphical abstract part 1

Initial A3B-induced damage in Kras-driven lung tumors is compasated by the inactivation of the p53 pathway. In addition, preliminary data suggest that A3B create more aggressive subclones that are no longer dependent in the initiator oncogene for survival.

2. Acute expression of human APOBEC3B in mice causes lethality and induces RNA editing

Summary of this part of the thesis:

- Acute levels of A3B cause lethality *in vivo*
- A3B is an RNA editing enzyme *in vitro* and *in vivo*
- RNA editing by A3B occurs at specific hotspots
- Apobec1 editing activity is influenced by A3B expression
- Continuous A3B expression is required for RNA editing
- A3B-induced lethality is deaminase independent
- A3B RNA editing is deaminase dependent

This work illustrates how elevated levels of A3B dramatically compromise cell and tissue homeostasis and identifies, for the first time, a new function of A3B in editing the RNA. These results highlight the importance of expanding our knowledge of C-to-U RNA-editing events. We expect this model to serve as a valuable preclinical tool to understand the emerging role of A3B as a potent driver of cancer evolution.

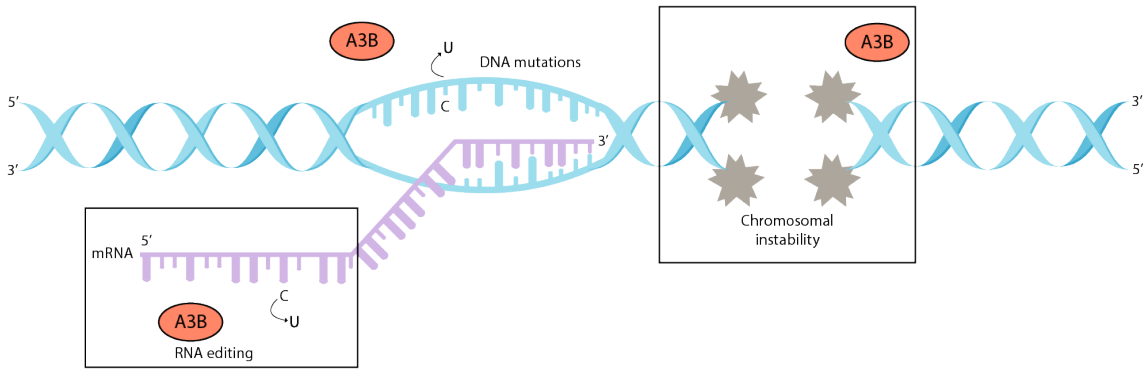

Figure 39: Graphical abstract part 2

Mutagenesis and chromosomal instability induced by A3B have been reported as mechanisms driving diversity and damage in cancer. The data presented in this thesis is the first evidence that A3B is an RNA editing enzyme.

Materials

Table 1: Mouse Alleles	
Strain	Source
A3B (KH2-APOBEC3B-GFP)	Sotillo Lab, DKFZ Transgenic animal facility
A3B-E255A	Sotillo Lab, DKFZ Transgenic animal facility
CAGs-rtTA3	Kindly provided by Prof. Dr. Darjus Tschaharganeh
Rosa26-rtTA	Integrated in the KH2 ES cells
Apobec1-KO	Kindly provided by Prof. Dr. Nina Papavasiliou
TetO-Kras^{G12D} /CCSP-rtTA	Sotillo Lb, (Sotillo et al., 2010)Kindly provided by Prof. Dr Harold Varmus
p53$^{flx/flx}$/LSL-Kras$^{G12D/+}$/LSL-rtTA-mKate	Kindly provided by Prof. Dr. Darjus Tschaharganeh and Prof. Dr. Claudia Scholl

Table 2: Mouse oligonucleotides - Genotyping			
Gene	Primer Name	Sequence	Product length (bp)
KH2	Primer Coll frt A	GCACAGCATTGCGGACATGC	WT: 300 Ki: 500
	Primer Coll frt B	CCCTCCATGTGTGACCAAGG	
	Primer Coll frt C1	GCAGAAGCGCGGCCGTCTGG	
A3B	A3B FW	GCTGGGACACCTTTGTGTACCG	325
	A3B RV	ATCACGTGGCTCAGCAGGTAGG	
Rosa26-rtTA	Common (HET)	AAA GTC GCT CTG AGT TGT TAT	WT: 650 MUT: 340
	Wild type Reverse (WT)	GGA GCG GGA GAA ATG GAT ATG	
	Mutant Reverse (MT)	GCG AAG AGT TTG TCC TCA ACC	
Apobec1	APO1-1	GACTATCCAGATCATGACAGAGC	WT: 600 KO: 250
	APO1-2	GGCCAGCTCATTCCTCCACTCATGAT	
	APO1-3	CCACAGATGGGGGTACCTTGGCCAAT	
TetO-KrasG12D	KrasF	GGGAATAAGTGTGATTTGCCT	320
	KrasR	GCCTGCGACGGCGGCATCTGC	
CCSP-rtTA	CCSP-rtTAF	AAGGTTTAACAACCCGTAAACTCG	380
	CCSP-rtTAR	GTGCATATAACGCGTTCTCTAGTG	
P53 floxed	P53-flox (Fwd)	GGTTAAACCCAGCTTGACCA	WT 270bp MUT: 390bp
	p53-flox (Rev)	GGAGGCAGAGACAGTTGGAG	
LSL-Kras	Kras G12D 1	ACCTCTATCGTAGGGTCATACTC	WT: 659 MUT: 554
	Kras G12D 2	CCAGCTTCGGCTTCCTATTT	
	Kras G12D 3	GCCACCATGGCTTGAGTAAGTCTGCA	
LSL-mkate	ROSA A (Kate)	AAAGTCGCTCTGAGTTGTTAT	WT:350bp MUT:297bp
	ROSA B (kate)	GCGAAGAGTTTGTCCTCAACC	
	ROSA C5 (Kate)	CCTCCAATTTTACACCTGTTC	

Table 3: Mouse oligonucleotides - qPCR		
Gene	Forward Primer (5' 3')	Reverse Primer (3' 5')
Human A3B	GCTGGGACACCTTTGTGTACCG	ATCACGTGGCTCAGCAGGTAGG

Mouse 18S	AAGGAGACTCTGGCATGCTAAC	CAGACATCTAAGGGCATCACAGAC
Mouse TBP	GGGGAGCTGTGATGTGAAGT	CCAGGAAATAATTCTGGCTCA
Mouse Actin B	GCTTCTTTGCAGCTCCTTCGT	ACCAGCCGCAGCGATATCG
TetO-KrasG12D	AAGGACAAGGTGTACAGTTATGTGA	CTCCGTCTGCGACATCTTC

Table 4: Mouse oligonucleotides – RNA editing validation

Gene	Forward Primer (5' 3')	Reverse Primer (3' 5')	Product length (bp)
Capzb	ACCGCTCCCTCCATCTTTTT	GACTCCAAGCAACTCCCACA	128
Larp4	GGCTTGAAGAATGCTATCTCT	CAAACTGATTGGTAGTCACAG	278
Arhgap	GAGAAGGCGTAGATGAGCAGATCAG	ATGCATGACCCTAAGAGCTGACC	323
Ccp110	TAAGCTTGATTTCCTTTGTTGAGAC	CACAAAACAATGTCTGGCAC	386
Bri3bp	ACCAATGACTTCTTCACAGTTGAG	CCAATTAATGTTTGCGCATGTG	150
Itsn1	CCGTCTTAGTCTCTGTTACGTG	ACTAGGACAGCTAGCAGGC	326
Ube2d2a	AACTGCTTTAGGCCTATTTCG	CACCACTAATCTTAGCTAGACC	207
Hsph1	TCACACGCTGGGATCAGAAT	TCACACCTCCACGGGACAAT	281
Dab2ip	AAATGCAAAGGTTGGATCGGC	ACAGAAATTGCACAGCCACAC	117
Clasp1	TGCTTCTCTGACCCTCCAAA	ACAGTAGCAGTGGGACAGTT	337
Slc25a37	ATACAGTTACCCTGCGTGC	GGGTCAACAGGAGACTACTA	337
Lclat1	GTGCATTTGTTAGTGGGAGAG	TCCTGGGCAACAAATTGC	289
Rasgrp3	GTGGCTGTGCTTGTAATGCC	AGGTGGCCAGGTGTATGCTG	117
Spast	ATAGCAAGCGTTCTGAGCTC	ACAAGGACTGATGCACATGC	316
Lpin2	GGCGTTGTGTGCAGATCCTG	AGCGCATGCCTAGACTATGC	185
Xdh	AGGAAAGAGCTGTATTCCACATGGAC	AGGTGACAGCGACCTCACTC	167
Clip4	TCTTCAGCCACATCTGCAGCA	AATGGTGCCTACTCGCTGGC	96
Myom1.1	AGCCACACTGGAGTGGAGAC	AGACGTAAGCACTGTACTGTTCG	123
Myom1.2	ATACAGATACCTCAGTGGTGG	TTCACCGGGTTGTTATTGC	127
Epb41l3	TACTACCTCTGCTTGCAGCT	GCGGAACTCACTGATGTAGTC	157
Birc6.1	GAACTTAAATAGATCCTCCAAGGG	GCTTATGATGGACAAGCTG	86
Birc6.2	CGTGACCACCAATACAACAG	ATGGCACTGCTATTACACAG	183
Unc45b	GAATCCACGATCGCTCCGAACC	TCACACCTCCACGGGACAAT	358
Scnn1a	CTTCTCCGTGACTGTTTCTG	CACCTGGGACTCGTAGTG	106
Lgals9	AAGCTTCAGGCTTACGGGTG	CGGAGCGAGCGGGGATCC	143
Rslcan18	CCTTTGCTAAGAGCTCGGTC	TCTCCGGTATGAACTCTTTGGT	388
Abca17	TTTGGATGAGCCCACCTCAG	GGACCCTTCCCAAAGTCACC	274
Gls2	GCCTCAATGGATACCTGAGCA	AGCGTGTCCTGGCTAAGATGG	245

Table 5: Antibodies			
Reagent	Dilution	Source	Identifier
anti-pH3 Ser10	(1:200)	Cell Signalling	9701
cleaved caspase 3	(1:200)	Cell Signalling	9661
yH2AX	(1:200)	Bethyl Labs	00059
APOBEC3B	(1:200)	gift from R. Harris	
tGFP	(1:200)	Origene	TA150041
ki67	(1:200)	Medac	275R-18
CD3	(1:200)	Dako	A045229
GAPDH	(1:200)	Millipore,	CB1001
Actin	(1:200)	Sigma	A2066

Anti-Prosurfactant Protein C (proSP-C)	(1:500)	Millipore	AB3786
CC10	(1:500)	Santa Cruz	SC-9772
TTF1	(1:200)	Abcam	Ab76013
Cytokeratin 5 (CK5)	(1:200)	Abcam	ab53121

Table 6: Plasmids

Plasmid	Manufacturer	Identifier
pAL8 (HrasV12)	Provided by Prof. Dr. Mariano Barbacid	
E1A	N/A	N/A
pSAPX2 (packaging plasmid)	N/A	N/A
pMD2.G (packaging plasmid)	N/A	N/A
pLenti-CMVtight-Hygro-DEST	Addgene	w769-1
pCAGGS-FLPe-puro	N/A	MES4488
TRE-A3B-tGFP	Dr. Kalman Somogy	
TRE-A3B-E255A-tGFP	Alicia Alonso de la Vega	

Table 7: Equipment

Equipment	Manufacturer
Hand-held glucose analyzer Accu-Chek Aviva	Roche
DRY-CHEM 500i analyzer	Fujifilm
Leica tissue processor ASP300S	Leica
RM 2135 microtome	Leica
Cellometer Auto T4	Nexcelom Biosciences
Neon™ Transfection system	Invitrogen
Molecular Imager GelDoc™ XR+	Biorad
Nanodrop Lite Spectrophotometer	Life Technologies
LightCycler II® 480	Roche
LabSystems 352 Multiskan MS Microplate Reader	Artisan
Electrophoresis chamber	Biorad
Trans-Blot Turbo Transfer System	Biorad
iBright CL1500 imaging system	Thermo Fisher Scientific
ZEISS Axio Observer	Zeiss
HiSeq 4000 Systems	Illumina
NovaSeq 6000	Illumina

Table 8: Commercial kits

Reagent	Source	Identifier
VECTASTAIN Elite ABC kits	Vector Labs	PK-6101 and BMK-2202
DAB Peroxidase Substrate kit	Vector Labs	SK-4100
AllPrep DNA/RNA Mini	Qiagen	80204
QuantiTect Reverse Transcription Kit	Qiagen	205313
QIAquick Gel Extraction kit	Qiagen	28706
NeonTM Transfection system	Thermo Scientific	MPK1025
pENTR/D-TOPO Cloning Kit	Life Technologies	K240020SP
Gateway LR-Clonase II Enzyme Mix system	Invitrogen	11791-020
QIAprep spin miniprep kit	Qiagen	12583
Q5 site directed mutagenesis kit	NEB	M0492L
Pierce BCA Protein Assay Kit	Life Technologies	23225
TruSeq Stranded kit	Illumina	20020596

Agilent Low Input Exom-Seq Mouse kit	Illumina	N/A

Table 9: Reagents and chemicals

Reagent	Source	Identifier
1XPBS	Life Technologies	14190169
10% formalin	Sigma	HT501128
unmasking solution	Vector Labs	H-3300
Hydrogen Peroxide	Sigma	H1009
Eosin G	Roth	3137.2
Hematoxylin QS	Linaris	H-3404
DPX mounting media	Sigma	06522
Ethanol ABSOLUTE 100%	DKFZ	14926
xylene	DKFZ	13435
Ethanol 96%	Roth	T171.3
Dulbecco's Modified Eagle Medium (DMEM)	Life Technologies	419650394
Penicillin-streptomycin	Gibco	15070-063
Fetal bovine serum (FBS)	Gibco	10270-106
L-Glutamine	Gibco	25030024
0.05% trypsin	Life Technologies	25300054
0.25% trypsin	Life Technologies	25200056
Doxycycline hydrochloride	Sigma-Aldrich Chemie GmbH	D9891-5G
Cristal Violet	Sigma-Aldrich	V5265
Lipofectamin 2000	Life Technologies	11668027
OPTI-MEM	Gibco	31985062
Polybrene	Millipore	TR-1003-G
Dulbecco’s MEM with Glutamax	Gibco	31966-021
KO-DMEM	Gibco	10829-018
2-Mercaptoetanol 50 mM	Gibco	31350-010
MEM NEAA (100x)	Gibco	11140-035
Fetal serum	Millipore	ES-009-B
Hygromycin B	Calbiochem	400051
Mitomycin-C	Sigma	M-0503
1x Dream Taq Green Buffer	Life Technologies	B71
dNTP mix	Promega	U1240
peqGreen DNA dye	VWR	732-2960
SYBR Green PCR Master Mix (2×)	Applied Biosystems	4364346
2-Mercaptoethanol	Life Technologies	31350010
30% Acrylamide	Biorad	161-0156
Ammonium persulfate	Sigma	A3678
TEMED	Sigma	T22500
Albumin from bovine serum	Sigma	SIALA7906
TransBlot Turbo transfer buffer	Biorad	1704270
RNaseA	Qiagen	19101
10X UGD buffer (NEB)	NEB	M0280S
Urea	Sigma	51456
NEBNext® High-Fidelity 2X PCR Master Mix	NEB	M0541S

Table 10: Software and algorithms

Tool	Source
TissueFAXS technology	TissueGnostics
StrataQuest software	TissueGnostics

Fiji Software	Wayne Rasband (NIH)
Benchling	Benchling.com
FastQC	https://www.bioinformatics.babraham.ac.uk/projects/fastqc/
STAR/2.7.1a	https://github.com/alexdobin/STAR/releases
Picard tools (version 2.18.16)	http://broadinstitute.github.io/picard/
CIGAR	N/A
Mutect2 from GATK (3.6)	(Cibulskis et al., 2013)
R v3.6.2	N/A
Kallisto v0.46.1.	(Bray et al., 2016)
javaGSEA Desktop Application v2.2.2	(Liberzon et al., 2015; Subramanian et al., 2005)
SpeedSeq	(Chiang et al., 2015)
GraphPad Prism v8	GraphPad Software
Omnigraffle	The Omni Group
BioRender	Biorender.com

Table 11: Summary of techniques
ES cells manipulation
Mouse handling
Mouse necropsy
Intratraqueal injection
Glucose tolerance test
Measurement of Serum Parameters
Mouse tissue processing
Immunohistochemistry and H&E
In vitro experiments
Mouse embryonic fibroblast (MEFs)
Cloning experiments
Genotyping
RNA/DNA isolation and cDNA synthesis
Quantitative Real Time PCR
Protein quantification and western blot
Deamination
Validation of RNA editing candidates
High throughput experiments

Methods

Some parts of the text have been taken and/or adapted from the previously manuscript originally co-written by myself (see author contributions).

1. ES cells manipulation

1.1. Mitomycin treatment of DR4 MEFs feeder cells culture

DR4 MEFS (resistant to hygromycin) were thaw and plated in p150 plates and cultured in 20 mL of DMEM (Gibco) supplemented with 1% Streptomycin and Penicillin (Gibco), 10% fetal bovine serum (FBS) (Gibco) and 1% L-Glutamine (Gibco). After expansion, DR4 MEFS were treated with 1 mL mitomycin C (10 µg/ml) for 3 hours to be used as feeder cells for ES cells.

1.2. KH2 ES cells culture and expansion

KH2 ES cells, were a gift from Sagrario Ortega and were generated by Konrad Hochedlinger and Rudolf Jaenisch (Beard et al., 2006b). Feeder cells were thawed and plated one day before plating ES cells on top. Cells were cultured in ES-KO media containing (500ml): 75 ml of fetal serum (Millipore), 6 ml MEM with Glutamax (Gibco), 6 ml NEAA non-essential aminoacids (Gibco), 6ml penicillin-streptomycin (Gibco), 1.2 ml of 2-mercaptoetanol (Gibco) and 12 µl of LIF. After two days in culture the ES cells reached 80% subconfluence and were expanded at 1:3-5 ratio. The medium was changed every day.

1.3. Electroporation and selection of KH2 ES cells

Two days after ES cells expansion, 2 cycles of 20 seconds 1200V electroporation was performed using NeonTM Transfection system and following the manufacturer;s intructions for electroporation of ES cells. KH2 ES were electroporated with 5 µg of the either TRE-A3B-tGFP or TRE-A3B-E255A-tGFP vector and 2.5 µg of the pCAGGS-flpE-puro vector (per well in a 6-well plate). After 48 hours from the electroporation, positive ES cell clones were selected by adding fresh medium containing 160µg/ml of hygromycin B for 12 days. Positive clones were then picked and expanded and all of them were confirmed to have inserted the A3B-tGFP transgene by genotyping

2. Mouse work

All animals were housed at the DKFZ (Deutsches Krebsforschungszentrum) animal facility under a constant 12-hour light-dark cycle and were maintained on a standard diet with ad

libitum with access to food and water. Mice were weaned at 3 weeks old and housed in same sex cages containing 3-5 animals. Experiments were conducted in compliance with institutional regulations and with ethical permission from the Regierungspräsidium Karlsruhe, Baden-Wurttemberg, Germany, under permit numbers G29/19 and G108/21.

Genetically engineered mice for human A3B (*A3B/Rosa26-rtTA*) and A3B deaminase mutant (*A3B-E255A/Rosa26-rtTA*) were generated at the DKFZ transgenic facility by Prof. Dr. Franciscus van der Hoeven and Brittney Armstrong, via injection of ES cells into 8 cell blastocysts and embryo transfer into FVB recipients. *A3B/Rosa26-rtTA* and *A3B-E255A/Rosa26-rtTA* heterozygous animals were bred out with FVB mice to exclude the *Rosa26-rtTA* transgene and bred to *CAGs-rtTA3* mice, kindly provided by Prof. Dr. Darjus Tschaharganeh (DKFZ, Heidelberg, Germany) (Dow et al., 2014). A3B mice were also bred to *TetO-Kras^{G12D} /CCSP-rtTA* mice (Fisher et al., 2001) to obtain triple transgenic animals. *Apobec1-KO* mice were kindly provided by Prof. Dr. Nina Papavasiliou. To obtain the mouse line *p53$^{flx/flx}$/LSL-Kras$^{G12D/+}$/TetO-A3B*/*LSL-rtTA-mKate*, Prof. Dr. Claudia Scholl kindly provided *p53$^{flx/flx}$/LSL-Kras$^{G12D/+}$* animals (KP model (Jackson et al., 2005). These mice were bred with the *TetO-A3B* mice and with *LSL-rtTA-mKate* obtained from Prof. Dr. Darjus Tschaharganeh. All mice were in a mixed background of C57BL/6 and FVB and only heterozygous animals for every transgene were included in this study.

For *in vivo* induction of *TetO-A3B, TetO-A3B-E255A* and *TetO-Kras^{G12D}* transgenes, adult mice aged 4-8 week old were administered with 625 ppm doxycycline impregnated food pellets (Harald-Teklad). Adenovirus containing Cre (Ad-Cre) recombinase (University of Iowa) were intratracheally injected in 6-week old *p53$^{flx/flx}$/LSL-Kras$^{G12D/+}$/TetO-A3B*/*LSL-rtTA-mKate* animals to allow for *p53* loss and mutant *Kras* and *rtTA* expression. For viral instillation, mice were anesthetized by intraperitoneal (i.p.) injection of 100 µg/g ketamine and 14 µg/g xylazine per mouse. Mice were injected with a viral dose of 2.5 x 10^7 PFU/ml diluted in DMEM (Life Technologies, 41965039) and 2M CaCl2 in a final volume of 50 µL per animal (DuPage et al., 2009). After virus instillation, mice were fed with 625 ppm doxycycline food pellets to also induce *A3B* expression.

Animals were monitored weekly or daily, in the case of *CAGs-rtTA3* mice, and were sacrificed when they reached the established humane endpoint with signs of sickness (heavy breathing, weight loss or signs of lethargy). For the tumor regression and relapse experiment *TetO-Kras^{G12D}/TetO-A3B/CCSP-rtTA* tumor growth was monitored 25 weeks post-doxycycline induction by µCT imaging every 2 weeks. Tumor volume was calculated using ImageJ2 software. When tumor volume reached a minimum of 15 mm^3 animals were changed to normal food. Animals were euthanized by cervical dislocation. To clean the tissues from blood, the

inferior vena cava was cut and mice were perfused with 1XPBS through the left ventricle of the heart. Intestines were also perfused to clean food rests. Tissues were either snap frozen in liquid nitrogen and then kept at -80°C for RNA/protein isolation or stored in 10% formalin solution for further histological analysis.

2.1. Glucose tolerance test GTT

Mice were fasted overnight, with doxycycline administration in the drinking water, and 16 hours later they received an intraperitoneal injection of glucose (1g/kg body weight). To measure glucose levels, blood samples from the tail vein were taken before glucose injection as well as 15, 30, 60, 90 and 120 min post glucose administration using a hand-held glucose analyzer (Accu-Chek Aviva, Roche).

2.2. Measurement of Serum Parameters

Blood samples were taken from the ventricle of mice hearts. After 10 min at room temperature, blood samples were centrifuged for 5 min at 14000rpm and the serum was separated and snap frozen. Serum samples were then used for analyzing AST, ALT enzymes with the DRY-CHEM 500i analyzer (Fujifilm, Japan) following the manufacturer's protocol.

2.3. Tissue processing/ Immunohistochemistry/ H&E

Mouse tissues were fixed in 10% formalin (Sigma) overnight, processed in a tissue processor (Leica, ASP300S) and embedded in paraffin. Sections of 3 µm were cut using a RM 2135 microtome (Leica) and placed onto superfrost slides (VWR International). For immunostaining, the sections were first subjected to two rounds of deparaffinization in Xylene (each 10min) and rehydrated through gradual exposure to decreasing percentage of alcohols (3x 100%, 96%, 70%) for 3 minutes each and 5 minutes in dH2O.

Antigen retrieval was performed using 0.09% (v/v) unmasking solution (Vector Labs) in a steamer at 60°C for 30 minutes, and then rinsed in dH2O for 5 min. To inactivate endogenous peroxidases, 3% hydrogen peroxide (Sigma) was used for 10 min. following the manufacturer's recommendations, blocking (30 min), secondary antibodies (30 min) and biotin-streptavidin incubation (30 min), specie-specific VECTASTAIN Elite ABC kits (Vector Labs) were used, depending on the species of the primary antibody. The primary antibodies used are listed in Table 5 and were incubated overnight at 4°C. For antibody detection, a DAB peroxidase substrate kit (Vector Labs) was used, hematoxylin QS (Linaris) was employed for nuclear counterstaining and eosin G (Roth) for cytoplasmic counterstaining. Finally, tissues were

dehydrated through increasing ethanol grades (96%, 2x 100%) and placed two times 5 minutes in Xylene. Then slides were mounted using DPX mounting media.

Sections were visualized and scanned with the TissueFAXS technology (TissueGnostic). The different staining analysis were done using the StrataQuest software (TissueGnostic). To determine the number or percentage of pH3, Casp3, ki67 and yH2AX in mouse tissues, 15 ROIs per section were assigned randomly. The total number of cells in each ROI was measured by counting the number of hematoxylin-stained nuclei. Nuclear DAB signal was used to determine the number of positive cells, and the percentage was calculated relative to the total number of cells in that particular ROI. Similarly, in lung tumors sections, each single nodule was analyzed. In the case of CD3 staining, the positive signal was quantified from DAB shades per mm^2 and multiplied by 10^3 for better data visualization. Tumor burden was calculated using hematoxylin and eosin-stained tissue sections. The area of each tumor and the total lung area were measured. Tumor burden was expressed in percentages and calculated by dividing the total tumor area by the total lung area.

3. In vitro experiments

3.1. Cell culture maintenance

MEFs and HEK-293T cells were maintained with Dulbecco's Modified Eagle Medium (DMEM) (Gibco) supplemented with 1% Streptomycin and Penicillin (Gibco), 10% fetal bovine serum (FBS) (Gibco) and 1% L-Glutamine (Gibco). Cells were grown at 37°C and 5% CO2 incubators. For collecting the cells, 0.05% trypsin was used for MEFs and 0.25% trypsin was used for HEK293T cells. For A3B induction, doxycycline (1µg/ml) was added to the media and replaced every time the media was changed. For all the experiments cells were counted with Cellometer Auto T4 (Nexcelom Biosciences).

3.2. Growth curve

For determination of cell growth rate, 100.000 cells per well were seeded in a 6-well plate. Every 24h during 6 consecutive days, one well was trypsinized and counted with the Cellometer Auto T4 (Nexcelom Biosciences). Confluence was calculated using the daily cell count relative to the highest cell count reached by the control on day 6.

3.3. Transformation assay

For determination of oncogenic capacities 1x10^6 cells were seeded in a p-100 plate. Transfection using calcium phosphate with the vectors containing HrasV12 and E1A was

performed 24 hours later. After 15 days, culture plates containing foci or colonies were fixed with ice-cold methanol and stained with Crystal Violet. Plates were scanned on a scanner and quantified using ImageJ.

3.4. Wound healing assay

For determination of the migration rate, 500.000 cells were seeded in a 6-well plate. When confluence was reached, a small pipette tip was used to draw a scratch in the well. Wells were washed with 1XPBS to remove the detached cells and fresh media was added with or without doxycycline. Images of the scratch in the same positions were taken 18, 24 and 48 hours later. Analysis of wound closure was performed using Fiji software.

3.5. Mouse embryonic fibroblast (MEFs)

Embryos in stage E12.5 were harvested from pregnant females coming from the lines *Rosa26-rtTA* or *CAGs-rtTA*. In a sterile environment, each embryo was separated from its embryonic sac. After releasing the embryo by extracting the remaining layers, the fetal liver was removed to prevent differentiated cells in the culture. DNA was extracted from the embryo's head in 200 µl of 0.5 M NaOH shaking at 98 ºC for one hour followed by neutralization with 20 µL of 1M Tris HCl. Later genotyping was done (described below) for selecting just the embryos with the required genotypes for processing the next day. The rest of the embryo's body was digested at 4 ºC in 500µl 0.05% Trypsin overnight and then carefully pipetted up and down to disaggregate the tissue. MEFs were grown in DMEM media (Figure 40).

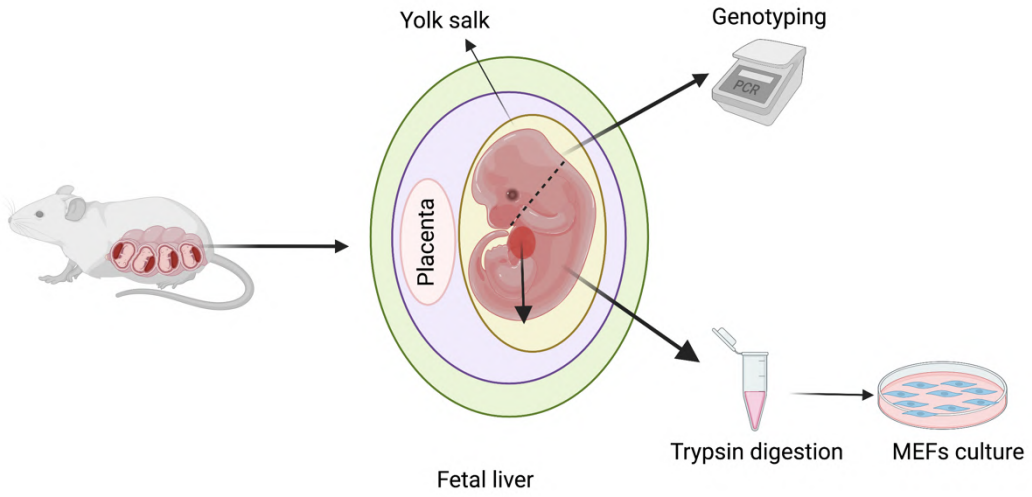

Figure 40: Generation of mouse embryonic fibroblasts

Scheme of the method used to generate mouse embryonic fibroblasts (MEFs). In the E12.5 stage of embryonic development, embryos are separated from the embryonic sac and the rest of the layers. The fetal liver is removed to avoid differentiated cells in the culture. The head of the embryo is used to asses the genotypes. The rest of the body is digested in trypsin overnight and then MEFs are plated and cultured.

3.6. Generation of transient or stable cell lines

For generating stable HEK293T-rtTA cells overexpressing A3B, $5x10^5$ HEK293T cells and $2x10^5$ HEK293T-rtTA cells were cultured in 6-well plates. HEK293T cells were transfected using lipofectamine 2000 together with 1.2µg of a lentiviral plasmid encoding A3B-tGFP, 0.9µg psPAx2 and 0.3µg pmD2.G plasmids and were incubated under these conditions overnight in order to produce lentiviruses containing A3B-tGFP plasmid.

Lipofectamine was incubated in 250µl OPTI-MEM (Gibco) and the three different plasmids were incubated all together also in 250µl OPTI-MEM for 5 minutes. Both solutions were then mixed and incubated for 20 minutes. After the incubation, the mixture was carefully added to the cells. 24 and 48 hours after transfection, the media from the transfected HEK293T cells was collected and filtered through a 0.45µm filter to remove cell debris. Before infection, (4µg/ml) Polybrene was added to increase the infection efficiency. Two days after transduction, cells were treated with 0.2mg/ml hygromycin for 10 days.(Beard et al., 2006)

4. Molecular biology methods

4.1. Generation of A3B vectors

For the generation of the A3B doxycycline inducible plasmid (TRE-A3B-tGFP) the cDNA containing the sequence of A3B fused to tGFP was amplified from the vector pCMV6-AC-A3B-tGFP purchased from Origene. Using standard cloning methods using restriction enzymes the A3B-tGFP fragment was ligated into an opened TRE plasmid used as a backbone. Ligation was transformed into competent cells (DH5-α *E.coli*) by heat shock and incubated at 37°C shaking overnight in LB medium plus ampicillin. In order to obtain the plasmid DNA from picked colonies, minipreps were performed using the QIAprep spin miniprep kit (Qiagen) following the manufacturer's instructions and verified by sequencing. This plasmid was used for electroporating the ES cells to generate the A3B transgenic mice and for generating the plasmids for the catalytic mutant A3B.

For the generation of the lentiviral A3B doxycycline-inducible vector, the Gateway cloning system was used. Briefly, cDNA encoding for A3B-tGFP was cloned into pENTR-D/TOPO (Invitrogen) following the manufacturer's instructions. Then recombined into the inducible destination vector pLenti-CMVtight-Hygro-DEST (Addgene) using the Gateway LR-Clonase II Enzyme Mix system (Invitrogen) and following "Cloning-Classic LR Reaction II" protocol from A. Untergasser laboratory. Plasmid DNA was isolated by QIAprep Spin Miniprep kit (Invitrogen) and verify by sequencing.

For generating the TRE-A3B-E255A-tGFP plasmid, site directed mutagenesis was performed by using Q5 site-directed mutagenesis kit (NEB) and following the manufacturer's instructions. Primers were designed to create targeted specific changes (E255A, adenine for cytosine in position 255) in the plasmid containing the wild-type A3B. This plasmid was used for electroporating the ES cells to generate the mutant A3B-E255A transgenic mice.

4.2. Genotyping

DNA was isolated from ear punches by incubating them with 100 µL of 0.05M NaOH 1 hour at 98°C, followed by neutralization with 10 µL of 1M Tris HCl, pH7.5. For the PCR reaction, 1 µL of DNA was used in a 20 µL reaction containing: 1x Dream Taq Green Buffer (Life Technologies, B71), 0.25 pmol/l forward primer, 0.25 pmol/l reverse primer, 200 M dNTPs mix, and 1U/20l Taq Polymerase enzyme. The primers used are described in Table 2. For all transgenes, the PCR program used was: 94°C for 2 min, 30 times [95°C for 30 s, 60°C for 30 s, 72°C for 30 s], and a final step at 72°C for 1 min. PCR products were run on a 2% agarose gel at 120V with peqGreen DNA dye and visualized with Molecular Imager GelDoc^{TM} XR+ (Biorad).

4.3. RNA/DNA isolation and cDNA synthesis

Snap frozen mouse tissues were grinded on dry ice using a mortar and pestle. No more than 30mg of tissue powder was used for further RNA and DNA extraction. For total RNA and genomic DNA isolation of mouse tissues and cell pellets, AllPrep DNA/RNA Mini (Qiagen, 80204) was used according to the manufacturer's instructions. In the case of mouse tissues, 2-Mercaptoethanol (10µl per mL of RLT plus buffer) was added to the lysis buffer to avoid degradation by tissue endogenous RNAses. DNA and RNA concentrations were measured using Nanodrop Lite Spectrophotometer (Life Technologies, ND-LITE).

For cDNA synthesis QuantiTect Reverse Transcription Kit (Qiagen, 205313) was used following the manufacturer's instructions. A maximum of 1200 ng of RNA was used in a 10 µL reaction. To avoid double-stranded DNA contamination, RNA was initially incubated for 2 min at 42°C. Reverse transcription was performed for 15 min at 42°C. Inactivation of the reverse transcriptase was achieved by incubating the reaction for 3 min at 95°C.

4.4. Quantitative Real Time PCR

Quantification using real-time PCR was initiated using 10 ng of cDNA with 5µl SYBR Green PCR Master Mix (2×) (Applied Biosystems) and 1µl of each primer (10nM) which are listed in Table 3. All reactions were run in triplicates in in a LightCycler II® 480 (Roche) using the following program: 95°C for 5 min, 45 times [95°C for 10 s, 60°C for 42 s], 95°C for 5 min

and a final step at 65°C for 1 min. Relative mRNA expression levels were calculated according to the ΔCt or ΔΔCt relative quantification method (Livak & Schmittgen, 2001) and were normalized to the housekeeping genes (18S; Actin; TBP) levels.

ΔCt= Ct(gene of interest) – Ct(reference gene)

ΔΔCt= ΔCt(sample) – ΔCt(negative control sample)

Fold Change= 2^(- ΔΔCt)

4.5. Protein quantification and Western Blot

Mouse tissue powder and cell pellets were lysed in RIPA lysis buffer (50 mM NaCl, 5 mM EDTA, 1.0% NP-40 or 0.1% Triton X-100, 0.5% sodium deoxycholate, 0.1% sodium dodecyl sulphate (SDS), 50 mM Tris-HCl pH 8.0-7.4, 1 tablet of Protease inhibitors/ 10mL) plus 1:100 PMFS for protein extraction. In addition, mouse tissues in RIPA buffer were resuspended with a syringe for proper homogenization. Lysis reactions were kept in ice for 15 min and vortex every 5 min followed by 20 min 13800 rmps centrifugation at 4°C. Protein quantification was performed by BCA assay and colorimetric detection at 540nm was done using Labsystems Multiskan Ms photometer.

For Western Blot 40µg of protein were used and samples were mix with 5X Laemmli buffer (10% SDS, 50% glycerol, 0.005% bromophenol blue, 0.5 M Tris-HCl pH 6.8, 20% 2-mercaptoethanol) and the boiled at 98°C for 5 min and cleared by centrifugation. Samples were run on 10% SDS polyacrylamide gels (4mL H20, 3.3mL 30% Acrylamide, 2.5mL 1.5M Tris pH 8.8, 50µl SDS 10%, 50µl ammonium persulfate, 5µl TEMED) with stacking gel (3.7mL H20, 670µl 30% Acrylamide, 625µl 1M Tris pH 6.8, 100µl SDS 10%, 100µl ammonium persulfate, 4µl TEMED) in 1X running buffer (30 g Tris base, 144 g glycine, 0.1% SDS, 1L dH2O) between 1.5 to 2 hours at 120V. Transfer to nitrocellulose membranes was performed using Trans-Blot Turbo Transfer System (Biorad) in TransBlot Turbo transfer buffer (25mM Tris, 250mM glycine, 20% methanol) (Biorad) at 1.3A, 25V, 13 min. Membranes were blocked in 1X TBS-T (30 g Tris base, 144 g glycine, 0.1% Tween) containing 5% bovine serum albumin (BSA). The primary antibodies and the dilutions used are listed in Table 5 and were incubated at 4°C overnight. Membranes were then incubated for 1h at room temperature with fluorescent species-specific secondary antibodies listed in Table 5. Membranes were washed using TBS-T. For protein detection iBright CL1500 imaging system (Thermo Fisher Scientific) was used.

4.6. Deamination assay

Using previously established techniques, DNA deaminase activity was evaluated in protein lysates from various tissues (Law et al., 2016). For the deamination reaction, 40µg of

protein was used in a final volume of 18µl. Each reaction was incubated 3h at 37°C and contained 3.5µl from the deamination master mix that was prepared as follows: 0.25µl RNaseA (10mg/mL), 1µl fluorescent oligo (4 µM) containing a single target cytosine (5′-ATTATTATTATTCGAATGGATTTATTTATTTATTTATTTATTT-fluorescein), 2µl 10X UGD buffer (NEB), 0.25µl UDG (NEB), 2µ 0.5M EDTA. Oligo cleavage is achieved by adding 2 µl of 1M NaOH and incubated at 98°C for 10 min. Samples were mixed with equal volume of 2 x Formamide Buffer (80% formamide, 1 x TBE (108 g Tris base, 55 g Boric acid, 0.25 M EDTA 80 ml pH 8.0), 0.05% Bromophenol blue and 0.01% Xylene cyanol) and run in a 15% Urea-TBE gel (Up to 15mL H20, 7.5ml 30% Acrylamide, 7.2g Urea, 1.5ml 10X TBE, 75µl ammonium persulfate, 7.5µl TEMED) for 1.5 h at 200V. Deamination activity was detected by fluorescence using iBright CL1500 imaging system (Thermo Fisher Scientific). If the protein extract contains A3B, the single cytosine in the fluorescent oligo will be deaminated, resulting in an uracil. UDG will remove the uracil creating an abasic site that can be cleaved by heating and alkaline conditions. Therefore, two bands can be detected: the top band or substrate (S), which belongs to the whole oligo, and the lower band or product (P), which corresponds to the deaminated oligo (Figure 41).

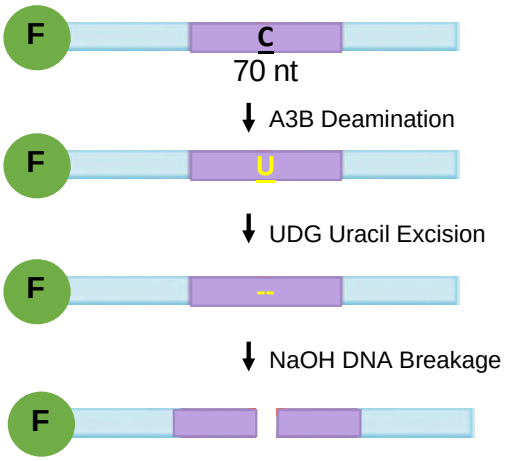

Figure 41: Deamination assay

Scheme of deaminase activity assay. Briefly, a fluorescent oligo containing a single target for A3B will be deaminated in the presence of A3B enzyme. The uracil will be removed by UDG enzyme, creating an abasic site that can be cleaved by heating and alkaline conditions. Therefore, two bands can be detected: the top band or substrate (S), which belongs to the whole oligo, and the lower band or product (P), which corresponds to the deaminated oligo

4.7. Validation of RNA editing candidates

In order to detect double peaks in Sanger sequences, candidate genes were chosen based on the criteria that at least 20% of the transcripts had to contain the C-to-T change. To amplify the target sequences, specific primers were designed and listed in Table 4. PCRs were performed using 30ng cDNA and 100ng DNA from liver, lung and pancreas tissues in 30µl

reactions (2x NebNext Buffer, 0.25 pmol/l forward primer, 0.25 pmol/l reverse primer). For all genes, the PCR program used was: 98°C for 30 s, 35 times [98°C for 10 s, 63-58°C for 30 s, 72°C for 30 s], and a final step at 72°C for 2 min. PCR products were run in 1% agarose gels and bands were separated. DNA was extracted using the QIAquick Gel Extraction kit (Qiagen) following the manufacturer's instructions. The isolated DNA was then submitted for sanger sequencing (Microsynth). Sanger sequences were aligned to the specified reference mouse gene using the online software Benchling to confirm the existence of an RNA editing event or a DNA mutation.

5. High throughput experiments

5.1. Total RNA sequencing

Libraries from total RNA from mouse tissues and single nodules were prepared with TruSeq Stranded kit for Illumina platforms using 1.2 ug starting material. HiSeq 2000 v4 technology (100-nucleotide paired-end reads) was employed for library sequencing of the liver, pancreas and lung mouse tissues. Novaseq 6000 technology (100-nucleotide paired-end reads) was employed for library sequencing of the single lung nodules.

5.2. RNA editing calling

RNA-seq data from liver, pancreas and lung tissues were subjected to quality control analysis with FastQC before and after trimming. After quality check, the reads were aligned to the mm10 build of the mouse reference genome using STAR/2.7.1a with basic two pass mode for realigning splice junctions enabled. Then Picard tools (version 2.18.16) was used to identify duplicate reads and CIGAR to split reads with Ns at the splice junctions. RNA edits were annotated using Mutect2 from GATK (3.6) having as a control RNA-seq data from pancreas/liver/lung tissues of litter mates. For downstream analysis, only editing events that passed the internal filter of mutect2 with at least 6 reads supporting the edit, a minimum of 20 total reads at the editing site, and a variant allele frequency larger than 0.05 were used for downstream analysis. RNA editing levels at Apobec1 target sites were extracted from the raw tables of the aligned reads before applying any filters for further analysis.

TPMs levels of various genes were extracted by generating the read-count matrix using the Bioconductor packages GenomicAlignments and GenomicFeatures in R.

5.3. Differential expression analysis

To investigate differentially expressed genes, the sequenced reads from mouse tissues and lung nodules were aligned to the mm10 reference genome using kallisto v0.46.1. The package from R DEseq2 was used to obtain the normalized counts from the raw counts (Love et al., 2014). Principal component analysis (PCA) was performed, to confirm that biological groups clustered together. Differential expression analysis was performed with javaGSEA Desktop Application v2.2.2. (GSEA, Broad Institute) (Liberzon et al., 2015; Subramanian et al., 2005). To asses p values, 1000 permutations for each gene set were used and corrected with the false discovery rate (FDR) method. Only pathways with an FDR-P value ≤ 0.25 were chosen as significantly enriched.

5.4. Whole Exome Sequencing and analysis

Libraries from total genomic DNA from mouse tissues, single nodules and normal matched DNA from tails (TK and TKA mice) were prepared with Agilent Low Input Exom-Seq Mouse kit for Illumina platforms using 0.5 ug starting material. HiSeq 2000 v4 technology (125-nucleotide paired-end reads) was employed for library sequencing of liver, lung and pancreas tissues. Novaseq 6000 technology (100-nucleotide paired-end reads) was employed for library sequencing of the single lung nodules. Whole exome reads from *A3B* and control tissues were aligned to the mm10 build of the mouse reference genome using SpeedSeq (Chiang et al., 2015). Then Picard tools (version 2.18.16) were used to identify duplicate PCR reads. Reads were locally realigned around Indels using GATK3 (version 3.6.0) tools. Single base substitutions and small InDels were called and annotated using Mutect2 from GATK (3.6) having as a control the pool of normal data from litter mates. For downstream analysis, only SBSs that passed the internal filter of GATK3 with at least 4 reads supporting each variant, a minimum of 20 total reads and a variant allele frequency larger than 0.05 were used to accurately call RNA editing events. Signature analysis used RNA editing events that were not found in the matching exome data for each sample. All sequence logos were constructed and displayed in R using the "ggseqlogo" tool.

6. Statistical analysis and representation

Statistical analysis was performed using GraphPad Prism software. Biological tests used are indicated in the figure legends. Unpaired t-test, one- or two-way ANOVA, or log-rank Mantel-Cox tests were performed. All data shown is displayed as mean±SD or mean±SEM. p values were as follows: *p < 0.05, **p < 0.01, ***p < 0.001, ****p < 0.0001. The number of animals is represented with n.

7. Schemes and images

All schemes and figures shown in the introduction, results and discussion part were generated by myself and with the help of Prof. Dr. Rocio Sotillo and Sandra Alonso de la Vega using the BioRender Software (Biorender.com) or Adobe Illustrator 2022.

8. Contributions

This thesis has been proofread and corrected by Prof. Dr. Rocio Sotillo. Dr. Lorena Salgueiro, Dr. Kalman Somogy and Prof. Dr Rocio Sotillo made the plasmid and the ES cells for generating the A3B mice. Pathological analysis in Figures 24 and 25 was performed by Prof. Dr. Albrecht Stenzinger and Prof. Dr. Tanja Poth. Mouse experiments shown in Figure 28B and 28C were assisted by Mirian Fernandez. Dr. Rafail Tasakis develop the pipeline and data analysis for Figure 29A and 29B. Dr. Nuri Alpay Temiz developed the pipeline and bioinformatic data analysis from Figures 30 and 31.

Additional technical and/or conceptual assistance was provided by Maria Ramos, Alberto Díaz, Sara Chocarro, Pan Fan, Sridhar Kandala, Ana Carbajo Uña, Dr. Bojana Stefanovska, Dr. Emily Law, Prof. Dr. Reuben Harris and Prof. Dr. Nina Papavasiliou.

Prof. Dr. Rocio Sotillo played a crucial role in helping to define and guide the project.

Acknowledgments

I need to start this section by thanking the person who has been at my side through both the darkest and the brightest moments of this journey. **Rocio** has been and continues to be a role model and someone I admire. I remember that during my master's internship in Madrid, I wanted to present in a journal club one of Rocio's articles, which I was fascinated about. In the end, I presented something different, but the coincidences in life took me to do a PhD in her lab. Thank you for choosing me, trusting me and let me do amazing science. You have been my supervisor, my boss and more importantly, my friend. Although it has not been an easy road for us, we have learned together how to overcome every obstacle. Your guidance in every aspect has been invaluable to me, and I really cannot describe how grateful I am to you in words. You have been my backbone these 4 years, and as I am always telling you, I don't know what I will do without you.

I want to go back in time and express my gratitude to those who helped me realize how much I like science. Thank you **Pedro Medina Vico** for allowing me to work in your lab and have the chance to live in Granada, one of Spain's most beautiful cities. **Paola**, I admire your constant patience and I hope I'm still your favorite student. Thank you, **Marcos Malumbres**, for allowing me to join your team at the CNIO, an excellent research center. **Guille**, I will be forever grateful to you for everything you taught me and for connecting me to Rocio.

I arrived to Rocio's lab to study chromosomal instability in cancer and I ended up doing my thesis in something completely different. However, I got the opportunity of working in this amazing project that has given me a lot of headaches, but also a lot of happy moments. This is not simply my effort, but the work of many brilliant scientists. Therefore, I want to thank all the collaborators working all around the world for your effort and support: Heidelberg University (**Albretch** and **Tanja**), Tel Avi University (**Uri** and **Eli**), University of Minnesota (**Alpay**), DKFZ (**Lars, Benedickt, Nina** and **Rafi**) **Rafi**, thanks for being a friend and for always being there for me. **Nina** thanks for all the feedback and the meetings to discuss the project. The last but not least, **Reuben** in Texas. Thank you for the amazing days in Texas, your unconditional support and for believing in my science. I will always remember your advice: "*Less is more*".

Next, I want to thank the DKFZ core facilities: the animal care takers, the microscopy, flow cytometry, animal imaging and functional genetics teams for providing excellent service and making my life much easier.

Additionally, I want to thank my TAC committee members **Prof. Dr. Rob Russel**, **Prof. Dr. Stefan Wiemann** and **Prof. Dr. Nina Papavasiliou** for great discussions and support. Moreover, I want to thank my thesis examiner **Prof. Dr. Michael Boutrous** for agreeing to participate in my PhD examination committee.

When you are surrounded by excellent scientists and even better people, incredible science happens. During these years, my lab mates became more than just coworkers; they were a family (bros and sis). I want to thank current and previous lab members: **Charles, Simone, Vanessa, Laura, Ana, Justin, Filiz** and the rest of the people that have been in the lab at some point. **Mr. Kalman** or cloning man, thanks for your love and dedication to the project. I will miss your rock music in cell culture, and our runs to send the samples for sequencing at 16:30. **Hilary** you are like a mom to me, I only have kind words for you. Thanks for making my life much easier. I am going to miss you and our long conversations about life. **Kandala** you are a mess bro, but also the best office mate. Thanks for all your support and for always trying to bring everyone together to do some fun staff (although it has not always worked). **Dr. Fan**, you are my favorite Chinese in the world! Don't think you will get rid of me because I will keep scaring you until the end! But…..it's oookkkkk. **Sarita**, cuantas cosas hemos pasado juntas, desde el principio hasta el final. Y como ya te he dicho muchas veces que bonita casualidad que seas tu la que me haya acompañado en esta etapa.

Mi **Alber**, hermano. Gracias por ser el estudiante repelente que todo el mundo odia. Soy demasiado afortunada de haber podido aprender de ti cada día y de disfrutar del corazón tan grande que tienes. Me has enseñado nuevos pasos de baile y como conservar carne en un falcon durante años. Gracias por ser el mejor amigo y compañero, te quiero mucho.

Mi **Mari**, mi ángel. No se que he hecho sin ti todos estos años. Literalmente somos la misma persona en cuerpos diferentes. Como se suele decir, por fin he encontrado a mi soul mate. No puedo estar mas feliz de que mi "hijo" ahora sea también el tuyo, y estoy convencida de que vas a hacer cosas gigantes, estoy súper orgullosa de ti. Eres la persona mas buena y con mas paciencia que conozco. Nunca podre agradecerte todo el amor que me has dado. Aun nos quedan mil cosas por hacer juntas, porque este solo es el principio de un para siempre amiga. Te quiero mucho.

This thesis would not have been possible without my GREAT Heidelberg friends! They have turned my workplace and the city of Heidelberg into a second home.

PhD resistance group (**Jeyan, Juliane, Karol, Laura, Gemma, Joshua**), although it is difficult to meet all together, when we manage we have so much fun! I will always remember our long dinners, Secret Santa's and laser tags. Thanks to you all and to many more people that have made me feel at home.

Alessa and **Cata**, amigas thank you for your friendship and love. Next, wine and cheese dinner should be in Paris.

Cocido-croquetas-bacalao family I could not feel homesick with friends like you. Antes de que me vaya tenemos que hacer los cocidos que tengo en el congelador, así que prepárense. Honestly, I could have not been luckier to have found such an amazing group of people. To the newcomers **Cristina, Sandra** y **Marta** you are amazing girls, take care of the rest when I am gone.

Dani. Mi compi de todo. Gracias por escucharme, por darme tantos buenos consejos y por ser de las personas mas detallistas que conozco. Aunque siempre llegas tarde, siempre llegas, y eso es lo importante.

Mirian. Quien me iba a decir con lo mal que me caías al principio lo mucho que te iba a terminar queriendo. Gracias por hacer de madre de todos y por hacer las mejores croquetas del mundo. Ohhhh yeah!

Nuria. Cuando nos encontramos de casualidad en Ámsterdam, aun no sabíamos la amistad tan grande que íbamos a crear. Gracias por contagiarme con tu risa que se oye desde la otra punta del mundo. Cuida a Alber y que él te cuide a ti.

Paula. Wiiiiiiii. Mi compañera desde el día 1. Gracias por todas tus caídas, por el contenido que creas allá donde vas y por siempre mantenernos hidratadas.

Damian. Mi pilar. Aunque a veces seas demasiado intenso y pesado, eres fundamental. Todo esto no ha sido fácil y tu has estado a mi lado en todo momento. Gracias por cuidarme y preocuparte tanto por mi churri.

Chicos os quiero muchísimo de verdad sois los mejores amigos y familia que podía haber tenido.

Dani. Gracias por haber aparecido y por haberme acompañado en esta etapa. Nosotros somos el claro ejemplo de que las cosas no son fáciles, y que con esfuerzo y amor todo se consigue. Gracias por todos los aufstehen a tu lado y por todas las pelis/series que no hemos visto porque te has quedado dormido. Gracias por cuidarme tan bien, pero sobre todo por quererme tanto. Londres nos espera. Te quiero novio.

A mis amigos de España,

Mis biosanis**. Andrea, Bea, Isa, Álvaro, Moyano, Didi, Marta** y **Pardi**s por todos los momentos que hemos pasado juntos y porque, aunque nos veamos de año en año parezca que el tiempo no ha pasado. Mis pajaritos voladores **Suni**, **Luli** y **Maria**. Gracias por vuestra amistad. La carrera me hizo un regalo que sois vosotras. Ojalá poder volver a estar todas

juntas en la misma ciudad sin tener que despedirnos continuamente. Lo importante es que se que estemos donde estemos, siempre nos vamos a tener las 4. Os quiero chicas.

Dicen que quien tiene amigos tiene un tesoro. Pues yo tengo la suerte de tener las mejores amigas del mundo. **Noe**, **Vir** y **Rais** gracias por todos los momentos juntas y por quererme tal y como soy. **Nur**, mi cara bonita. Gracias por complementarnos tan bien, por ser mi compañera de aventuras internacionales y mi una hora menos en Canarias. **Andre**, aún recuerdo la primera vez que te conocí en el parque de atracciones. Desde entonces he sabido que serías una de mis personas favoritas en el mundo.

Silvia. Tendría que escribir otra tesis entera para darte las gracias por todo lo que has hecho por mi. Sabes que lo nuestro es especial y que nuestra conexión es MAGIA. Gracias por tu paciencia, por darme tranquilidad, pero también locura. Eres una persona preciosa, llena de bondad y alegría. Gracias por una vez mas haberme acompañado en uno de los momentos mas importantes de mi vida. Te quiero, AlwayS.

A mi maravillosa familia, todos mis tíos, a mis abuelos, **Luis**, **Carmen** y **Pedro**, a mi madrina **Montse**, a mi primo **Miguel** y a mis tíos postizos **Luisa** y **Baltita** gracias por haber creído siempre en ese terremoto de niña.

A mis **padres**. Una vez me dijisteis: todo llega cariño mío, todo a su tiempo. Pues lo he conseguido. Lo he conseguido gracias a los maravillosos padres que tengo. Gracias por haber hecho todo lo que estaba en vuestra mano para que pueda ser la mujer que soy hoy. Papi, siempre seré tu niña (favorita) pase el tiempo que pase. Admiro tu esfuerzo, amor, dedicación. Gracias por haberme enseñado a ser la mejor amiga de mis amigos, porque tu sin duda lo eres. Mamita gracias por ser tan “especial” y mi confidente en mis peores momentos. Me has enseñado que a veces no hay que tomarse las cosas tan en serio, y que la risa lo cura todo. Gracias a los dos por ser el motor de mi vida y por ser los mejores padres del mundo. Os quiero.

A mi hermana **Sandra**. Mi mitad, mi bebe, mi todo. Gracias por ser mi persona, la que se que va a estar de principio a fin. No sabes lo orgullosa que estoy de la mujer en la que te has convertido. Eres preciosa por fuera y por dentro. Gracias por brillar como lo haces y por ser una artista (reflejado está en la tesis). Gracias por apoyarme siempre y por quererme incondicionalmente con todos mis defectos. Eres el sol de mi vida. Te quiero.

A mi abuela **Alicia**. El miedo a perderte fue lo que mi hizo tener claro que quería ser científica. Quería intentar frenar todo lo que te estaba pasando. Esto fue hace mas de 15 años y aún sigues aquí, luchando cada día. Gracias por criarme y por ser la luz que me guía. Todo esto es por ti.

Supplementary material

1. List of abbreviations

Numbers

18S	Ribosomal rRNA of the 40S Ribosome Subunit

A

A-to-I	Adenosine to Inosine
A1	APOBEC1
A1CF	APOBEC1 complementation factor
A2	APOBEC2
A3	APOBEC3
A3A	APOBEC3A
A3B	APOBEC3B
A3C	APOBEC3C
A3D	APOBEC3D
A3F	APOBEC3F
A3G	APOBEC3G
A3H	APOBEC3H
A4	APOBEC4
AAH	Atypical adenomous hyperplasia
Ad-Cre	Adenovirus containing Cre
ADAR	Adenosine deaminase acting on RNA
AID	Activation-induced-deaminase
ALT	Alanine transaminase
AP	Apurinic/apyrimidinic site
APE1	Endonuclease 1
ApoB	Apolipoprotein B mRNA
APOBEC	Editing catalytic polypeptide-like Apolipoprotein B
APS	Ammonium persulfate
AST	Aspartate transaminase
ATR	Ataxia Telangiectasia and Rad3-related

B

BER	Base excision repair
BSA	Bovine serum albumin

C

C-terminal	Carboxil-terminal
C-to-U	cytosine to uracil
C57BL/6	Black 6 strain
CAGs	Cytomegalovirus actin globin promoter
Casp3	Caspase 3
CC10	Club cell protein

CCSP	Clara cell secretory protein promoter
CD3	Cluster of differentiation 3
CDK5	Cytokeratin 5
CHK1	Checkpoint kinase
ColA1	Collagenase I locus
Cre	Cre recombinase
CSR	Class-switch recombination
cDNA	Complementary DNA
CDT	Carboxy-terminal domain

D

DKFZ	Deutsches Krebsforschungszentrum
DMEM	Dulbecco's Modified Eagle's Medium
DNA	Deoxyribonucleic acid
dNTP	Deoxynucleotide Triphosphate
Dox	Doxycycline
DSBs	Double-strand breaks

E

EDTA	Ethylenediaminetetraacetic acid
EGFR	Epidermal Growth Factor receptor
ES cells	Embryonic stem cells

F

FBS	Fetal Bovine Serum
FDR	False Discovery Rate
FVB	Sensitive to Friend Leukemia Virus B strain

G

gDNA	Genomic DNA
GEMM	Genetic engineered mouse model
GSEA	Gene Set Enrichment Analysis
GTPases	Guanosintriphosphatase
GTT	Glucose tolerance test

H

H&E	Hematoxylin-Eosin
HBV	Hepatitis-B-Virus
HEK	Human Embryonic Kidney cells
HIV	Human Immunodeficiency Virus
HPV	Human Papillomavirus

I

i.p	Intraperitoneal
IFN	Interferon type-I
Ig	Immunoglobulin
IHC	Immunohistochemestry

K

kDA	Kilodalton
KO	Knock-Out
KP	p53flx/flx/LSL- KrasG12D/+/ LSL-rtTA-mKate
KPA	p53flx/flx/LSL-KrasG12D/+/TetO-A3/LSL-rtTA-mKate
KRAS	Kirsten Rat Sarcoma Viral Oncogene Homolog

L

LINE	Class I transposable elements
Log2FC	Logarithmic Fold Change
LoxP	Locus of X-over P1
LSL	Lox-Stop-Lox
LUAD	Lung adenocarcinoma

M

MEF	Mouse embryonic fibroblast
MEK1/2	Mitogen-activated protein kinase
miRNA	MicroRNAs
mRNA	Messenger Ribonucleic acid

N

n.s	Not significant
NaOH	Sodium hydroxide
NAT1	N-Acetyltransferase 1
NES	Normalized Enrichment Score
NF-kB	Nuclear factor kappa-light-chain-enhancer of activated B cells
NF1	Neurofibromin 1
NSCLC	Non-small cell lung cancer

P

padj	Adjusted p value
PBS	Phosphate Buffered Saline
PCA	Principal component analysis
pH3	phospho Histone 3
PIK3CA	Phosphatidylinositol-4,5-Bisphosphate 3-Kinase Catalytic Subunit Alpha

R

RBM47	RNA-binding motif protein 47
RIPA	Radioimmunoprecipitation Assay
RNA	Ribonucleic acid
RT-qPCR	Quantitative real-time PCR
rtTA	Reverse Tetracycline Transactivator

S

SBSs	Single-base substitution signatures
SCLC	Small cell lung cancer
SD	Standard deviation
SDS	Sodium dodecyl sulfate
SDS-PAGE	Sodium dodecylsulfate polyacrylamide gel electrophoresis
SEM	Standard Error of the Mean
Seq	Sequencing
SHM	Somatic hypermutation
SMARC4	SWI/SNF Related, Matrix Associated, Actin Dependent Regulator of Chromatin, Subfamily A, Member 4
SPC	Surfactant protein C
ssDNA	Single-stranded RNAs
ssRNA	Single-stranded-DNA
STAT2	Signal Transducer and Activator of Transcription 2
STK11	Serine/Threonine Kinase 11

T

TBS-T	Tris-buffered saline supplemented with 1 % Tween20
TCGA	The Cancer Genome Atlas
TEMED	Tetramethylethylenediamine
TetO	Tetracycline-inducible operator
tGFP	Turbo Green fluorescent protein
TK	*TetO-Kras^{G12D}/CCSP-rtTA*
TKA	*TetO-Kras^{G12D}/TetO-A3B/CCSP-rtTA*
TKI	Tyrosine kinase inhibitors
TLS	Translesion synthesis
TRE	Tetracycline response element
TTF1	Thyroid transcription factor-1

U

uCT	Micro Computed Tomography
UNG	Uracil-DNA glycosylase
UTR	Untranslated región

W

WG	Whole-genome-sequencing
WT	Wild Type
WT1	Wilms Tumor 1

X

XRCC1	X-ray repair cross-complementing protein 1

Z

Zn^{2+}	Zinc ion
ZDD	Zinc-dependent deaminase domain

2. Table of figures

3. List of Tables

References

Akre, M. K., Starrett, G. J., Quist, J. S., Temiz, N. A., Carpenter, M. A., Tutt, A. N. J., Grigoriadis, A., & Harris, R. S. (2016). Mutation Processes in 293-Based Clones Overexpressing the DNA Cytosine Deaminase APOBEC3B. *PLoS ONE*, *11*(5), e0155391. https://doi.org/10.1371/journal.pone.0155391

Alexandrov, L. B., Kim, J., Haradhvala, N. J., Huang, M. N., Ng, A. W. T., Wu, Y., Boot, A., Covington, K. R., Gordenin, D. A., Bergstrom, E. N., Islam, S. M. A., Lopez-Bigas, N., Klimczak, L. J., McPherson, J. R., Morganella, S., Sabarinathan, R., Wheeler, D. A., Mustonen, V., Alexandrov, L. B., … Stratton, M. R. (2020). The repertoire of mutational signatures in human cancer. *Nature*, *578*(7793), 94–101. https://doi.org/10.1038/s41586-020-1943-3

Alexandrov, L. B., Nik-Zainal, S., Wedge, D. C., Aparicio, S. A. J. R., Behjati, S., Biankin, A. V., Bignell, G. R., Bolli, N., Borg, A., Børresen-Dale, A.-L., Boyault, S., Burkhardt, B., Butler, A. P., Caldas, C., Davies, H. R., Desmedt, C., Eils, R., Eyfjörd, J. E., Foekens, J. A., … PedBrain, I. (2013). Signatures of mutational processes in human cancer. *Nature*, *500*(7463), 415–421. https://doi.org/10.1038/nature12477

Allen, E. M. V., Wagle, N., Sucker, A., Treacy, D. J., Johannessen, C. M., Goetz, E. M., Place, C. S., Taylor-Weiner, A., Whittaker, S., Kryukov, G. V., Hodis, E., Rosenberg, M., McKenna, A., Cibulskis, K., Farlow, D., Zimmer, L., Hillen, U., Gutzmer, R., Goldinger, S. M., … (DeCOG), D. C. O. G. of G. (2014). The Genetic Landscape of Clinical Resistance to RAF Inhibition in Metastatic Melanoma. *Cancer Discovery*, *4*(1), 94–109. https://doi.org/10.1158/2159-8290.cd-13-0617

Alqassim, E. Y., Sharma, S., Khan, A. N. M. N. H., Emmons, T. R., Gomez, E. C., Alahmari, A., Singel, K. L., Mark, J., Davidson, B. A., McGray, A. J. R., Liu, Q., Lichty, B. D., Moysich, K. B., Wang, J., Odunsi, K., Segal, B. H., & Baysal, B. E. (2021). RNA editing enzyme APOBEC3A promotes pro-inflammatory M1 macrophage polarization. *Communications Biology*, *4*(1), 102. https://doi.org/10.1038/s42003-020-01620-x

Angus, L., Smid, M., Wilting, S. M., Riet, J. van, Hoeck, A. V., Nguyen, L., Nik-Zainal, S., Steenbruggen, T. G., Tjan-Heijnen, V. C. G., Labots, M., Riel, J. M. G. H. van, Bloemendal, H. J., Steeghs, N., Lolkema, M. P., Voest, E. E., Werken, H. J. G. van de, Jager, A., Cuppen, E., Sleijfer, S., & Martens, J. W. M. (2019). The genomic landscape of metastatic breast cancer highlights changes in mutation and signature frequencies. *Nature Genetics*, *51*(10), 1450–1458. https://doi.org/10.1038/s41588-019-0507-7

Asaoka, M., Ishikawa, T., Takabe, K., & Patnaik, S. K. (2019). APOBEC3-Mediated RNA Editing in Breast Cancer is Associated with Heightened Immune Activity and Improved Survival. *International Journal of Molecular Sciences*, *20*(22), 5621. https://doi.org/10.3390/ijms20225621

Barka, A., Berríos, K. N., Bailer, P., Schutsky, E. K., Wang, T., & Kohli, R. M. (2022). The Base-Editing Enzyme APOBEC3A Catalyzes Cytosine Deamination in RNA with Low

Proficiency and High Selectivity. *ACS Chemical Biology*, *17*(3), 629–636. https://doi.org/10.1021/acschembio.1c00919

Baylin, S. B., & Jones, P. A. (2011). A decade of exploring the cancer epigenome — biological and translational implications. *Nature Reviews Cancer*, *11*(10), 726–734. https://doi.org/10.1038/nrc3130

Baysal, B. E., Sharma, S., Hashemikhabir, S., & Janga, S. C. (2017). RNA Editing in Pathogenesis of Cancer. *Cancer Research*, *77*(14), 3733–3739. https://doi.org/10.1158/0008-5472.can-17-0520

Beard, C., Hochedlinger, K., Plath, K., Wutz, A., & Jaenisch, R. (2006a). Efficient method to generate single-copy transgenic mice by site-specific integration in embryonic stem cells. *Genesis*, *44*(1), 23–28. https://doi.org/10.1002/gene.20180

Beard, C., Hochedlinger, K., Plath, K., Wutz, A., & Jaenisch, R. (2006b). Efficient method to generate single-copy transgenic mice by site-specific integration in embryonic stem cells. *Genesis*, *44*(1), 23–28. https://doi.org/10.1002/gene.20180

Bertucci, F., Ng, C. K. Y., Patsouris, A., Droin, N., Piscuoglio, S., Carbuccia, N., Soria, J. C., Dien, A. T., Adnani, Y., Kamal, M., Garnier, S., Meurice, G., Jimenez, M., Dogan, S., Verret, B., Chaffanet, M., Bachelot, T., Campone, M., Lefeuvre, C., … André, F. (2019). Genomic characterization of metastatic breast cancers. *Nature*, *569*(7757), 560–564. https://doi.org/10.1038/s41586-019-1056-z

Blanc, V., Henderson, J. O., Newberry, R. D., Xie, Y., Cho, S.-J., Newberry, E. P., Kennedy, S., Rubin, D. C., Wang, H. L., Luo, J., & Davidson, N. O. (2007). Deletion of the AU-Rich RNA Binding Protein Apobec-1 Reduces Intestinal Tumor Burden in Apcmin Mice. *Cancer Research*, *67*(18), 8565–8573. https://doi.org/10.1158/0008-5472.can-07-1593

Blanc, V., Park, E., Schaefer, S., Miller, M., Lin, Y., Kennedy, S., Billing, A. M., Hamidane, H. B., Graumann, J., Mortazavi, A., Nadeau, J. H., & Davidson, N. O. (2014). Genome-wide identification and functional analysis of Apobec-1-mediated C-to-U RNA editing in mouse small intestine and liver. *Genome Biology*, *15*(6), R79–R79. https://doi.org/10.1186/gb-2014-15-6-r79

Bonvin, M., Achermann, F., Greeve, I., Stroka, D., Keogh, A., Inderbitzin, D., Candinas, D., Sommer, P., Wain-Hobson, S., Vartanian, J., & Greeve, J. (2006). Interferon-inducible expression of APOBEC3 editing enzymes in human hepatocytes and inhibition of hepatitis B virus replication. *Hepatology*, *43*(6), 1364–1374. https://doi.org/10.1002/hep.21187

Borghaei, H., Paz-Ares, L., Horn, L., Spigel, D. R., Steins, M., Ready, N. E., Chow, L. Q., Vokes, E. E., Felip, E., Holgado, E., Barlesi, F., Kohlhäufl, M., Arrieta, O., Burgio, M. A., Fayette, J., Lena, H., Poddubskaya, E., Gerber, D. E., Gettinger, S. N., … Brahmer, J. R. (2015). Nivolumab versus Docetaxel in Advanced Nonsquamous Non–Small-Cell Lung Cancer. *The New England Journal of Medicine*, *373*(17), 1627–1639. https://doi.org/10.1056/nejmoa1507643

Boumelha, J., Trécesson, S. de C., Law, E. K., Romero-Clavijo, P., Coelho, M., Ng, K., Mugarza, E., Moore, C., Rana, S., Caswell, D. R., Murillo, M., Hancock, D. C., Argyris, P. P., Brown, W. L., Durfee, C., Larson, L. K., Vogel, R. I., Suarez-Bonnet, A., Priestnall, S.

L., … Downward, J. (2022). An immunogenic model of KRAS-mutant lung cancer enables evaluation of targeted therapy and immunotherapy combinations. *Cancer Research*. https://doi.org/10.1158/0008-5472.can-22-0325

Bransteitter, R., Pham, P., Scharff, M. D., & Goodman, M. F. (2003). Activation-induced cytidine deaminase deaminates deoxycytidine on single-stranded DNA but requires the action of RNase. *Proceedings of the National Academy of Sciences*, *100*(7), 4102–4107. https://doi.org/10.1073/pnas.0730835100

Bray, N. L., Pimentel, H., Melsted, P., & Pachter, L. (2016). Near-optimal probabilistic RNA-seq quantification. *Nature Biotechnology*, *34*(5), 525–527. https://doi.org/10.1038/nbt.3519

Bruin, E. C. de, McGranahan, N., Mitter, R., Salm, M., Wedge, D. C., Yates, L., Jamal-Hanjani, M., Shafi, S., Murugaesu, N., Rowan, A. J., Grönroos, E., Muhammad, M. A., Horswell, S., Gerlinger, M., Varela, I., Jones, D., Marshall, J., Voet, T., Loo, P. V., … Swanton, C. (2014). Spatial and temporal diversity in genomic instability processes defines lung cancer evolution. *Science*, *346*(6206), 251–256. https://doi.org/10.1126/science.1253462

Buisson, R., Langenbucher, A., Bowen, D., Kwan, E. E., Benes, C. H., Zou, L., & Lawrence, M. S. (2019). Passenger hotspot mutations in cancer driven by APOBEC3A and mesoscale genomic features. *Science*, *364*(6447). https://doi.org/10.1126/science.aaw2872

Burns, M. B., Lackey, L., Carpenter, M. A., Rathore, A., Land, A. M., Leonard, B., Refsland, E. W., Kotandeniya, D., Tretyakova, N., Nikas, J. B., Yee, D., Temiz, N. A., Donohue, D. E., Mcdougle, R. M., Brown, W. L., Law, E. K., & Harris, R. S. (2013). APOBEC3B is an enzymatic source of mutation in breast cancer. *Nature*. https://doi.org/10.1038/nature11881

Byeon, I.-J. L., Byeon, C.-H., Wu, T., Mitra, M., Singer, D., Levin, J. G., & Gronenborn, A. M. (2016). Nuclear Magnetic Resonance Structure of the APOBEC3B Catalytic Domain: Structural Basis for Substrate Binding and DNA Deaminase Activity. *Biochemistry*, *55*(21), 2944–2959. https://doi.org/10.1021/acs.biochem.6b00382

Cannataro, V. L., Gaffney, S. G., Sasaki, T., Issaeva, N., Grewal, N. K. S., Grandis, J. R., Yarbrough, W. G., Burtness, B., Anderson, K. S., & Townsend, J. P. (2019). APOBEC-induced mutations and their cancer effect size in head and neck squamous cell carcinoma. *Oncogene*, *38*(18), 3475–3487. https://doi.org/10.1038/s41388-018-0657-6

Cappione, A. J., French, B. L., & Skuse, G. R. (1997). A potential role for NF1 mRNA editing in the pathogenesis of NF1 tumors. *American Journal of Human Genetics*, *60*(2), 305–312.

Cárcer, G. de, Venkateswaran, S. V., Salgueiro, L., Bakkali, A. E., Somogyi, K., Rowald, K., Montañés, P., Sanclemente, M., Escobar, B., Martino, A. de, McGranahan, N., Malumbres, M., & Sotillo, R. (2018). Plk1 overexpression induces chromosomal instability and suppresses tumor development. *Nature Communications*, *9*(1), 3012. https://doi.org/10.1038/s41467-018-05429-5

Carmi, S., Church, G. M., & Levanon, E. Y. (2011). Large-scale DNA editing of retrotransposons accelerates mammalian genome evolution. *Nature Communications*, *2*(1), 519. https://doi.org/10.1038/ncomms1525

Caswell, D. R., Chuang, C.-H., Ma, R. K., Winters, I. P., Snyder, E. L., & Winslow, M. M. (2018). Tumor Suppressor Activity of Selenbp1, a Direct Nkx2-1 Target, in Lung Adenocarcinoma. *Molecular Cancer Research : MCR*, *16*(11), 1737–1749. https://doi.org/10.1158/1541-7786.mcr-18-0392

Caswell, D. R., Mayekar, M. K., Gui, P., Law, E. K., Vokes, N. I., Ruiz, C. M., Dietzen, M., Angelova, M., Bailey, C., Pich, O., Bakker, B., Wu, W., Humpton, T. J., Kerr, D. L., Hill, W., Lu, W.-T., Haderk, F., Blakely, C. M., Bakir, M. A., … Swanton, C. (2022). The role of APOBEC3B in lung tumour evolution and targeted therapy resistance. *BioRxiv*, 2020.12.18.423280. https://doi.org/10.1101/2020.12.18.423280

Caswell, D. R., & Swanton, C. (2017). The role of tumour heterogeneity and clonal cooperativity in metastasis, immune evasion and clinical outcome. *BMC Medicine*, *15*(1), 133. https://doi.org/10.1186/s12916-017-0900-y

Caval, V., Jiao, W., Berry, N., Khalfi, P., Pitŕe, E., Thiers, V., Vartanian, J.-P., Wain-Hobson, S., & Suspène, R. (2019). Mouse APOBEC1 cytidine deaminase can induce somatic mutations in chromosomal DNA. *BMC Genomics*, *20*(1), 858. https://doi.org/10.1186/s12864-019-6216-x

Caval, V., Suspène, R., Shapira, M., Vartanian, J.-P., & Wain-Hobson, S. (2014). A prevalent cancer susceptibility APOBEC3A hybrid allele bearing APOBEC3B 3′UTR enhances chromosomal DNA damage. *Nature Communications*, *5*(1), 5129. https://doi.org/10.1038/ncomms6129

Caval, V., Suspène, R., Vartanian, J.-P., & Wain-Hobson, S. (2014). Orthologous Mammalian APOBEC3A Cytidine Deaminases Hypermutate Nuclear DNA. *Molecular Biology and Evolution*, *31*(2), 330–340. https://doi.org/10.1093/molbev/mst195

Chan, K., Roberts, S. A., Klimczak, L. J., Sterling, J. F., Saini, N., Malc, E. P., Kim, J., Kwiatkowski, D. J., Fargo, D. C., Mieczkowski, P. A., Getz, G., & Gordenin, D. A. (2015). An APOBEC3A hypermutation signature is distinguishable from the signature of background mutagenesis by APOBEC3B in human cancers. *Nature Genetics*, *47*(9), 1067–1072. https://doi.org/10.1038/ng.3378

Chapman, J. H., Custance, M. F., Tricola, G. M., Shen, B., & Furano, A. V. (2020). The effect of APOBEC3B deaminase on double-stranded DNA. *BioRxiv*, 750877. https://doi.org/10.1101/750877

CHEN, C.-X., CHO, D.-S. C., WANG, Q., LAI, F., CARTER, K. C., & NISHIKURA, K. (2000). A third member of the RNA-specific adenosine deaminase gene family, ADAR3, contains both single- and double-stranded RNA binding domains. *RNA*, *6*(5), 755–767. https://doi.org/10.1017/s1355838200000170

Chen, H., Lilley, C. E., Yu, Q., Lee, D. V., Chou, J., Narvaiza, I., Landau, N. R., & Weitzman, M. D. (2006). APOBEC3A Is a Potent Inhibitor of Adeno-Associated Virus

and Retrotransposons. *Current Biology*, *16*(5), 480–485. https://doi.org/10.1016/j.cub.2006.01.031

Chen, L., Li, Y., Lin, C. H., Chan, T. H. M., Chow, R. K. K., Song, Y., Liu, M., Yuan, Y.-F., Fu, L., Kong, K. L., Qi, L., Li, Y., Zhang, N., Tong, A. H. Y., Kwong, D. L.-W., Man, K., Lo, C. M., Lok, S., Tenen, D. G., & Guan, X.-Y. (2013). Recoding RNA editing of AZIN1 predisposes to hepatocellular carcinoma. *Nature Medicine*, *19*(2), 209–216. https://doi.org/10.1038/nm.3043

Chen, S.-H., Habib, G., Yang, C.-Y., Gu, Z.-W., Lee, B. R., Weng, S.-A., Silberman, S. R., Cai, S.-J., Deslypere, J. P., Rosseneu, M., Jr., A. M. G., Li, W.-H., & Chan, L. (1987). Apolipoprotein B-48 Is the Product of a Messenger RNA with an Organ-Specific In-Frame Stop Codon. *Science*, *238*(4825), 363–366. https://doi.org/10.1126/science.3659919

Chiang, C., Layer, R. M., Faust, G. G., Lindberg, M. R., Rose, D. B., Garrison, E. P., Marth, G. T., Quinlan, A. R., & Hall, I. M. (2015). SpeedSeq: ultra-fast personal genome analysis and interpretation. *Nature Methods*, *12*(10), 966–968. https://doi.org/10.1038/nmeth.3505

Christofi, T., & Zaravinos, A. (2019). RNA editing in the forefront of epitranscriptomics and human health. *Journal of Translational Medicine*, *17*(1), 319. https://doi.org/10.1186/s12967-019-2071-4

Cibulskis, K., Lawrence, M. S., Carter, S. L., Sivachenko, A., Jaffe, D., Sougnez, C., Gabriel, S., Meyerson, M., Lander, E. S., & Getz, G. (2013). Sensitive detection of somatic point mutations in impure and heterogeneous cancer samples. *Nature Biotechnology*, *31*(3), 213–219. https://doi.org/10.1038/nbt.2514

Concepcion, C. P., Ma, S., LaFave, L. M., Bhutkar, A., Liu, M., DeAngelo, L. P., Kim, J. Y., Priore, I. D., Schoenfeld, A. J., Miller, M., Kartha, V. K., Westcott, P. M. K., Sanchez-Rivera, F. J., Meli, K., Gupta, M., Bronson, R. T., Riely, G. J., Rekhtman, N., Rudin, C. M., … Jacks, T. (2021). SMARCA4 inactivation promotes lineage-specific transformation and early metastatic features in the lung. *Cancer Discovery*, *12*(2), candisc.0248.2021. https://doi.org/10.1158/2159-8290.cd-21-0248

Conticello, S. G. (2008). The AID/APOBEC family of nucleic acid mutators. *Genome Biology*, *9*(6), 229. https://doi.org/10.1186/gb-2008-9-6-229

Conticello, S. G., Thomas, C. J. F., Petersen-Mahrt, S. K., & Neuberger, M. S. (2005). Evolution of the AID/APOBEC Family of Polynucleotide (Deoxy)cytidine Deaminases. *Molecular Biology and Evolution*, *22*(2), 367–377. https://doi.org/10.1093/molbev/msi026

DeWeerd, R. A., Németh, E., Póti, Á., Petryk, N., Chen, C.-L., Hyrien, O., Szüts, D., & Green, A. M. (2022). Prospectively defined patterns of APOBEC3A mutagenesis are prevalent in human cancers. *Cell Reports*, *38*(12), 110555. https://doi.org/10.1016/j.celrep.2022.110555

DiMarco, A. V., Qin, X., McKinney, B., Garcia, N. M. G., Alsten, S. C. V., Mendes, E. A., Force, J., Hanks, B. A., Troester, M. A., Owzar, K., Xie, J., & Alvarez, J. V. (2021). APOBEC mutagenesis inhibits breast cancer growth through induction of T cell-mediated antitumor immune responses. *Cancer Immunology Research*, *10*(1), canimm.CIR-21-0146-E.2021. https://doi.org/10.1158/2326-6066.cir-21-0146

Dow, L. E., Nasr, Z., Saborowski, M., Ebbesen, S. H., Manchado, E., Tasdemir, N., Lee, T., Pelletier, J., & Lowe, S. W. (2014). Conditional Reverse Tet-Transactivator Mouse Strains for the Efficient Induction of TRE-Regulated Transgenes in Mice. *PLOS ONE*, *9*(4), e95236. https://doi.org/10.1371/journal.pone.0095236

Driscoll, C. B., Schuelke, M. R., Kottke, T., Thompson, J. M., Wongthida, P., Tonne, J. M., Huff, A. L., Miller, A., Shim, K. G., Molan, A., Wetmore, C., Selby, P., Samson, A., Harrington, K., Pandha, H., Melcher, A., Pulido, J. S., Harris, R., Evgin, L., & Vile, R. G. (2020). APOBEC3B-mediated corruption of the tumor cell immunopeptidome induces heteroclitic neoepitopes for cancer immunotherapy. *Nature Communications*, *11*(1), 790. https://doi.org/10.1038/s41467-020-14568-7

Drosten, M., & Barbacid, M. (2022). Targeting KRAS mutant lung cancer: light at the end of the tunnel. *Molecular Oncology*, *16*(5), 1057–1071. https://doi.org/10.1002/1878-0261.13168

DuPage, M., Dooley, A. L., & Jacks, T. (2009). Conditional mouse lung cancer models using adenoviral or lentiviral delivery of Cre recombinase. *Nature Protocols*, *4*(7), 1064–1072. https://doi.org/10.1038/nprot.2009.95

Eisenberg, E., & Levanon, E. Y. (2018). A-to-I RNA editing — immune protector and transcriptome diversifier. *Nature Reviews Genetics*, *19*(8), 473–490. https://doi.org/10.1038/s41576-018-0006-1

Faden, D. L., Ding, F., Lin, Y., Zhai, S., Kuo, F., Chan, T. A., Morris, L. G., & Ferris, R. L. (2019). APOBEC mutagenesis is tightly linked to the immune landscape and immunotherapy biomarkers in head and neck squamous cell carcinoma. *Oral Oncology*, *96*, 140–147. https://doi.org/10.1016/j.oraloncology.2019.07.020

Ferrer, I., Zugazagoitia, J., Herbertz, S., John, W., Paz-Ares, L., & Schmid-Bindert, G. (2018). KRAS-Mutant non-small cell lung cancer: From biology to therapy. *Lung Cancer*, *124*, 53–64. https://doi.org/10.1016/j.lungcan.2018.07.013

Fisher, G. H., Wellen, S. L., Klimstra, D., Lenczowski, J. M., Tichelaar, J. W., Lizak, M. J., Whitsett, J. A., Koretsky, A., & Varmus, H. E. (2001). Induction and apoptotic regression of lung adenocarcinomas by regulation of a K-Ras transgene in the presence and absence of tumor suppressor genes. *Genes & Development*, *15*(24), 3249–3262. https://doi.org/10.1101/gad.947701

Fumagalli, D., Gacquer, D., Rothé, F., Lefort, A., Libert, F., Brown, D., Kheddoumi, N., Shlien, A., Konopka, T., Salgado, R., Larsimont, D., Polyak, K., Willard-Gallo, K., Desmedt, C., Piccart, M., Abramowicz, M., Campbell, P. J., Sotiriou, C., & Detours, V. (2015). Principles Governing A-to-I RNA Editing in the Breast Cancer Transcriptome. *Cell Reports*, *13*(2), 277–289. https://doi.org/10.1016/j.celrep.2015.09.032

Green, A. M., Landry, S., Budagyan, K., Avgousti, D. C., Shalhout, S., Bhagwat, A. S., & Weitzman, M. D. (2016). APOBEC3A damages the cellular genome during DNA replication. *Cell Cycle*, *15*(7), 998–1008. https://doi.org/10.1080/15384101.2016.1152426

Grillo, M. J., Jones, K. F. M., Carpenter, M. A., Harris, R. S., & Harki, D. A. (2022). The current toolbox for APOBEC drug discovery. *Trends in Pharmacological Sciences*, *43*(5), 362–377. https://doi.org/10.1016/j.tips.2022.02.007

Hakata, Y., & Miyazawa, M. (2020). Deaminase-Independent Mode of Antiretroviral Action in Human and Mouse APOBEC3 Proteins. *Microorganisms*, *8*(12), 1976. https://doi.org/10.3390/microorganisms8121976

Han, L., Diao, L., Yu, S., Xu, X., Li, J., Zhang, R., Yang, Y., Werner, H. M. J., Eterovic, A. K., Yuan, Y., Li, J., Nair, N., Minelli, R., Tsang, Y. H., Cheung, L. W. T., Jeong, K. J., Roszik, J., Ju, Z., Woodman, S. E., … Liang, H. (2015). The Genomic Landscape and Clinical Relevance of A-to-I RNA Editing in Human Cancers. *Cancer Cell*, *28*(4), 515–528. https://doi.org/10.1016/j.ccell.2015.08.013

Harris, R. S. (2015). Molecular mechanism and clinical impact of APOBEC3B-catalyzed mutagenesis in breast cancer. *Breast Cancer Research*, *17*(1), 8. https://doi.org/10.1186/s13058-014-0498-3

Harris, R. S., & Dudley, J. P. (2015). APOBECs and virus restriction. *Virology*, *479*, 131–145. https://doi.org/10.1016/j.virol.2015.03.012

Harris, R. S., Petersen-Mahrt, S. K., & Neuberger, M. S. (2002). RNA Editing Enzyme APOBEC1 and Some of Its Homologs Can Act as DNA Mutators. *Molecular Cell*, *10*(5), 1247–1253. https://doi.org/10.1016/s1097-2765(02)00742-6

Helleday, T., Eshtad, S., & Nik-Zainal, S. (2014). Mechanisms underlying mutational signatures in human cancers. *Nature Reviews Genetics*, *15*(9), 585–598. https://doi.org/10.1038/nrg3729

Henderson, S., Chakravarthy, A., Su, X., Boshoff, C., & Fenton, T. R. (2014). APOBEC-Mediated Cytosine Deamination Links PIK3CA Helical Domain Mutations to Human Papillomavirus-Driven Tumor Development. *Cell Reports*, *7*(6), 1833–1841. https://doi.org/10.1016/j.celrep.2014.05.012

Henderson, S., & Fenton, T. (2015). APOBEC3 genes: retroviral restriction factors to cancer drivers. *Trends in Molecular Medicine*, *21*(5), 274–284. https://doi.org/10.1016/j.molmed.2015.02.007

Higuchi, M., Maas, S., Single, F. N., Hartner, J., Rozov, A., Burnashev, N., Feldmeyer, D., Sprengel, R., & Seeburg, P. H. (2000). Point mutation in an AMPA receptor gene rescues lethality in mice deficient in the RNA-editing enzyme ADAR2. *Nature*, *406*(6791), 78–81. https://doi.org/10.1038/35017558

Higuchi, M., Single, F. N., Köhler, M., Sommer, B., Sprengel, R., & Seeburg, P. H. (1993). RNA editing of AMPA receptor subunit GluR-B: A base-paired intron-exon structure determines position and efficiency. *Cell*, *75*(7), 1361–1370. https://doi.org/10.1016/0092-8674(93)90622-w

Hirano, K.-I., Young, S. G., Farese, R. V. Jr., Ng, J., Sande, E., Warburton, C., Powell-Braxton, L. M., & Davidson, N. O. (1996). Targeted Disruption of the Mouse apobec-1 Gene Abolishes Apolipoprotein B mRNA Editing and Eliminates Apolipoprotein B48 (∗).

Journal of Biological Chemistry, *271*(17), 9887–9890. https://doi.org/10.1074/jbc.271.17.9887

Hoopes, J. I., Cortez, L. M., Mertz, T. M., Malc, E. P., Mieczkowski, P. A., & Roberts, S. A. (2016). APOBEC3A and APOBEC3B Preferentially Deaminate the Lagging Strand Template during DNA Replication. *Cell Reports*, *14*(6), 1273–1282. https://doi.org/10.1016/j.celrep.2016.01.021

Hou, S., Silvas, T. V., Leidner, F., Nalivaika, E. A., Matsuo, H., Yilmaz, N. K., & Schiffer, C. A. (2018). Structural Analysis of the Active Site and DNA Binding of Human Cytidine Deaminase APOBEC3B. *Journal of Chemical Theory and Computation*, *15*(1), 637–647. https://doi.org/10.1021/acs.jctc.8b00545

Huff, A. L., Wongthida, P., Kottke, T., Thompson, J. M., Driscoll, C. B., Schuelke, M., Shim, K. G., Harris, R. S., Molan, A., Pulido, J. S., Selby, P. J., Harrington, K. J., Melcher, A., Evgin, L., & Vile, R. G. (2018). APOBEC3 Mediates Resistance to Oncolytic Viral Therapy. *Molecular Therapy - Oncolytics*, *11*, 1–13. https://doi.org/10.1016/j.omto.2018.08.003

Hunter, J. C., Manandhar, A., Carrasco, M. A., Gurbani, D., Gondi, S., & Westover, K. D. (2015). Biochemical and Structural Analysis of Common Cancer-Associated KRAS Mutations. *Molecular Cancer Research*, *13*(9), 1325–1335. https://doi.org/10.1158/1541-7786.mcr-15-0203

Isozaki, H., Abbasi, A., Nikpour, N., Langenbucher, A., Su, W., Stanzione, M., Cabanos, H. F., Siddiqui, F. M., Phan, N., Jalili, P., Oh, S., Timonina, D., Bilton, S., Gomez-Caraballo, M., Archibald, H. L., Nangia, V., Dionne, K., Riley, A., Lawlor, M., … Hata, A. N. (2021). APOBEC3A drives acquired resistance to targeted therapies in non-small cell lung cancer. *BioRxiv*, 2021.01.20.426852. https://doi.org/10.1101/2021.01.20.426852

Jackson, E. L., Olive, K. P., Tuveson, D. A., Bronson, R., Crowley, D., Brown, M., & Jacks, T. (2005). The Differential Effects of Mutant p53 Alleles on Advanced Murine Lung Cancer. *Cancer Research*, *65*(22), 10280 LP – 10288. https://doi.org/10.1158/0008-5472.can-05-2193

Jackson, E. L., Willis, N., Mercer, K., Bronson, R. T., Crowley, D., Montoya, R., Jacks, T., & Tuveson, D. A. (2001). Analysis of lung tumor initiation and progression using conditional expression of oncogenic K-ras. *Genes & Development*, *15*(24), 3243–3248. https://doi.org/10.1101/gad.943001

Jalili, P., Bowen, D., Langenbucher, A., Park, S., Aguirre, K., Corcoran, R. B., Fleischman, A. G., Lawrence, M. S., Zou, L., & Buisson, R. (2020). Quantification of ongoing APOBEC3A activity in tumor cells by monitoring RNA editing at hotspots. *Nature Communications*, *11*(1), 2971. https://doi.org/10.1038/s41467-020-16802-8

Jamal-Hanjani, M., Wilson, G. A., McGranahan, N., Birkbak, N. J., Watkins, T. B. K., Veeriah, S., Shafi, S., Johnson, D. H., Mitter, R., Rosenthal, R., Salm, M., Horswell, S., Escudero, M., Matthews, N., Rowan, A., Chambers, T., Moore, D. A., Turajlic, S., Xu, H., … Swanton, C. (2017). Tracking the Evolution of Non–Small-Cell Lung Cancer. *New England Journal of Medicine*, *376*(22), 2109–2121. https://doi.org/10.1056/nejmoa1616288

Jarvis, M. C., Carpenter, M. A., Temiz, N. A., Brown, M. R., Richards, K. A., Argyris, P. P., Brown, W. L., Yee, D., & Harris, R. S. (2022). Mutational impact of APOBEC3B and APOBEC3A in a human cell line. *BioRxiv*, 2022.04.26.489523. https://doi.org/10.1101/2022.04.26.489523

Ji, H., Ramsey, M. R., Hayes, D. N., Fan, C., McNamara, K., Kozlowski, P., Torrice, C., Wu, M. C., Shimamura, T., Perera, S. A., Liang, M.-C., Cai, D., Naumov, G. N., Bao, L., Contreras, C. M., Li, D., Chen, L., Krishnamurthy, J., Koivunen, J., … Wong, K.-K. (2007). LKB1 modulates lung cancer differentiation and metastasis. *Nature*, *448*(7155), 807–810. https://doi.org/10.1038/nature06030

Jiang, Q., Isquith, J., Ladel, L., Mark, A., Holm, F., Mason, C., He, Y., Mondala, P., Oliver, I., Pham, J., Ma, W., Reynoso, E., Ali, S., Morris, I. J., Diep, R., Nasamran, C., Xu, G., Sasik, R., Rosenthal, S. B., … Jamieson, C. (2021). Inflammation-driven deaminase deregulation fuels human pre-leukemia stem cell evolution. *Cell Reports*, *34*(4), 108670. https://doi.org/10.1016/j.celrep.2020.108670

Johnson, L., Mercer, K., Greenbaum, D., Bronson, R. T., Crowley, D., Tuveson, D. A., & Jacks, T. (2001). Somatic activation of the K-ras oncogene causes early onset lung cancer in mice. *Nature*, *410*(6832), 1111–1116. https://doi.org/10.1038/35074129

Kanu, N., Cerone, M. A., Goh, G., Zalmas, L.-P., Bartkova, J., Dietzen, M., McGranahan, N., Rogers, R., Law, E. K., Gromova, I., Kschischo, M., Walton, M. I., Rossanese, O. W., Bartek, J., Harris, R. S., Venkatesan, S., & Swanton, C. (2016). DNA replication stress mediates APOBEC3 family mutagenesis in breast cancer. *Genome Biology*, *17*(1), 185. https://doi.org/10.1186/s13059-016-1042-9

Klemm, L., Duy, C., Iacobucci, I., Kuchen, S., Levetzow, G. von, Feldhahn, N., Henke, N., Li, Z., Hoffmann, T. K., Kim, Y., Hofmann, W.-K., Jumaa, H., Groffen, J., Heisterkamp, N., Martinelli, G., Lieber, M. R., Casellas, R., & Müschen, M. (2009). The B Cell Mutator AID Promotes B Lymphoid Blast Crisis and Drug Resistance in Chronic Myeloid Leukemia. *Cancer Cell*, *16*(3), 232–245. https://doi.org/10.1016/j.ccr.2009.07.030

Koning, F. A., Newman, E. N. C., Kim, E.-Y., Kunstman, K. J., Wolinsky, S. M., & Malim, M. H. (2009). Defining APOBEC3 Expression Patterns in Human Tissues and Hematopoietic Cell Subsets. *Journal of Virology*, *83*(18), 9474–9485. https://doi.org/10.1128/jvi.01089-09

Kumar, S., & Mohapatra, T. (2021). Deciphering Epitranscriptome: Modification of mRNA Bases Provides a New Perspective for Post-transcriptional Regulation of Gene Expression. *Frontiers in Cell and Developmental Biology*, *9*, 628415. https://doi.org/10.3389/fcell.2021.628415

Kung, C.-P., Maggi, L. B., & Weber, J. D. (2018). The Role of RNA Editing in Cancer Development and Metabolic Disorders. *Frontiers in Endocrinology*, *9*, 762. https://doi.org/10.3389/fendo.2018.00762

Kurkowiak, M., Arcimowicz, Ł., Chruściel, E., Urban-Wójciuk, Z., Papak, I., Keegan, L., O'Connell, M., Kowalski, J., Hupp, T., & Marek-Trzonkowska, N. (2021). The effects of RNA editing in cancer tissue at different stages in carcinogenesis. *RNA Biology*, *18*(11), 1524–1539. https://doi.org/10.1080/15476286.2021.1877024

Lackey, L., Law, E. K., Brown, W. L., & Harris, R. S. (2014). Subcellular localization of the APOBEC3 proteins during mitosis and implications for genomic DNA deamination. *Cell Cycle*, *12*(5), 762–772. https://doi.org/10.4161/cc.23713

Land, A. M., Law, E. K., Carpenter, M. A., Lackey, L., Brown, W. L., & Harris, R. S. (2013). Endogenous APOBEC3A DNA Cytosine Deaminase Is Cytoplasmic and Nongenotoxic*. *Journal of Biological Chemistry*, *288*(24), 17253–17260. https://doi.org/10.1074/jbc.m113.458661

Landry, S., Narvaiza, I., Linfesty, D. C., & Weitzman, M. D. (2011). APOBEC3A can activate the DNA damage response and cause cell-cycle arrest. *EMBO Reports*, *12*(5), 444–450. https://doi.org/10.1038/embor.2011.46

Larijani, M., & Martin, A. (2007). Single-Stranded DNA Structure and Positional Context of the Target Cytidine Determine the Enzymatic Efficiency of AID. *Molecular and Cellular Biology*, *27*(23), 8038–8048. https://doi.org/10.1128/mcb.01046-07

Law, E. K., Levin-Klein, R., Jarvis, M. C., Kim, H., Argyris, P. P., Carpenter, M. A., Starrett, G. J., Temiz, N. A., Larson, L. K., Durfee, C., Burns, M. B., Vogel, R. I., Stavrou, S., Aguilera, A. N., Wagner, S., Largaespada, D. A., Starr, T. K., Ross, S. R., & Harris, R. S. (2020). APOBEC3A catalyzes mutation and drives carcinogenesis in vivo. *Journal of Experimental Medicine*, *217*(12). https://doi.org/10.1084/jem.20200261

Law, E. K., Sieuwerts, A. M., LaPara, K., Leonard, B., Starrett, G. J., Molan, A. M., Temiz, N. A., Vogel, R. I., Gelder, M. E. M., Sweep, F. C. G. J., Span, P. N., Foekens, J. A., Martens, J. W. M., Yee, D., & Harris, R. S. (2016). The DNA cytosine deaminase APOBEC3B promotes tamoxifen resistance in ER-positive breast cancer. *Science Advances*, *2*(10), e1601737–e1601737. https://doi.org/10.1126/sciadv.1601737

Lawrence, M. S., Stojanov, P., Polak, P., Kryukov, G. V., Cibulskis, K., Sivachenko, A., Carter, S. L., Stewart, C., Mermel, C. H., Roberts, S. A., Kiezun, A., Hammerman, P. S., Mckenna, A., Drier, Y., Zou, L., Ramos, A. H., Pugh, T. J., Stransky, N., Helman, E., … Getz, & G. (2013). Mutational heterogeneity in cancer and the search for new cancer-associated genes. *Nature*. https://doi.org/10.1038/nature12213

Leonard, B., McCann, J. L., Starrett, G. J., Kosyakovsky, L., Luengas, E. M., Molan, A. M., Burns, M. B., McDougle, R. M., Parker, P. J., Brown, W. L., & Harris, R. S. (2015). The PKC/NF-κB Signaling Pathway Induces APOBEC3B Expression in Multiple Human Cancers. *Cancer Research*, *75*(21), 4538–4547. https://doi.org/10.1158/0008-5472.can-15-2171-t

Lerner, T., Papavasiliou, F. N., & Pecori, R. (2018). RNA Editors, Cofactors, and mRNA Targets: An Overview of the C-to-U RNA Editing Machinery and Its Implication in Human Disease. *Genes*, *10*(1), 13. https://doi.org/10.3390/genes10010013

Li, L., Su, N., Cui, M., Li, H., Zhang, Q., Yu, N., Wu, S., & Cao, Z. (2019). Activation-induced cytidine deaminase expression in colorectal cancer. *International Journal of Clinical and Experimental Pathology*, *12*(11), 4119–4124.

Li, M., Wang, I. X., Li, Y., Bruzel, A., Richards, A. L., Toung, J. M., & Cheung, V. G. (2011). Widespread RNA and DNA Sequence Differences in the Human Transcriptome. *Science*, *333*(6038), 53–58. https://doi.org/10.1126/science.1207018

Liberzon, A., Birger, C., Thorvaldsdóttir, H., Ghandi, M., Mesirov, J. P., & Tamayo, P. (2015). The Molecular Signatures Database Hallmark Gene Set Collection. *Cell Systems*, *1*(6), 417–425. https://doi.org/10.1016/j.cels.2015.12.004

Liddicoat, B. J., Piskol, R., Chalk, A. M., Ramaswami, G., Higuchi, M., Hartner, J. C., Li, J. B., Seeburg, P. H., & Walkley, C. R. (2015). RNA editing by ADAR1 prevents MDA5 sensing of endogenous dsRNA as nonself. *Science*, *349*(6252), 1115–1120. https://doi.org/10.1126/science.aac7049

Livak, K. J., & Schmittgen, T. D. (2001). Analysis of Relative Gene Expression Data Using Real-Time Quantitative PCR and the 2−ΔΔC T Method. *Methods*, *25*(4), 402–408. https://doi.org/10.1006/meth.2001.1262

Lorenzo, J. P., Molla, L., Ibarra, I. L., Ruf, S., Ridani, J., Subramani, P. G., Boulais, J., Harjanto, D., Vonica, A., Noia, J. M. D., Dieterich, C., Zaugg, J. B., & Papavasiliou, F. N. (2021). APOBEC2 is a Transcriptional Repressor required for proper Myoblast Differentiation. *BioRxiv*, 2020.07.29.223594. https://doi.org/10.1101/2020.07.29.223594

Love, M. I., Huber, W., & Anders, S. (2014). Moderated estimation of fold change and dispersion for RNA-seq data with DESeq2. *Genome Biology*, *15*(12), 550. https://doi.org/10.1186/s13059-014-0550-8

Luo, C., Wang, S., Liao, W., Zhang, S., Xu, N., Xie, W., & Zhang, Y. (2021). Upregulation of the APOBEC3 Family Is Associated with a Poor Prognosis and Influences Treatment Response to Raf Inhibitors in Low Grade Glioma. *International Journal of Molecular Sciences*, *22*(19), 10390. https://doi.org/10.3390/ijms221910390

Luo, J., Ostrem, J., Pellini, B., Imbody, D., Stern, Y., Solanki, H. S., Haura, E. B., & Villaruz, L. C. (2022). Overcoming KRAS -Mutant Lung Cancer. *American Society of Clinical Oncology Educational Book*, *42*(42), 700–710. https://doi.org/10.1200/edbk_360354

Ma, W., Ho, D. W., Sze, K. M., Tsui, Y., Chan, L., Lee, J. M., & Ng, I. O. (2019). APOBEC3B promotes hepatocarcinogenesis and metastasis through novel deaminase-independent activity. *Molecular Carcinogenesis*, *58*(5), 643–653. https://doi.org/10.1002/mc.22956

Maciejowski, J., Li, Y., Bosco, N., Campbell, P. J., & de Lange, T. (2015). Chromothripsis and Kataegis Induced by Telomere Crisis. *Cell*, *163*(7), 1641–1654. https://doi.org/10.1016/j.cell.2015.11.054

Mannion, N. M., Greenwood, S. M., Young, R., Cox, S., Brindle, J., Read, D., Nellåker, C., Vesely, C., Ponting, C. P., McLaughlin, P. J., Jantsch, M. F., Dorin, J., Adams, I. R., Scadden, A. D. J., Öhman, M., Keegan, L. P., & O'Connell, M. A. (2014). The RNA-Editing Enzyme ADAR1 Controls Innate Immune Responses to RNA. *Cell Reports*, *9*(4), 1482–1494. https://doi.org/10.1016/j.celrep.2014.10.041

Maruyama, W., Shirakawa, K., Matsui, H., Matsumoto, T., Yamazaki, H., Sarca, A. D., Kazuma, Y., Kobayashi, M., Shindo, K., & Takaori-Kondo, A. (2016). Classical NF-κB pathway is responsible for APOBEC3B expression in cancer cells. *Biochemical and Biophysical Research Communications*, *478*(3), 1466–1471. https://doi.org/10.1016/j.bbrc.2016.08.148

McFadden, D. G., Politi, K., Bhutkar, A., Chen, F. K., Song, X., Pirun, M., Santiago, P. M., Kim-Kiselak, C., Platt, J. T., Lee, E., Hodges, E., Rosebrock, A. P., Bronson, R. T., Socci, N. D., Hannon, G. J., Jacks, T., & Varmus, H. (2016). Mutational landscape of EGFR-, MYC-, and Kras-driven genetically engineered mouse models of lung adenocarcinoma. *Proceedings of the National Academy of Sciences*, *113*(42), E6409–E6417. https://doi.org/10.1073/pnas.1613601113

Mcgranahan, N., Favero, F., Bruin, E. C. D., Birkbak, N. J., Szallasi, Z., & Swanton, C. (2015). Clonal status of actionable driver events and the timing of mutational processes in cancer evolution. *Science Translational Medicine*, *7*(283), 283ra54-283ra54. https://doi.org/10.1126/scitranslmed.aaa1408

McGranahan, N., & Swanton, C. (2017). Clonal Heterogeneity and Tumor Evolution: Past, Present, and the Future. *Cell*, *168*(4), 613–628. https://doi.org/10.1016/j.cell.2017.01.018

Menendez, D., Nguyen, T.-A., Snipe, J., & Resnick, M. A. (2017). The Cytidine Deaminase APOBEC3 Family Is Subject to Transcriptional Regulation by p53. *Molecular Cancer Research*, *15*(6), 735–743. https://doi.org/10.1158/1541-7786.mcr-17-0019

Methot, S. P., & Noia, J. M. D. (2017). Chapter Two Molecular Mechanisms of Somatic Hypermutation and Class Switch Recombination. *Advances in Immunology*, *133*, 37–87. https://doi.org/10.1016/bs.ai.2016.11.002

Meuwissen, R., Linn, S. C., Valk, M. van der, Mooi, W. J., & Berns, A. (2001). Mouse model for lung tumorigenesis through Cre/lox controlled sporadic activation of the K-Ras oncogene. *Oncogene*, *20*(45), 6551–6558. https://doi.org/10.1038/sj.onc.1204837

Molina-Arcas, M., Samani, A., & Downward, J. (2021). Drugging the Undruggable: Advances on RAS Targeting in Cancer. *Genes*, *12*(6), 899. https://doi.org/10.3390/genes12060899

Mori, S., Takeuchi, T., Ishii, Y., Yugawa, T., Kiyono, T., Nishina, H., & Kukimoto, I. (2017). Human Papillomavirus 16 E6 Upregulates APOBEC3B via the TEAD Transcription Factor. *Journal of Virology*, *91*(6). https://doi.org/10.1128/jvi.02413-16

Mukhopadhyay, D., Anant, S., Lee, R. M., Kennedy, S., Viskochil, D., & Davidson, N. O. (2002). C→U Editing of Neurofibromatosis 1 mRNA Occurs in Tumors That Express Both the Type II Transcript and apobec-1, the Catalytic Subunit of the Apolipoprotein B mRNA–Editing Enzyme. *The American Journal of Human Genetics*, *70*(1), 38–50. https://doi.org/10.1086/337952

Muramatsu, M., Kinoshita, K., Fagarasan, S., Yamada, S., Shinkai, Y., & Honjo, T. (2000). Class Switch Recombination and Hypermutation Require Activation-Induced Cytidine Deaminase (AID), a Potential RNA Editing Enzyme. *Cell*, *102*(5), 553–563. https://doi.org/10.1016/s0092-8674(00)00078-7

Muramatsu, M., Sankaranand, V. S., Anant, S., Sugai, M., Kinoshita, K., Davidson, N. O., & Honjo, T. (1999). Specific Expression of Activation-induced Cytidine Deaminase (AID), a Novel Member of the RNA-editing Deaminase Family in Germinal Center B Cells*. *Journal of Biological Chemistry*, *274*(26), 18470–18476. https://doi.org/10.1074/jbc.274.26.18470

Nabel, C. S., Jia, H., Ye, Y., Shen, L., Goldschmidt, H. L., Stivers, J. T., Zhang, Y., & Kohli, R. M. (2012). AID/APOBEC deaminases disfavor modified cytosines implicated in DNA demethylation. *Nature Chemical Biology*, *8*(9), 751–758. https://doi.org/10.1038/nchembio.1042

Nakamuta, M., Chang, B. H.-J., Zsigmond, E., Kobayashi, K., Lei, H., Ishida, B. Y., Oka, K., Li, E., & Chan, L. (1996). Complete Phenotypic Characterization of apobec-1 Knockout Mice with a Wild-type Genetic Background and a Human Apolipoprotein B Transgenic Background, and Restoration of Apolipoprotein B mRNA Editing by Somatic Gene Transfer of Apobec-1*. *Journal of Biological Chemistry*, *271*(42), 25981–25988. https://doi.org/10.1074/jbc.271.42.25981

Nelson, V. R., Heaney, J. D., Tesar, P. J., Davidson, N. O., & Nadeau, J. H. (2012). Transgenerational epigenetic effects of the Apobec1 cytidine deaminase deficiency on testicular germ cell tumor susceptibility and embryonic viability. *Proceedings of the National Academy of Sciences*, *109*(41), E2766–E2773. https://doi.org/10.1073/pnas.1207169109

Niavarani, A., Currie, E., Reyal, Y., Anjos-Afonso, F., Horswell, S., Griessinger, E., Sardina, J. L., & Bonnet, D. (2015). APOBEC3A Is Implicated in a Novel Class of G-to-A mRNA Editing in WT1 Transcripts. *PLoS ONE*, *10*(3), e0120089. https://doi.org/10.1371/journal.pone.0120089

Nikkilä, J., Kumar, R., Campbell, J., Brandsma, I., Pemberton, H. N., Wallberg, F., Nagy, K., Scheer, I., Vertessy, B. G., Serebrenik, A. A., Monni, V., Harris, R. S., Pettitt, S. J., Ashworth, A., & Lord, C. J. (2017). Elevated APOBEC3B expression drives a kataegic-like mutation signature and replication stress-related therapeutic vulnerabilities in p53-defective cells. *British Journal of Cancer*, *117*(1), 113–123. https://doi.org/10.1038/bjc.2017.133

Nik-Zainal, S., Alexandrov, L. B., Wedge, D. C., Loo, P. V., Greenman, C. D., Raine, K., Jones, D., Hinton, J., Marshall, J., Stebbings, L. A., Menzies, A., Martin, S., Leung, K., Chen, L., Leroy, C., Ramakrishna, M., Rance, R., Lau, K. W., Mudie, L. J., … Cancer, B. (2012). *Mutational Processes Molding the Genomes of 21 Breast Cancers*. https://doi.org/10.1016/j.cell.2012.04.024

Nik-Zainal, S., Davies, H., Staaf, J., Ramakrishna, M., Glodzik, D., Zou, X., Martincorena, I., Alexandrov, L. B., Martin, S., Wedge, D. C., Loo, P. V., Ju, Y. S., Smid, M., Brinkman, A. B., Morganella, S., Aure, M. R., Lingjærde, O. C., Langerød, A., Ringnér, M., … Stratton, M. R. (2016). Landscape of somatic mutations in 560 breast cancer whole-genome sequences. *Nature*, *534*(7605), 47–54. https://doi.org/10.1038/nature17676

Nik-Zainal, S., Wedge, D. C., Alexandrov, L. B., Petljak, M., Butler, A. P., Bolli, N., Davies, H. R., Knappskog, S., Martin, S., Papaemmanuil, E., Ramakrishna, M., Shlien, A., Simonic, I., Xue, Y., Tyler-Smith, C., Campbell, P. J., & Stratton, M. R. (2014).

Association of a germline copy number polymorphism of APOBEC3A and APOBEC3B with burden of putative APOBEC-dependent mutations in breast cancer. *Nature Genetics*, *46*(5), 487–491. https://doi.org/10.1038/ng.2955

Nishikura, K. (2016). A-to-I editing of coding and non-coding RNAs by ADARs. *Nature Reviews Molecular Cell Biology*, *17*(2), 83–96. https://doi.org/10.1038/nrm.2015.4

Oakes, E., Anderson, A., Cohen-Gadol, A., & Hundley, H. A. (2017). Adenosine Deaminase That Acts on RNA 3 (ADAR3) Binding to Glutamate Receptor Subunit B Pre-mRNA Inhibits RNA Editing in Glioblastoma*. *Journal of Biological Chemistry*, *292*(10), 4326–4335. https://doi.org/10.1074/jbc.m117.779868

Oh, S., Bournique, E., Bowen, D., Jalili, P., Sanchez, A., Ward, I., Dananberg, A., Manjunath, L., Tran, G. P., Semler, B. L., Maciejowski, J., Seldin, M., & Buisson, R. (2021). Genotoxic stress and viral infection induce transient expression of APOBEC3A and pro-inflammatory genes through two distinct pathways. *Nature Communications*, *12*(1), 4917. https://doi.org/10.1038/s41467-021-25203-4

Okazaki, I., Hiai, H., Kakazu, N., Yamada, S., Muramatsu, M., Kinoshita, K., & Honjo, T. (2003). Constitutive Expression of AID Leads to Tumorigenesis. *Journal of Experimental Medicine*, *197*(9), 1173–1181. https://doi.org/10.1084/jem.20030275

Okuyama, S., Marusawa, H., Matsumoto, T., Ueda, Y., Matsumoto, Y., Endo, Y., Takai, A., & Chiba, T. (2012). Excessive activity of apolipoprotein B mRNA editing enzyme catalytic polypeptide 2 (APOBEC2) contributes to liver and lung tumorigenesis. *International Journal of Cancer*, *130*(6), 1294–1301. https://doi.org/10.1002/ijc.26114

Pasqualucci, L., Bhagat, G., Jankovic, M., Compagno, M., Smith, P., Muramatsu, M., Honjo, T., Morse, H. C., Nussenzweig, M. C., & Dalla-Favera, R. (2008). AID is required for germinal center–derived lymphomagenesis. *Nature Genetics*, *40*(1), 108–112. https://doi.org/10.1038/ng.2007.35

Paz-Yaacov, N., Bazak, L., Buchumenski, I., Porath, H. T., Danan-Gotthold, M., Knisbacher, B. A., Eisenberg, E., & Levanon, E. Y. (2015). Elevated RNA Editing Activity Is a Major Contributor to Transcriptomic Diversity in Tumors. *Cell Reports*, *13*(2), 267–276. https://doi.org/10.1016/j.celrep.2015.08.080

Pecori, R., Giorgio, S. D., Lorenzo, J. P., & Papavasiliou, F. N. (2022). Functions and consequences of AID/APOBEC-mediated DNA and RNA deamination. *Nature Reviews. Genetics*, 1–14. https://doi.org/10.1038/s41576-022-00459-8

Peng, X., Xu, X., Wang, Y., Hawke, D. H., Yu, S., Han, L., Zhou, Z., Mojumdar, K., Jeong, K. J., Labrie, M., Tsang, Y. H., Zhang, M., Lu, Y., Hwu, P., Scott, K. L., Liang, H., & Mills, G. B. (2018). A-to-I RNA Editing Contributes to Proteomic Diversity in Cancer. *Cancer Cell*, *33*(5), 817-828.e7. https://doi.org/10.1016/j.ccell.2018.03.026

Periyasamy, M., Singh, A. K., Gemma, C., Farzan, R., Allsopp, R. C., Shaw, J. A., Charmsaz, S., Young, L. S., Cunnea, P., Coombes, R. C., Győrffy, B., Buluwela, L., & Ali, S. (2021). Induction of APOBEC3B expression by chemotherapy drugs is mediated by DNA-PK-directed activation of NF-κB. *Oncogene*, *40*(6), 1077–1090. https://doi.org/10.1038/s41388-020-01583-7

Periyasamy, M., Singh, A. K., Gemma, C., Kranjec, C., Farzan, R., Leach, D. A., Navaratnam, N., Pálinkas, H. L., Vértessy, B. G., Fenton, T. R., Doorbar, J., Fuller-Pace, F., Meek, D. W., Coombes, R. C., Buluwela, L., & Ali, S. (2017). p53 controls expression of the DNA deaminase APOBEC3B to limit its potential mutagenic activity in cancer cells. *Nucleic Acids Research*, *45*(19), 11056–11069. https://doi.org/10.1093/nar/gkx721

Petersen-Mahrt, S. K., & Neuberger, M. S. (2003). In Vitro Deamination of Cytosine to Uracil in Single-stranded DNA by Apolipoprotein B Editing Complex Catalytic Subunit 1 (APOBEC1)*. *Journal of Biological Chemistry*, *278*(22), 19583–19586. https://doi.org/10.1074/jbc.c300114200

Petljak, M., Alexandrov, L. B., Brammeld, J. S., Price, S., Wedge, D. C., Grossmann, S., Dawson, K. J., Ju, Y. S., Iorio, F., Tubio, J. M. C., Koh, C. C., Georgakopoulos-Soares, I., Rodríguez–Martín, B., Otlu, B., O'Meara, S., Butler, A. P., Menzies, A., Bhosle, S. G., Raine, K., … Stratton, M. R. (2019). Characterizing Mutational Signatures in Human Cancer Cell Lines Reveals Episodic APOBEC Mutagenesis. *Cell*, *176*(6), 1282-1294.e20. https://doi.org/10.1016/j.cell.2019.02.012

Powell, L. M., Wallis, S. C., Pease, R. J., Edwards, Y. H., Knott, T. J., & Scott, J. (1987). A novel form of tissue-specific RNA processing produces apolipoprotein-B48 in intestine. *Cell*, *50*(6), 831–840. https://doi.org/10.1016/0092-8674(87)90510-1

Powell-Braxton, L., Véniant, M., Latvala, R. D., Hirano, K.-I., Won, W. B., Ross, J., Dybdal, N., Zlot, C. H., Young, S. G., & Davidson, N. O. (1998). A mouse model of human familial hypercholesterolemia: Markedly elevated low density lipoprotein cholesterol levels and severe atherosclerosis on a low-fat chow diet. *Nature Medicine*, *4*(8), 934–938. https://doi.org/10.1038/nm0898-934

Rayon-Estrada, V., Harjanto, D., Hamilton, C. E., Berchiche, Y. A., Gantman, E. C., Sakmar, T. P., Bulloch, K., Gagnidze, K., Harroch, S., McEwen, B. S., & Papavasiliou, F. N. (2017). Epitranscriptomic profiling across cell types reveals associations between APOBEC1-mediated RNA editing, gene expression outcomes, and cellular function. *Proceedings of the National Academy of Sciences of the United States of America*, *114*(50), 13296–13301. https://doi.org/10.1073/pnas.1714227114

Rebhandl, S., Huemer, M., Gassner, F. J., Zaborsky, N., Hebenstreit, D., Catakovic, K., Gr, E. M., Greil, R., & Geisberger, R. (1929). APOBEC3 signature mutations in chronic lymphocytic leukemia. *Leukemia*. https://doi.org/10.1038/leu.2014.160

Refsland, E. W., & Harris, R. S. (2013). The APOBEC3 Family of Retroelement Restriction Factors. *Current Topics in Microbiology and Immunology*, *371*, 1–27. https://doi.org/10.1007/978-3-642-37765-5_1

Roberts, S. A., & Gordenin, D. A. (2015). Hypermutation in human cancer genomes: footprints and mechanisms. *Nature Publishing Group*. https://doi.org/10.1038/nrc3816

Roberts, S. A., Lawrence, M. S., Klimczak, L. J., Grimm, S. A., Fargo, D., Stojanov, P., Kiezun, A., Kryukov, G. V., Carter, S. L., Saksena, G., Harris, S., Shah, R. R., Resnick, M. A., Getz, G., & Gordenin, D. A. (2013). An APOBEC cytidine deaminase mutagenesis pattern is widespread in human cancers. *Nature Genetics*, *45*(9), 970–976. https://doi.org/10.1038/ng.2702

Roberts, S. A., Sterling, J., Thompson, C., Harris, S., Mav, D., Shah, R., Klimczak, L. J., Kryukov, G. V., Malc, E., Mieczkowski, P. A., Resnick, M. A., & Gordenin, D. A. (2012). Clustered Mutations in Yeast and in Human Cancers Can Arise from Damaged Long Single-Strand DNA Regions. *Molecular Cell*, *46*(4), 424–435. https://doi.org/10.1016/j.molcel.2012.03.030

Rogozin, I. B., Basu, M. K., Jordan, I. K., Pavlov, Y. I., & Koonin, E. V. (2005). APOBEC4, a New Member of the AID/APOBEC Family of Polynucleotide (Deoxy)Cytidine Deaminases Predicted by Computational Analysis. *Cell Cycle*, *4*(9), 1281–1285. https://doi.org/10.4161/cc.4.9.1994

Rogozin, I. B., & Diaz, M. (2004). Cutting Edge: DGYW/WRCH Is a Better Predictor of Mutability at G:C Bases in Ig Hypermutation Than the Widely Accepted RGYW/WRCY Motif and Probably Reflects a Two-Step Activation-Induced Cytidine Deaminase-Triggered Process. *The Journal of Immunology*, *172*(6), 3382–3384. https://doi.org/10.4049/jimmunol.172.6.3382

Rogozin, I. B., & Kolchanov, N. A. (1992). Somatic hypermutagenesis in immunoglobulin genes II. Influence of neighbouring base sequences on mutagenesis. *Biochimica et Biophysica Acta (BBA) - Gene Structure and Expression*, *1171*(1), 11–18. https://doi.org/10.1016/0167-4781(92)90134-l

Roper, N., Gao, S., Maity, T. K., Banday, A. R., Zhang, X., Venugopalan, A., Cultraro, C. M., Patidar, R., Sindiri, S., Brown, A.-L., Goncearenco, A., Panchenko, A. R., Biswas, R., Thomas, A., Rajan, A., Carter, C. A., Kleiner, D. E., Hewitt, S. M., Khan, J., … Guha, U. (2019). APOBEC Mutagenesis and Copy-Number Alterations Are Drivers of Proteogenomic Tumor Evolution and Heterogeneity in Metastatic Thoracic Tumors. *Cell Reports*, *26*(10), 2651-2666.e6. https://doi.org/10.1016/j.celrep.2019.02.028

Rosenberg, B. R., Hamilton, C. E., Mwangi, M. M., Dewell, S., & Papavasiliou, F. N. (2011). Transcriptome-wide sequencing reveals numerous APOBEC1 mRNA-editing targets in transcript 3′ UTRs. *Nature Structural & Molecular Biology*, *18*(2), 230–236. https://doi.org/10.1038/nsmb.1975

Roth, S. H., Danan-Gotthold, M., Ben-Izhak, M., Rechavi, G., Cohen, C. J., Louzoun, Y., & Levanon, E. Y. (2018). Increased RNA Editing May Provide a Source for Autoantigens in Systemic Lupus Erythematosus. *Cell Reports*, *23*(1), 50–57. https://doi.org/10.1016/j.celrep.2018.03.036

Rowald, K., Mantovan, M., Passos, J., Buccitelli, C., Mardin, B. R., Korbel, J. O., Jechlinger, M., & Sotillo, R. (2016). Negative Selection and Chromosome Instability Induced by Mad2 Overexpression Delay Breast Cancer but Facilitate Oncogene-Independent Outgrowth. *Cell Reports*, *15*(12). https://doi.org/10.1016/j.celrep.2016.05.048

Rubio, T., Weyershaeuser, J., Montero, M. G., Hoffmann, A., Lujan, P., Jechlinger, M., Sotillo, R., & Köhn, M. (2021). The phosphatase PRL-3 affects intestinal homeostasis by altering the crypt cell composition. *Journal of Molecular Medicine*, *99*(10), 1413–1426. https://doi.org/10.1007/s00109-021-02097-9

Salamango, D. J., McCann, J. L., Demir, Ö., Brown, W. L., Amaro, R. E., & Harris, R. S. (2018). APOBEC3B Nuclear Localization Requires Two Distinct N-Terminal Domain

Surfaces. *Journal of Molecular Biology*, *430*(17), 2695–2708. https://doi.org/10.1016/j.jmb.2018.04.044

Salter, J. D., Bennett, R. P., & Smith, H. C. (2016). The APOBEC Protein Family: United by Structure, Divergent in Function. *Trends in Biochemical Sciences*, *41*(7), 578–594. https://doi.org/10.1016/j.tibs.2016.05.001

Salter, J. D., & Smith, H. C. (2018). Modeling the Embrace of a Mutator: APOBEC Selection of Nucleic Acid Ligands. *Trends in Biochemical Sciences*, *43*(8), 606–622. https://doi.org/10.1016/j.tibs.2018.04.013

Saraconi, G., Severi, F., Sala, C., Mattiuz, G., & Conticello, S. G. (2014). The RNA editing enzyme APOBEC1 induces somatic mutations and a compatible mutational signature is present in esophageal adenocarcinomas. *Genome Biology*, *15*(7), 417. https://doi.org/10.1186/s13059-014-0417-z

Sato, Y., Ohtsubo, H., Nihei, N., Kaneko, T., Sato, Y., Adachi, S., Kondo, S., Nakamura, M., Mizunoya, W., Iida, H., Tatsumi, R., Rada, C., & Yoshizawa, F. (2018). Apobec2 deficiency causes mitochondrial defects and mitophagy in skeletal muscle. *The FASEB Journal*, *32*(3), 1428–1439. https://doi.org/10.1096/fj.201700493r

Sawyer, S. L., Emerman, M., & Malik, H. S. (2004). Ancient Adaptive Evolution of the Primate Antiviral DNA-Editing Enzyme APOBEC3G. *PLoS Biology*, *2*(9), e275. https://doi.org/10.1371/journal.pbio.0020275

Sharma, S., & Baysal, B. E. (2017). Stem-loop structure preference for site-specific RNA editing by APOBEC3A and APOBEC3G. *PeerJ*, *5*, e4136. https://doi.org/10.7717/peerj.4136

Sharma, S., Patnaik, S. K., Kemer, Z., & Baysal, B. E. (2016). Transient overexpression of exogenous APOBEC3A causes C-to-U RNA editing of thousands of genes. *RNA Biology*, *14*(5), 00–00. https://doi.org/10.1080/15476286.2016.1184387

Sharma, S., Patnaik, S. K., Taggart, R. T., & Baysal, B. E. (2016). The double-domain cytidine deaminase APOBEC3G is a cellular site-specific RNA editing enzyme. *Scientific Reports*, *6*(1), 39100. https://doi.org/10.1038/srep39100

Sharma, S., Patnaik, S. K., Taggart, R. T., Kannisto, E. D., Enriquez, S. M., Gollnick, P., & Baysal, B. E. (2015). APOBEC3A cytidine deaminase induces RNA editing in monocytes and macrophages. *Nature Communications*, *6*(1), 6881. https://doi.org/10.1038/ncomms7881

Sharma, S., Wang, J., Alqassim, E., Portwood, S., Gomez, E. C., Maguire, O., Basse, P. H., Wang, E. S., Segal, B. H., & Baysal, B. E. (2019). Mitochondrial hypoxic stress induces widespread RNA editing by APOBEC3G in natural killer cells. *Genome Biology*, *20*(1), 37. https://doi.org/10.1186/s13059-019-1651-1

Shi, K., Carpenter, M. A., Banerjee, S., Shaban, N. M., Kurahashi, K., Salamango, D. J., McCann, J. L., Starrett, G. J., Duffy, J. V., Demir, Ö., Amaro, R. E., Harki, D. A., Harris, R. S., & Aihara, H. (2017). Structural basis for targeted DNA cytosine deamination and

mutagenesis by APOBEC3A and APOBEC3B. *Nature Structural & Molecular Biology*, *24*(2), 131–139. https://doi.org/10.1038/nsmb.3344

Shi, K., Demir, Ö., Carpenter, M. A., Wagner, J., Kurahashi, K., Harris, R. S., Amaro, R. E., & Aihara, H. (2017). Conformational Switch Regulates the DNA Cytosine Deaminase Activity of Human APOBEC3B. *Scientific Reports*, *7*(1), 17415. https://doi.org/10.1038/s41598-017-17694-3

Siegel, R. L., Miller, K. D., Fuchs, H. E., & Jemal, A. (2022). Cancer statistics, 2022. *CA: A Cancer Journal for Clinicians*, *72*(1), 7–33. https://doi.org/10.3322/caac.21708

Sieuwerts, A. M., Willis, S., Burns, M. B., Look, M. P., Gelder, M. E. M.-V., Schlicker, A., Heideman, M. R., Jacobs, H., Wessels, L., Leyland-Jones, B., Gray, K. P., Foekens, J. A., Harris, R. S., & Martens, J. W. M. (2014). Elevated APOBEC3B correlates with poor outcomes for estrogen-receptor-positive breast cancers. *Hormones & Cancer*, *5*(6), 405–413. https://doi.org/10.1007/s12672-014-0196-8

Siriwardena, S. U., Guruge, T. A., & Bhagwat, A. S. (2015). Characterization of the Catalytic Domain of Human APOBEC3B and the Critical Structural Role for a Conserved Methionine. *Journal of Molecular Biology*, *427*(19), 3042–3055. https://doi.org/10.1016/j.jmb.2015.08.006

Skoulidis, F., & Heymach, J. V. (2019). Co-occurring genomic alterations in non-small-cell lung cancer biology and therapy. *Nature Reviews Cancer*, *19*(9), 495–509. https://doi.org/10.1038/s41568-019-0179-8

Skuse, G. R., Cappione, A. J., Sowden, M., Metheny, L. J., & Smith, H. C. (1996). The Neurofibromatosis Type I Messenger RNA Undergoes Base-Modification RNA Editing. *Nucleic Acids Research*, *24*(3), 478–486. https://doi.org/10.1093/nar/24.3.478

Soleymanjahi, S., Blanc, V., & Davidson, N. O. (2021). APOBEC1 mediated C-to-U RNA editing: target sequence and trans -acting factor contribution to 177 RNA editing events in 119 murine transcripts in vivo. *RNA*, *27*(8), 876–890. https://doi.org/10.1261/rna.078678.121

Sotillo, R., Schvartzman, J.-M., Socci, N. D., & Benezra, R. (2010). *LETTERS Mad2-induced chromosome instability leads to lung tumour relapse after oncogene withdrawal*. https://doi.org/10.1038/nature08803

Starrett, G. J., Luengas, E. M., McCann, J. L., Ebrahimi, D., Temiz, N. A., Love, R. P., Feng, Y., Adolph, M. B., Chelico, L., Law, E. K., Carpenter, M. A., & Harris, R. S. (2016). The DNA cytosine deaminase APOBEC3H haplotype I likely contributes to breast and lung cancer mutagenesis. *Nature Communications*, *7*(1), 12918. https://doi.org/10.1038/ncomms12918

Stenglein, M. D., Burns, M. B., Li, M., Lengyel, J., & Harris, R. S. (2010). APOBEC3 proteins mediate the clearance of foreign DNA from human cells. *Nature Structural & Molecular Biology*, *17*(2), 222–229. https://doi.org/10.1038/nsmb.1744

Storb, U. (2014). Chapter Seven Why Does Somatic Hypermutation by AID Require Transcription of Its Target Genes? *Advances in Immunology*, *122*, 253–277. https://doi.org/10.1016/b978-0-12-800267-4.00007-9

Subramanian, A., Tamayo, P., Mootha, V. K., Mukherjee, S., Ebert, B. L., Gillette, M. A., Paulovich, A., Pomeroy, S. L., Golub, T. R., Lander, E. S., & Mesirov, J. P. (2005). Gene set enrichment analysis: A knowledge-based approach for interpreting genome-wide expression profiles. *Proceedings of the National Academy of Sciences*, *102*(43), 15545–15550. https://doi.org/10.1073/pnas.0506580102

Swanton, C., Mcgranahan, N., Starrett, G. J., & Harris, R. S. (2015). *APOBEC Enzymes: Mutagenic Fuel for Cancer Evolution and Heterogeneity THE IMPORTANCE OF CANCER DIVERSITY*. https://doi.org/10.1158/2159-8290.cd-15-0344

Tasakis, R. N., Laganà, A., Stamkopoulou, D., Melnekoff, D. T., Nedumaran, P., Leshchenko, V., Pecori, R., Parekh, S., & Papavasiliou, F. N. (2020). ADAR1 can drive Multiple Myeloma progression by acting both as an RNA editor of specific transcripts and as a DNA mutator of their cognate genes. *BioRxiv*, 2020.02.11.943845. https://doi.org/10.1101/2020.02.11.943845

Tasakis, R. N., Samaras, G., Jamison, A., Lee, M., Paulus, A., Whitehouse, G., Verkoczy, L., Papavasiliou, F. N., & Diaz, M. (2021). SARS-CoV-2 variant evolution in the United States: High accumulation of viral mutations over time likely through serial Founder Events and mutational bursts. *PLoS ONE*, *16*(7), e0255169. https://doi.org/10.1371/journal.pone.0255169

Taylor, B. J., Nik-Zainal, S., Wu, Y. L., Stebbings, L. A., Raine, K., Campbell, P. J., Rada, C., Stratton, M. R., & Neuberger, M. S. (2013). *DNA deaminases induce break-associated mutation showers with implication of APOBEC3B and 3A in breast cancer kataegis*. *2*, 534. https://doi.org/10.7554/elife.00534

Teng, B., Burant, C. F., & Davidson, N. O. (1993). Molecular Cloning of an Apolipoprotein B Messenger RNA Editing Protein. *Science*, *260*(5115), 1816–1819. https://doi.org/10.1126/science.8511591

Travis, W. D. (2002). Pathology of lung cancer. *Clinics in Chest Medicine*, *23*(1), 65–81. https://doi.org/10.1016/s0272-5231(03)00061-3

Turajlic, S., Sottoriva, A., Graham, T., & Swanton, C. (2019). Resolving genetic heterogeneity in cancer. *Nature Reviews Genetics*, *20*(7), 1–13. https://doi.org/10.1038/s41576-019-0114-6

Vega, A. A. de la, Temiz, N. A., Tasakis, R., Somogyi, K., Reuveni, E., Ben-David, U., Stenzinger, A., Poth, T., Papavasiliou, F. N., Harris, R. S., & Sotillo, R. (2022). *Acute expression of human APOBEC3B in mice causes lethality associated with RNA editing*. https://doi.org/10.1101/2022.06.01.494353

Venkatesan, S., Angelova, M., Puttick, C., Zhai, H., Caswell, D. R., Lu, W.-T., Dietzen, M., Galanos, P., Evangelou, K., Bellelli, R., Lim, E. L., Watkins, T. B. K., Rowan, A., Teixeira, V. H., Zhao, Y., Chen, H., Ngo, B., Zalmas, L.-P., Bakir, M. A., … Consortium, Tracer. (2021). Induction of APOBEC3 exacerbates DNA replication stress and

chromosomal instability in early breast and lung cancer evolution. *Cancer Discovery*, candisc.0725.2020. https://doi.org/10.1158/2159-8290.cd-20-0725

Venkatesan, S., Rosenthal, R., Kanu, N., McGranahan, N., Bartek, J., Quezada, S. A., Hare, J., Harris, R. S., & Swanton, C. (2018). Perspective: APOBEC mutagenesis in drug resistance and immune escape in HIV and cancer evolution. *Annals of Oncology*, *29*(3), 563–572. https://doi.org/10.1093/annonc/mdy003

Vieira, V. C., Leonard, B., White, E. A., Starrett, G. J., Temiz, N. A., Lorenz, L. D., Lee, D., Soares, M. A., Lambert, P. F., Howley, P. M., & Harris, R. S. (2014). Human Papillomavirus E6 Triggers Upregulation of the Antiviral and Cancer Genomic DNA Deaminase APOBEC3B. *MBio*, *5*(6), e02234-14. https://doi.org/10.1128/mbio.02234-14

Wang, D., Li, X., Li, J., Lu, Y., Zhao, S., Tang, X., Chen, X., Li, J., Zheng, Y., Li, S., Sun, R., Yan, M., Yu, D., Cao, G., & Yang, Y. (2019). APOBEC3B interaction with PRC2 modulates microenvironment to promote HCC progression. *Gut*, *68*(10), 1846. https://doi.org/10.1136/gutjnl-2018-317601

Wang, R., Hozumi, Y., Zheng, Y.-H., Yin, C., & Wei, G.-W. (2020). Host Immune Response Driving SARS-CoV-2 Evolution. *Viruses*, *12*(10), 1095. https://doi.org/10.3390/v12101095

Wang, S., Jia, M., He, Z., & Liu, X.-S. (2018). APOBEC3B and APOBEC mutational signature as potential predictive markers for immunotherapy response in non-small cell lung cancer. *Oncogene*, *37*(29), 3924–3936. https://doi.org/10.1038/s41388-018-0245-9

Warren, C. J., Xu, T., Guo, K., Griffin, L. M., Westrich, J. A., Lee, D., Lambert, P. F., Santiago, M. L., & Pyeon, D. (2015). APOBEC3A Functions as a Restriction Factor of Human Papillomavirus. *Journal of Virology*, *89*(1), 688–702. https://doi.org/10.1128/jvi.02383-14

Weinstein, J. N., Akbani, R., Broom, B. M., Wang, W., Verhaak, R. G. W., McConkey, D., Lerner, S., Morgan, M., Creighton, C. J., Smith, C., Kwiatkowski, D. J., Cherniack, A. D., Kim, J., Pedamallu, C. S., Noble, M. S., Al-Ahmadie, H. A., Reuter, V. E., Rosenberg, J. E., Bajorin, D. F., … Eley, G. (2014). Comprehensive molecular characterization of urothelial bladder carcinoma. *Nature*, *507*(7492), 315–322. https://doi.org/10.1038/nature12965

Wörmann, S. M., Zhang, A., Thege, F. I., Cowan, R. W., Rupani, D. N., Wang, R., Manning, S. L., Gates, C., Wu, W., Levin-Klein, R., Rajapakshe, K. I., Yu, M., Multani, A. S., Kang, Y., Taniguchi, C. M., Schlacher, K., Bellin, M. D., Katz, M. H. G., Kim, M. P., … Rhim, A. D. (2021). APOBEC3A drives deaminase domain-independent chromosomal instability to promote pancreatic cancer metastasis. *Nature Cancer*, *2*(12), 1338–1356. https://doi.org/10.1038/s43018-021-00268-8

Xiao, X., Yang, H., Arutiunian, V., Fang, Y., Besse, G., Morimoto, C., Zirkle, B., & Chen, X. S. (2017). Structural determinants of APOBEC3B non-catalytic domain for molecular assembly and catalytic regulation. *Nucleic Acids Research*, *45*(12), gkx564-. https://doi.org/10.1093/nar/gkx564

Xie, Y., Luo, J., Kennedy, S., & Davidson, N. O. (2007). Conditional Intestinal Lipotoxicity in Apobec-1 -/- Mttp-IKO Mice A SURVIVAL ADVANTAGE FOR MAMMALIAN INTESTINAL APOLIPOPROTEIN B mRNA EDITING*. *Journal of Biological Chemistry*, *282*(45), 33043–33051. https://doi.org/10.1074/jbc.m705386200

Yamanaka, S., Balestra, M. E., Ferrell, L. D., Fan, J., Arnold, K. S., Taylor, S., Taylor, J. M., & Innerarity, T. L. (1995). Apolipoprotein B mRNA-editing protein induces hepatocellular carcinoma and dysplasia in transgenic animals. *Proceedings of the National Academy of Sciences*, *92*(18), 8483 LP – 8487. https://doi.org/10.1073/pnas.92.18.8483

Yamanaka, S., Poksay, K. S., Arnold, K. S., & Innerarity, T. L. (1997). A novel translational repressor mRNA is edited extensively in livers containing tumors caused by the transgene expression of the apoB mRNA-editing enzyme. *Genes & Development*, *11*(3), 321–333. https://doi.org/10.1101/gad.11.3.321

Yan, S., He, F., Gao, B., Wu, H., Li, M., Huang, L., Liang, J., Wu, Q., & Li, Y. (2016). Increased APOBEC3B Predicts Worse Outcomes in Lung Cancer: A Comprehensive Retrospective Study. *Journal of Cancer*, *7*(6), 618–625. https://doi.org/10.7150/jca.14030

Zhang, H., Chen, Z., Wang, Z., Dai, Z., Hu, Z., Zhang, X., Hu, M., Liu, Z., & Cheng, Q. (2021). Correlation Between APOBEC3B Expression and Clinical Characterization in Lower-Grade Gliomas. *Frontiers in Oncology*, *11*, 625838. https://doi.org/10.3389/fonc.2021.625838

Zhang, J., Fujimoto, J., Zhang, J., Wedge, D. C., Song, X., Zhang, J., Seth, S., Chow, C.-W., Cao, Y., Gumbs, C., Gold, K. A., Kalhor, N., Little, L., Mahadeshwar, H., Moran, C., Protopopov, A., Sun, H., Tang, J., Wu, X., … Futreal, P. A. (2014). Intratumor heterogeneity in localized lung adenocarcinomas delineated by multiregion sequencing. *Science*, *346*(6206), 256–259. https://doi.org/10.1126/science.1256930

Zhang, J., & Webb, D. M. (2004). Rapid evolution of primate antiviral enzyme APOBEC3G. *Human Molecular Genetics*, *13*(16), 1785–1791. https://doi.org/10.1093/hmg/ddh183